

THE INVESTIGATION OF CONFIGURATIONALLY STABLE LONGITUDINALLY
TWISTED ACENES AND THE DEVELOPMENT OF A SILORANE-BASED
BIOMATERIAL FOR USE AS AN ANTIMICROBIAL DELIVERY DEVICE

A DISSERTATION IN
Chemistry
and
Pharmaceutical Science

Presented to the Faculty of the University
of Missouri-Kansas City in partial fulfillment of
the requirements for the degree

DOCTOR OF PHILOSOPHY

by
ELIZABETH MICHOL MENUHEY
B.S. Rockhurst University, 2010

Kansas City, Missouri
2019

© 2019
ELIZABETH MICHOL MENUHEY
ALL RIGHTS RESERVED

THE INVESTIGATION OF CONFIGURATIONALLY STABLE LONGITUDINALLY
TWISTED ACENES AND THE DEVELOPMENT OF A SILORANE-BASED
BIOMATERIAL FOR USE AS AN ANTIMICROBIAL DELIVERY DEVICE

Elizabeth Michol Menuey, Candidate for the Doctor of Philosophy Degree

University of Missouri-Kansas City, 2019

ABSTRACT

Longitudinally twisted acenes (LTAs) adopt a helical twist in order to alleviate steric congestion caused by bulky substituents along the acene backbone and are inherently chiral. As is observed in helicenes, this helical twist gives rise to *M* and *P* enantiomers, which may possess theoretically interesting chiroptical properties. In order to study the chiroptical properties of these compounds, they must be configurationally stable. One approach to configurational stability is through the extension of the acene core. Semiempirical calculations at the AM1 level resulted in values that align well with the experimentally determined crystal structure values. DFT calculations generated similar results, albeit with slightly larger differences. Inducing an energetically favored twist bias through the incorporation of bulky naphthyl groups in a dissymmetric fashion is an alternative approach to configurationally stable compounds. A twist bias was observed for all naphthyl substituted compounds. From

this study, it is apparent that the twist bias is not directly proportional to the overall twist and is affected by many factors, including sterics.

The number of joint replacement procedures is expected to rise exponentially over the next few decades. As with any surgery, a number of complications can occur including prosthetic joint infection (PJI), an infection of the surrounding bone and tissues. These risks are further compounded when presented with additional risk factors including previous joint infections, obesity, and diabetes. PJI affects approximately 2% of all primary hip and knee replacements, but increases to 15.8% for multiple replacements/revisions. Treatment options are limited to heat and chemically stable antimicrobials due to the composition and curing temperatures ($>70\text{ }^{\circ}\text{C}$) of commercially available poly(methyl methacrylate) (PMMA) bone cements. With the number of antibiotic and antifungal resistant pathogens on the rise, it is pertinent to expand the number of antimicrobials that can be incorporated into and eluted from bone cement. We have developed a novel silorane-based biomaterial that has the potential to serve as a delivery device for a breadth of antimicrobials including those unsuited for use in PMMA while displaying none of the drawbacks typical of commercial bone cements. The silorane-based biomaterial exhibits a lower exotherm ($\sim 26\text{ }^{\circ}\text{C}$), is non-toxic, has less shrinkage, and maintains comparable mechanical strength to commercial PMMA bone cements *in vitro* and *in vivo*. PMMA compatible and incompatible antimicrobials have been incorporated into silorane bone cement. The elution profiles and the effect of incorporation on the retention of antimicrobial activity and mechanical properties were measured. Our preliminary results have demonstrated the ability of silorane to serve as an antimicrobial delivery device.

APPROVAL PAGE

The faculty listed below, appointed by the Dean of the School of Graduate Studies have examined a thesis titled “The Investigation of Configurationally Stable Longitudinally Twisted Acenes and the Development of a Silorane-Based Biomaterial for Use as an Antimicrobial Delivery Device,” presented by Elizabeth Michol Menuey, candidate for the Doctor of Philosophy degree, and certify that in their opinion it is worthy of acceptance.

Supervisory Committee

Kathleen V. Kilway, Ph.D., Committee Chair
Department of Chemistry

Andrew J. Holder, Ph.D.
Department of Chemistry

Zhonghua Peng, Ph.D.
Department of Chemistry

Simon H. Friedman, Ph.D.
Department of Pharmaceutical Sciences

James B. Murowchick, Ph.D.
Department of Geosciences

CONTENTS

ABSTRACT	iii
LIST OF ILLUSTRATIONS	x
LIST OF TABLES	xv
ACKNOWLEDGEMENTS	xvii
Chapter	
1. INVESTIGATION OF CONFIGURATIONALLY STABLE LONGITUDINALLY TWISTED ACENES	1
Introduction	1
Twisted Acenes	5
Anthracenes and Tetracenes	9
Pentacene and Larger LTAs	11
Synthesis	17
Benzyne Approach	17
Quinone Approach	20
Chirality and Configurational Stability	22
Variable Temperature NMR Spectroscopy	23
Chiral Resolution	25
Twist Bias	27
Alternative Routes to Configurationally Stable LTAs	28
Prospective Applications	29
Summary	31
Results and Discussion	32

Prediction of the End-to-End Twists of LTAs	32
Barriers to Enantiomerization	37
Twist Bias.....	42
Summary.....	52
Future Work.....	53
Materials and Methods	54
REFERENCES	55
2. DEVELOPMENT OF A SILORANE-BASED BIOMATERIAL	61
Introduction	61
Commercial PMMA-Based Bone Cement	62
Alternative Bone Cements.....	64
Silorane-Based Bone Cement.....	65
Composition	65
Biocompatibility.....	71
Mechanical Properties	72
Pullout Strength.....	74
Silorane Moisture Investigation – Drying.....	75
<i>In Vivo</i> Pullout Testing.....	76
Summary.....	78
Results and Discussion	79
Synthesis and Optimization.....	79
Investigation of the Role of Si-H in Polymerization.....	83

CYGEP Optimization	90
Summary	91
<i>In Vivo</i> Animal Studies	92
Histology	95
Pullout Testing	95
Summary.....	101
Materials and Methods	102
3. SILORANE-BASED BIOMATERIAL AS AN ANTIMICROBIAL DELIVERY DEVICE.....	108
Introduction	108
Pathogeneses of PJIs.....	109
Treatment of PJIs.....	111
Antimicrobial-Laden Bone Cements	113
Antimicrobial Selection.....	114
Current ALBCS.....	115
Alternatives to PMMA-Based ALBCS	118
Summary.....	119
Results and Discussion	120
Proof of Concept Studies.....	121
Antimicrobial-Incorporated Silorane Bone Cement	130
Vancomycin Incorporation.....	130
Rifampin Incorporation.....	133
PMMA Incompatibility.....	133

Rifampin-Incorporated Silorane-Based Bone Cement.....	139
Summary.....	143
Future Work	144
Materials and Methods	146
REFERENCES	148
VITA.....	158

ILLUSTRATIONS

Figure	Page
1.1. Naphthalene and decacene.....	1
1.2. Synthetic route to heptacene (1)	2
1.3. Formation of the endoperoxide 8 in the presence of oxygen.....	3
1.4. Heptacene dimer 9	3
1.5. Substituted pentacene derivatives	5
1.6. Comparison 9,10,11,12,21,22,23,24-octaphenyltetrabenzo[<i>a,c,n,p</i>]hexacene and heptahelicene	6
1.7. Dihedral angle (ABCD or BADC) used to determine the end-to-end twist of the molecule	6
1.8. Structure of 9,10,11,12,21,22,23,24-octaphenyltetrabenzo[<i>a,c,n,p</i>]- hexacene (14)	7
1.9. X-ray crystal structure of hexacene 14 illustrating the 183° twist along the acene backbone.....	7
1.10. Structure of rubrene (15) next to its x-ray crystal structure displaying the planar acene core.....	8
1.11. Effects of substitution pattern on the end-to end twist of anthracenes along with their x-ray crystal structure displaying the overall twist.....	10
1.12. Structures of highly twisted tetracenes along with the x-ray crystal structure illustrating the overall twist	11
1.13. LTAs with centers of inversion alongside their x-ray crystal structures	13
1.14. Endoperoxide 27 of pentacene 24	13
1.15. Structure of dodecacene 28 in addition to the x-ray crystal structure depicting the net 0° twist	14
1.16. Pyrene capped hexacene 29 (135°) compared to phenanthrene capped pentacene 30 (144°)	15

1.17. <i>Meta</i> -xylene substituted (31 , 148°) and 1-naphthyl substituted (32 , 141°) pentacenes	16
1.18. Heptacene 33	17
1.19. Pascal’s decaphenylanthracene (16) synthesis.....	18
1.20. LTAs generated from the benzyne approach	19
1.21. Fully phenylated pentacene 41	20
1.22. Kilway’s decaphenylanthracene (16) synthesis	21
1.23. LTAs generated utilizing the “quinone” approach	22
1.24. Designation of <i>P</i> (plus) and <i>M</i> (minus) enantiomer based on the conformational orientation.....	23
1.25. Pascal’s isopropyl anthracene derivative 49	24
1.26. Miller’s isopropyl substituted LTA derivatives 50 and 51	25
1.27. Successfully resolved pentacene derivatives 30 and 52	26
1.28. A route to configurationally stable LTAs through naphthyl substituted naphthalene 53	28
1.29. Controlled anthracene LTA through the use of an ether tether	29
1.30. Structures of heptacene 55 and naphthalene 56	31
1.31. DFT B3LYP/6-31g(d) calculated twist of 30 , 32 , and 14	34
1.32. DFT B3LYP/6-31g(d) calculated twist of 48 , 57 , 29 , and 55	36
1.33. Synthetic route for the half-add isopropyl anthracene 58	38
1.34. Half-add isopropyl anthracene 62	39
1.35. ¹ H VT NMR spectra of 62 in 1,1,2,2-tetrachloroethane- <i>d</i> ₂	40
1.36. Half-add phenylated isopropyl anthracene 63	41
1.37. ¹ H VT NMR spectra of 63 in CDCl ₃	41

1.38. Structures with increasingly congested environments.....	43
1.39. Example of interconversion from the <i>trans-P</i> to <i>trans-M</i> diastereomer.....	44
1.40. DFT B3LYP/6-31g(d) optimized structures and relative energies of the two conformations of 66	45
1.41. DFT B3LYP/6-31g(d) optimized structures and relative energies of the six conformations of 67	46
1.42. DFT B3LYP/6-31g(d) optimized structures and relative energies of the six conformations of 68	47
1.43. DFT B3LYP/6-31g(d) optimized structures and relative energies of the six conformations of 69	48
1.44. DFT B3LYP/6-31g(d) optimized structures and relative energies of the six conformations of 70	51
2.1. Structures of bone cement components: PMMA (71), benzoyl peroxide (72), methyl methacrylate (73), N,N-dimethyl- <i>p</i> -toluidine (74), and hydroquinone (75).....	62
2.2. General reaction scheme of commercial bone cement polymerization.....	63
2.3. Examples of a siloxane 77 and an oxirane 78	65
2.4. Structures of CYGEP (79) and PHEPSI (80) monomers.....	66
2.5. Synthesis of CYGEP (79).....	67
2.6. Synthesis of PHEPSI (80).....	67
2.7. Structures of glass filler modifications: ECHE (84), 1TOSU (85), and 3TOSU (86).....	68
2.8. Chemical components of Filtek™ P90 light initiation system.....	69
2.9. Composition of the silorane dual-cured initiation system: CPQ (88), PIH (91), EDMAB (89), and LMC (90).....	70
2.10. Biocompatibility of DY5-1TOSU silorane bone cement <i>in vitro</i> . (A) Effect of bone cements on cell number and (B) Effect of bone cements on percent live and dead cells.....	72

2.11. Mimic pullout strengths of different glass-filled silorane formulations	74
2.12. <i>Ex vivo</i> pullout strength of silorane formulations compared to Simplex™ P	75
2.13. Effects of moisture and percent filler on pullout strengths of dried DY5-1TOSU bone cement one-week PO	77
2.14. Pullout strength of dried 65% DY5-1TOSU silorane and Simplex™ P bone cements eight-week PO.....	78
2.15. Proposed by-products of the CYGEP synthesis	80
2.16. ¹ H NMR spectra of our attempts to eliminate the di- and tri-substituted CYGEP byproducts.....	81
2.17. Proposed mechanism for polymerization initiation in our dual-cured biomaterial	84
2.18. Proposed silane reduction of the phenyliodonium salt in our monomer system	86
2.19. Side-by-side comparison of the old and new pig pullout apparatuses.....	97
2.20. X-rays of Simplex™ P (top) and silorane (bottom) pig femurs	99
2.21. Photographs of the titanium rod exposure at the midshaft illustrating the variability in filling the marrow cavity within and between Simplex™ P (top) and silorane (bottom) samples	100
2.22. Longitudinally cut femurs displaying differences in cement filling between silorane (left) and Simplex™ P (right)	101
3.1. Common pathogens associated with prosthetic joint infections	110
3.2. Schematic of treatment options for PJIs	112
3.3. Vancomycin (103) structure	121
3.4. Compressive strength of vancomycin-laden silorane cement.....	122
3.5. Compressive modulus of vancomycin-laden silorane cement.....	123
3.6. Weight-adjusted daily elution for vancomycin-incorporated PMMA and	

silorane bone cements	124
3.7. Amphotericin B (104)	125
3.8. Weight-adjusted average amphotericin B daily elution.....	126
3.9. Compressive strength of amphotericin B-laden silorane biomaterial on Day 7 (n=3)	128
3.10. Compressive modulus of amphotericin B-laden silorane biomaterial on Day 7 (n=3)	128
3.11. Elution profiles for vancomycin-incorporated SmartSet™ and silorane bone cements.....	131
3.12. Effect of vancomycin-incorporation on the compressive strength of SmartSet™ and silorane bone cements over time	132
3.13. Effect of vancomycin-incorporation on the compressive modulus of SmartSet™ and silorane bone cements over time	132
3.14. Chemical structure of rifampin (105)	133
3.15. Typical UV-Vis spectra of DPPH assay	134
3.16. Schematic of the reduction reaction of DPPH*	135
3.17. Structures of ascorbic acid (108), hydroquinone (75), 1-methylpiperazine (107), and gentamicin (110).....	135
3.18. Log scale EC50 values.....	136
3.19. Effects of rifampin (RIF), ascorbic acid (AA), and hydroquinone (HQ) on the compressive strength of SmartSet™ over time.....	138
3.20. Elution profiles for vancomycin-incorporated SmartSet™ and silorane bone cements.....	141
3.21. Effects of rifampin incorporation on the compressive strength of SmartSet™ (PMMA) and silorane (SIL) bone cements	142
3.22. Effects of rifampin incorporation on the compressive modulus of SmartSet™ (PMMA) and silorane (SIL) bone cements	142

TABLES

Table	Page
1.1. Comparison of experimental and calculated ΔG_{rac} for LTAs and helicenes...27	27
1.2. Comparison of the theoretical and experimental end-to-end twists.....37	37
1.3. DFT B3LYP/6-31g(d) calculated overall twist and twist bias of 65-69 for the diastereomers.....49	49
2.1. Comparison of the chemical composition of PMMA and silorane bone cements.....71	71
2.2. Summary of the effects of the surface modified glass fillers on the material properties of the silorane bone cement. The ISO 5833 standard is given as a reference.....73	73
2.3. Composition of silorane formulations tested <i>in vivo</i>76	76
2.4. Average <i>in vivo</i> rat pullout strength – 8 wk PO.....78	78
2.5. Attempts to obtain pure tetrasubstituted CYGEP.....82	82
2.6. Integration of CYGEP ^1H NMR spectra with respect to the Si-H peak.....87	87
2.7. In-house and commercial LMC polymerization results.....89	89
2.8. Effects of reaction time on CYGEP yield.....90	90
2.9. Effect of solvent on CYGEP synthesis.....91	91
2.10. Optimization of the rate of LMC addition.....91	91
2.11. Amount of silorane material required per animal.....93	93
2.12. Pig pullout strength.....98	98
2.13. Average pig pullout strength.....98	98
3.1. PMMA-compatible antimicrobials.....117	117
3.2. Compressive strength and modulus of vancomycin-laden silorane biomaterial.....123	123

3.3. Amphotericin B-laden silorane biomaterial formulations	126
3.4. Compressive strength and modulus of amphotericin-laden silorane biomaterial.....	129
3.5. Formulations of samples for the vancomycin investigation	130
3.6. Setting time and maximum curing temperature for rifampin-, hydroquinone-, and ascorbic acid-laden SmartSet™ bone cement.....	137
3.7. Formulations and polymerization times of silorane-based bone cement with increasing concentrations of rifampin.....	139
3.8. Sample formulation for rifampin-incorporated elution and mechanical testing	140

ACKNOWLEDGEMENTS

I would like to express my deepest appreciation to my advisor, Dr. Kathleen V. Kilway, for her support and mentorship over the years. Dr. Kilway was a constant source of encouragement and consistently pushed me to seek new opportunities for both professional and personal growth inside and outside the lab and for that I will be ever grateful.

I would also like to thank my committee, Drs. Andrew J. Holder, Zhonghua Peng, Simon H. Friedman, and James B. Murowchick, for their valuable advice and feedback. In addition, I would like to thank our collaborators who were willing to impart knowledge and guidance throughout these projects and without whom this work would not have been completed: Dr. Terrence McIff, Dr. Thomas Schuman, Dr. Lynda Bonewald, Grahmm Funk, and Jennifer Rosser. I would also like to thank Dr. Donna Pacicca and Dr. Lianxiang Bi for their role with the animal surgeries. I would also like to extend my gratitude to the undergraduate students who have assisted in the completion of this work. I am grateful for the support and stimulating conversations provided by my fellow graduate students and lab mates, in particular Dr. Robert Clevenger.

Finally, I would like to thank my family and friends for their unwavering support throughout this endeavor. I am indebted to my parents, Michael and Dianne Horn, for instilling a love for learning and their profound belief in my abilities. Last, but not least, I cannot begin to express my gratitude to my husband, Travis, for his love, support, and friendship.

DEDICATION

To my husband and parents, with love.

CHAPTER 1

INVESTIGATION OF CONFIGURATIONALLY STABLE LONGITUDINALLY TWISTED ACENES

Introduction

Acenes are defined as “polycyclic aromatic hydrocarbons consisting of fused benzene rings in a rectilinear arrangement,”¹ and experimentally observed up to and including decacene (one to ten linearly fused rings) (Figure 1.1).²⁻⁴

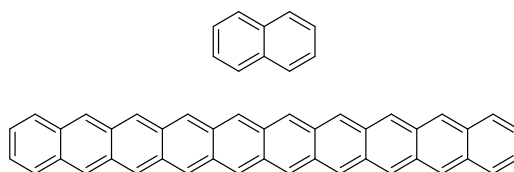


Figure 1.1. Naphthalene and decacene.

The smaller acenes (naphthalene and anthracene) can be extracted from petroleum products whereas, tetracene and larger acenes must be synthesized.⁵ However, due to the decreased solubility and increased reactivity, hexacene remained the longest “true” acene from 1930 to 2006.⁶ At which point, there was a successful synthetic approach to hexacene and longer acenes, which employs the Strating–Zwanenburg photodecarbonylation reaction.^{3,4,7,8} In general, these compounds must be generated either in an inert matrix (argon or PMMA) or on surfaces at very low temperatures (5-30 K) due to the inherent reactivity either through dimerization or photooxidation.²⁻⁴ Mondal, Shah, and Neckers first reported the synthesis of

heptacene (**1**) more than a decade (2006) ago.⁴ It was prepared through a Diels-Alder reaction between 2,3-dibromonaphthalene (**2**) and bicyclo[2.2.2]oct-2,3,5,6,7-pentaene (**3**), followed by subsequent aromatization to obtain **5**. The bridge alkene was then oxidized by OsO₄ (**6**) followed by a Swern oxidation to arrive at the diketone heptacene precursor **7** at an 18% yield for these five steps. The heptacene precursor then underwent Strating-Zwanenburg photodecarbonylation in a PMMA matrix to obtain heptacene, **1** (Figure 1.2).⁴

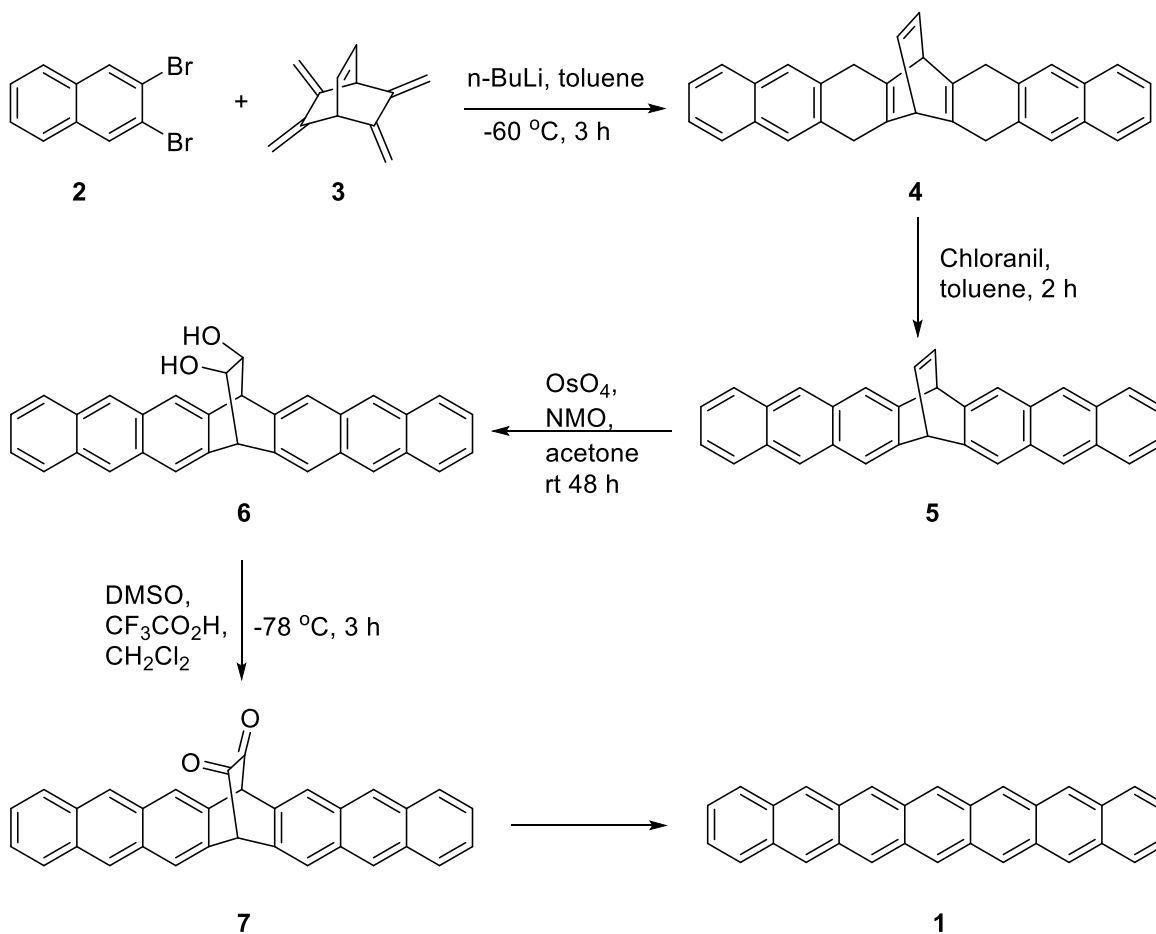


Figure 1.2. Synthetic route to heptacene (**1**).

As with pentacene and hexacene to this point, the heptacene immediately reacts with air to form oxygen adducts in solution (Figure 1.3, **8**).^{4,9} However, even in a PMMA matrix, heptacene has a half-life of 4 h.⁴ In addition to oxygen adducts, these longer acenes can undergo dimerization (Figure 1.4, **9**).^{5,7,10,11}

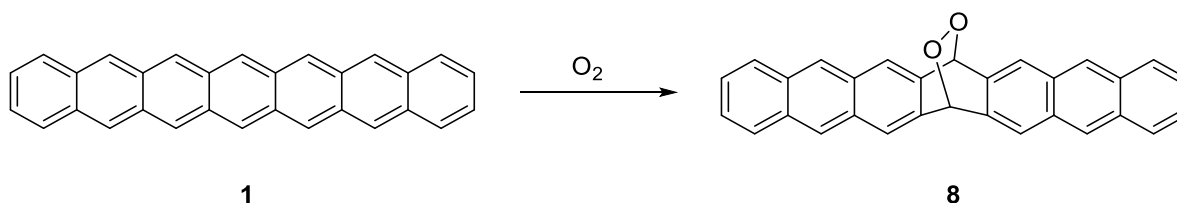


Figure 1.3. Formation of the endoperoxide **8** in the presence of oxygen.

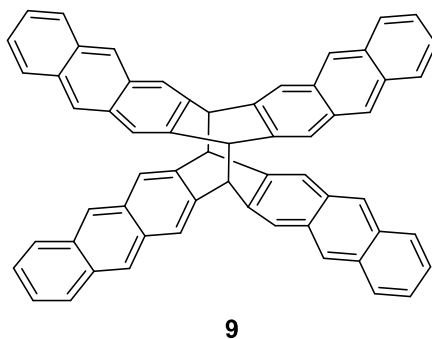


Figure 1.4. Heptacene dimer **9**.

This class of compounds has become of interest as they possess a variety of enticing electronic and optical characteristics that are expected to scale with size.^{12,13} These characteristics include an increase in charge-carrier mobility, decrease in HOMO-LUMO gap, and decrease in optical band gap.^{12,13} As a result, a number of acenes and their derivatives have

already been investigated for use in a variety of organic devices including organic light emitting diodes (OLEDs), organic field effect transistors (OFETs), photovoltaic cells, and biosensors, among others.^{5,14,15} For example, pentacene has been investigated for use in thin-film transistors and photovoltaic cells.¹⁶⁻¹⁸ Moreover, it has one of the highest charge carrier mobilities of $>1 \text{ cm}^2 \text{ V}^{-1} \text{ s}^{-1}$, utilizing the field effect method.^{18,19} The reactivity of pentacene and larger “true” acenes, however, has made it difficult to benefit from their scaling properties (e.g., decreased HOMO-LUMO gap). This issue coupled with the need to synthesize the larger acenes by means of complex multiple step reactions and in matrices, have made them not only difficult to study, but also unrealistic for use in large scale material production.

The reactivity and synthetic shortcomings of acenes, however, can be overcome to a certain extent through the addition of substituents to the acene backbone. These additions can modify or enhance particular properties, such as the stability and/or solubility of the compound.²⁰ A number of substituents including aryl, fluoro-, thio-, and silylethynyl groups have been added to the acene backbone to demonstrate this trend (Figure 1.5).²⁰⁻²³

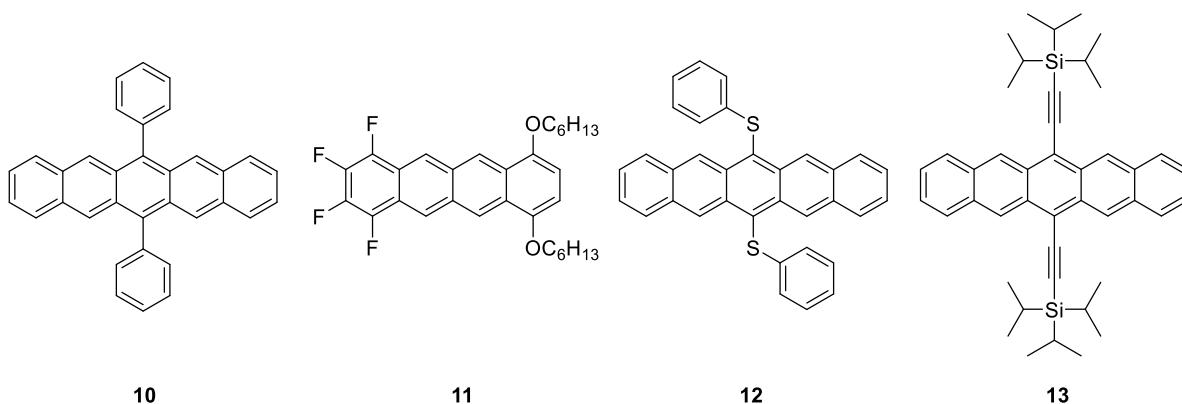


Figure. 1.5. Substituted pentacene derivatives.

Improvement of the stability and solubility allows for the utilization of the electronic trends and offsets some of the reactivity of these compounds. For example, the addition of trisopropylsilylethynyl groups (TIPS, **13**) at the 6 and 13 positions leads to a 50-fold enhancement in stability in solution than the unsubstituted pentacene.²⁴ However, the placement of the substituents along the acene backbone can play a large role in the susceptibility to photooxidation, with the most stable species being substituted at the central ring.^{7,20,25}

Twisted Acenes

As mentioned previously, the addition of strategically placed substituents along the acene backbone not only offers improved stability and solubility, but can produce another remarkable property, distortion from planarity.²⁶⁻²⁸ This distortion most commonly occurs along the horizontal axis due to the steric congestion that arises between bulky substituents along the acene backbone, giving rise to a helical twist reminiscent of helicenes (Figure 1.6).

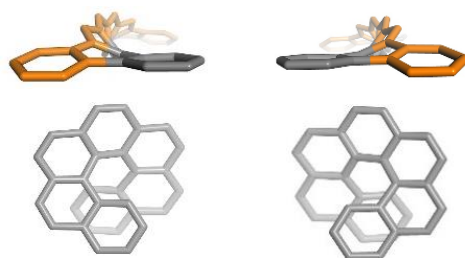


Figure 1.6. Comparison 9,10,11,12,21,22,23,24-octaphenyltetraabenzoc[*a,c,n,p*]-hexacene and heptahelicene.

For our purposes, the twist is reported as the largest end-to-end twist represented either by dihedral angle ABCD or BADC (Figure 1.7).

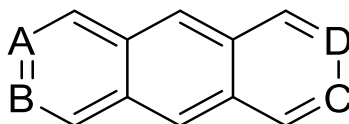
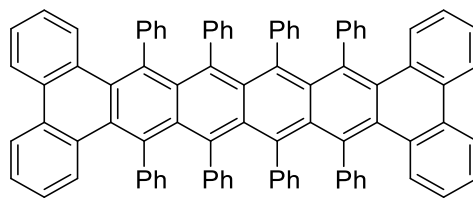


Figure 1.7. Dihedral angle (ABCD or BADC) used to determine the end-to-end twist of the molecule.

By fusing benzo, pyrene, or phenanthrene groups to the acene core, we deviate from the classical definition of acenes. However, for simplicity, we will refer to both substituted and benzannulated acenes as longitudinally twisted acenes (LTAs) or more commonly known as twistacenes. They will be named in the same manner as acenes (by the longest chain of linearly fused benzene rings). A modular approach to the design and synthesis of LTAs can be employed in which the fusion of pyrene, phenanthrene, or acenaphthene groups to the acene

core can be thought of as caps. Additionally, the acene core itself can be substituted. Thus, LTAs can vary not only in length, but in substituents and substitution pattern as well. Consequently, they span a broad array of degrees of twist with the most twisted LTA reported to date being hexacene **14** with an overall twist of 183° (Figures 1.8 and 1.9).²⁹



14

Figure 1.8. Structure of 9,10,11,12,21,22,23,24-octaphenyltetraabenzohexacene (**14**).

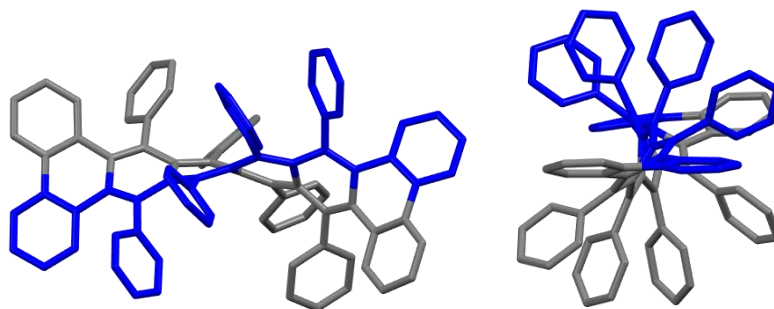


Figure 1.9. X-ray crystal structure of hexacene **14** illustrating the 183° twist along the acene backbone.

The twist of these compounds is not only affected by the steric repulsion between aryl hydrogens, but is also impacted by crystal packing forces. In fact, less than 5 kcal/mol energy can be the difference between a planar compound and an LTA with a twist greater than 20° .^{26,30}

For example, the planar structure of rubrene (**15**) was calculated (at the B3LYP/6-31g(d) level of theory) to lie 3.8 kcal/mol above the twisted minimum (calculated twist of 44°).³⁰ Thus, the well-known planar structure of rubrene is most likely the result of crystal packing forces (Figure 1.10).

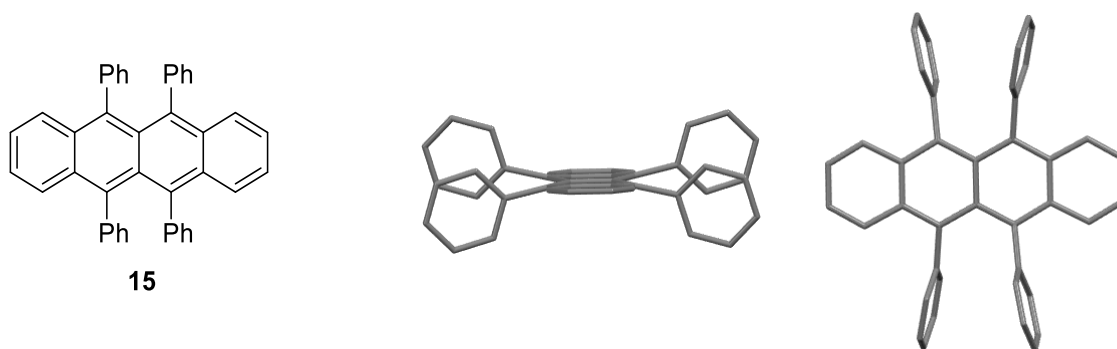


Figure 1.10. Structure of rubrene (**15**) next to its x-ray crystal structure displaying the planar acene core.³¹

Paraskar *et. al.* proposed further confirmation of the non-planarity of **15** in solution based on the differences observed in the field-effect mobility between single crystals and thin films.³⁰ Despite the fact that minimal energy is required to distort LTAs out of plane, the overall twist is an intrinsic property of these compounds.^{25,32-34} Due to the considerable variety of LTAs and minimal energy required to distort these compounds out of plane, only a select number of highly twisted, purely hydrocarbon twistacenes will be highlighted here in this chapter.

Anthracenes and Tetracenes

For two simple systems, hexaphenylbenzene and octaphenylnaphthalene, they are planar in the solid state as determined by x-ray crystallography even though the latter is predicted to have a twist of 31° (as determined at the AM1 level of theory).³⁵ When one extends the system to anthracene, decaphenylanthracene, **16**, possesses an overall twist of 63° (Figure 1.11).³⁵ Furthermore, benzannulation often results in additional distortion. This is observed for 9,18-diphenyltetrabenz[*a,c,h,j*]anthracene, **17**. Compound **17** has an end-to-end twist of 66° just slightly more twisted than the fully phenylated **16**.³⁶ Other twisted anthracenes include compounds **18**, **19**, and **20**, which possess end-to-end twists of 60° , 57° , and 40° , respectively.³⁷

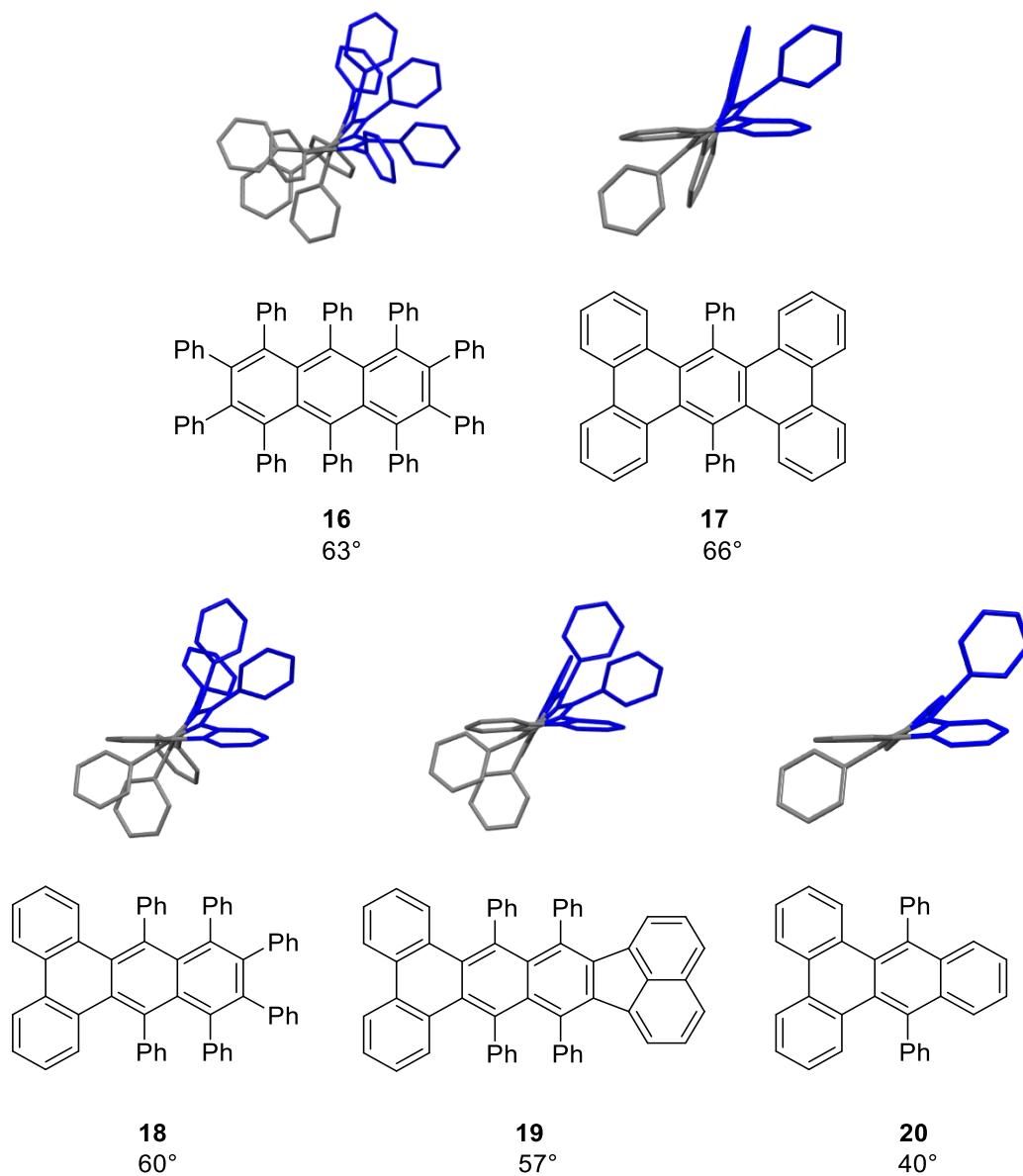


Figure 1.11. Effects of substitution pattern on the end-to end twist of anthracenes along with their x-ray crystal structure displaying the overall twist.

Not surprisingly, variation of the substitution pattern, the end caps, or the length of acene core affects the overall twist. For example, when comparing the anthracene **18** to the tetracene analogue, octaphenyldibenzo[*a,c*]naphthacene (**21**), a 45° increase in twist was

observed. The latter was the first LTA to have an overall twist greater than 100° . It was followed by the benzannulated tetracene **22** almost a decade later (Figure 1.12). Surprisingly, both **21** and **22** have end-to-end twists of 105° .^{38,39} More recently, the fully phenylated dodecaphenyltetracene (**23**) has been successfully synthesized. As observed in the anthracene series, the fully phenylated derivative is less twisted than the pyrene capped derivative, 97° versus 105° , respectively.⁴⁰

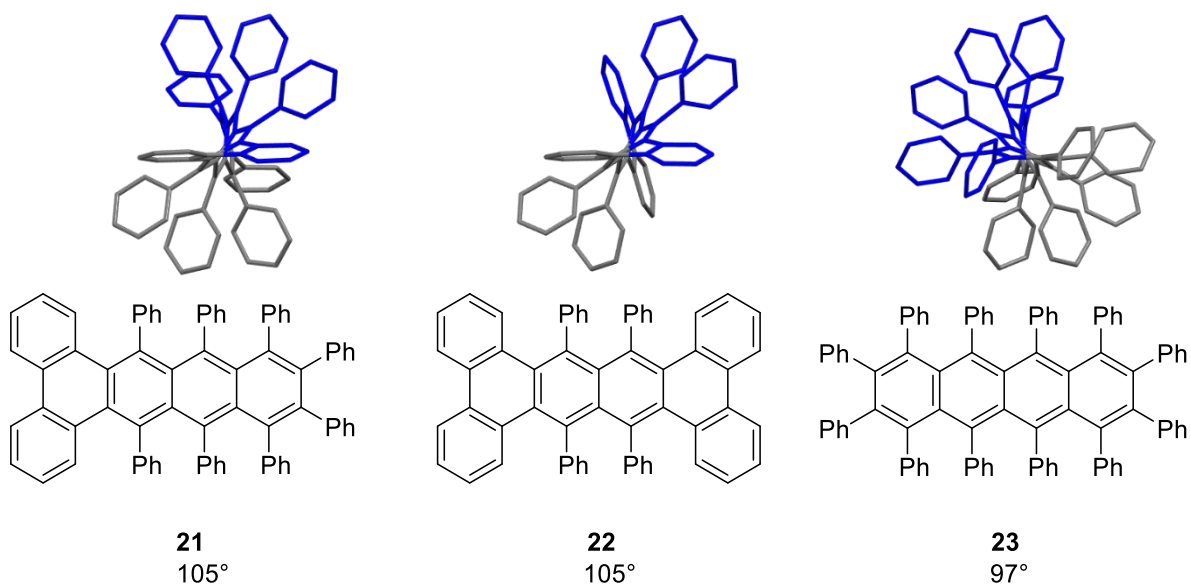


Figure 1.12. Structures of highly twisted tetracenes along with the x-ray crystal structure illustrating the overall twist.

Pentacene and Larger LTAs

While it was generally thought that extension of the core leads to more highly twisted acenes, it is not always the case. The choice of substitution pattern and benzannulation has a

large effect on the overall twist. LTAs **24-26** exhibit a center of inversion, and as a result, have a net twist of 0° (Figure 1.13).^{25,27,34} For **24**, theoretical studies at the B3LYP/6-31g(d) level of theory revealed the 0° net twist for C_{2h} structure. It lies 3 kcal/mol above the calculated D_2 twisted ground, which was predicted to possess a 92° end-to-end twist.³⁴ This discrepancy between the theoretical and experimental results most likely arises due to crystal packing forces. Furthermore, **24** is air and light sensitive in solution rapidly forming endoperoxide **27** within an hour.³⁴ It has been proposed that the accessibility of the central aromatic ring (unsubstituted) is directly related to its sensitivity as shown previously.^{20,25} When the central ring is substituted, the molecules become more stable as in **26**, and no photooxidation nor dimerization is observed. Surprisingly, this reactivity at the central ring for **25** is not observed in solution even though it exhibits the same solid state structure. While researchers have proposed that the phenyl substituents “protect” the central “core”, there is no support of this hypothesis through solid state analysis. Both adjacent phenyl groups are splayed the same in the pyrene and phenanthrene end-capped systems.^{25,34}

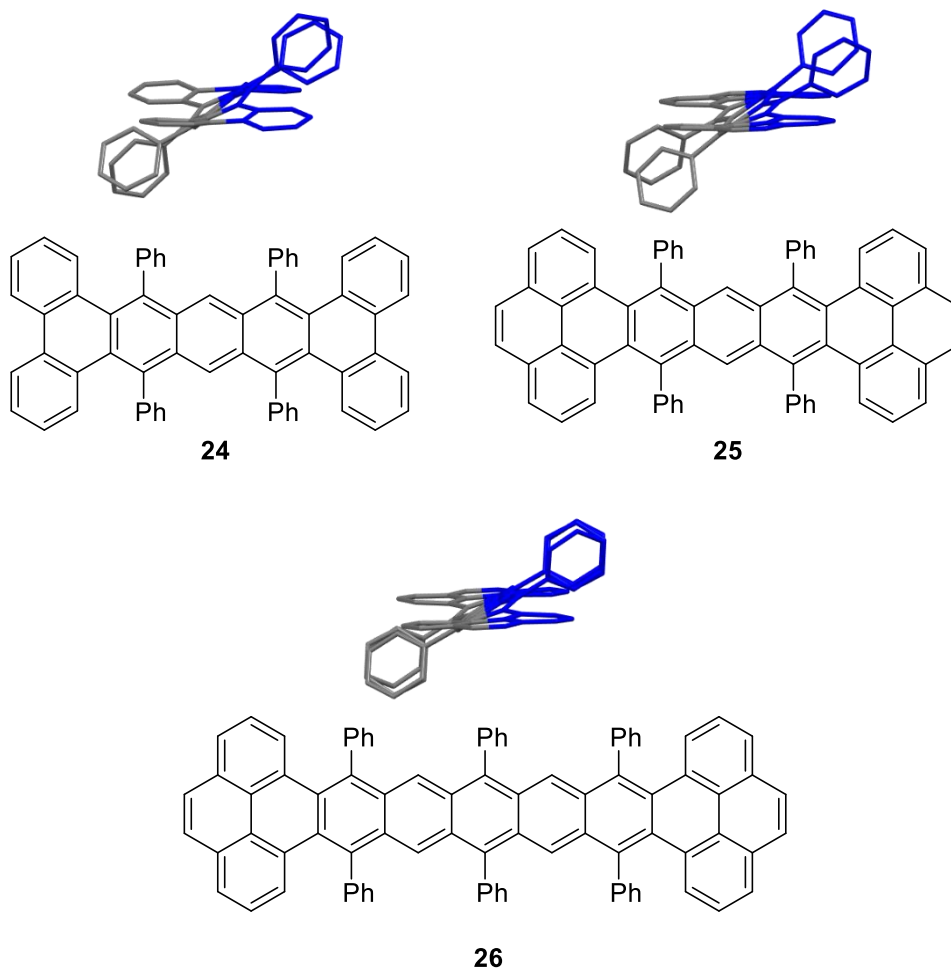


Figure 1.13. LTAs with centers of inversion alongside their x-ray crystal structures.

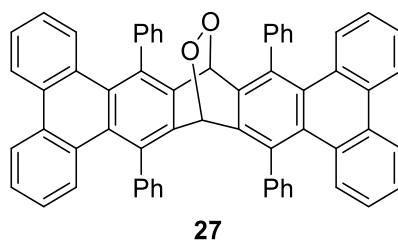


Figure 1.14. Endoperoxide **27** of pentacene **24**.

To the best of our knowledge, the longest “twistacene” to date is dodecatwistacene **28**.⁴¹ This compound does not adopt a twisted conformation in the solid state, but instead the two pentacene units relative to the central pyrene unit are rotated in opposite directions with the pyrene end units lying parallel to one another. As a result, **28** has an overall twist of 0°.⁴¹

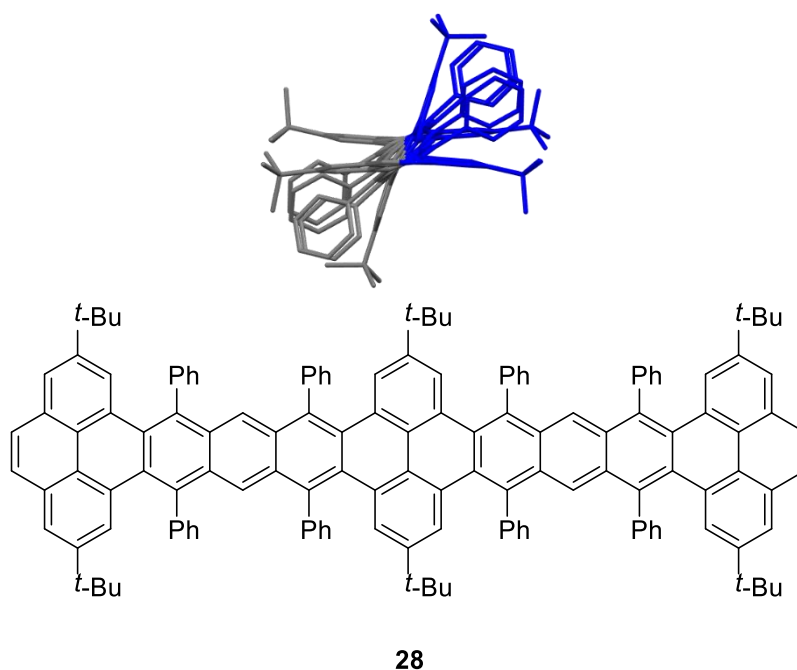


Figure 1.15. Structure of dodecatwistacene **28** in addition to the x-ray crystal structure depicting the net 0° twist.

The presence of pyrene “caps” appears to reduce the overall twist and is probably due to the less flexible nature of these end units as compared to phenanthrene or phenyl groups. Both ends do not need to be pyrene capped in order to see this effect as illustrated in Figure

1.16. The mono-pyrene capped hexacene **29** is twisted 135° , nine degrees less than the diphenanthrene capped pentacene **30**.⁴²

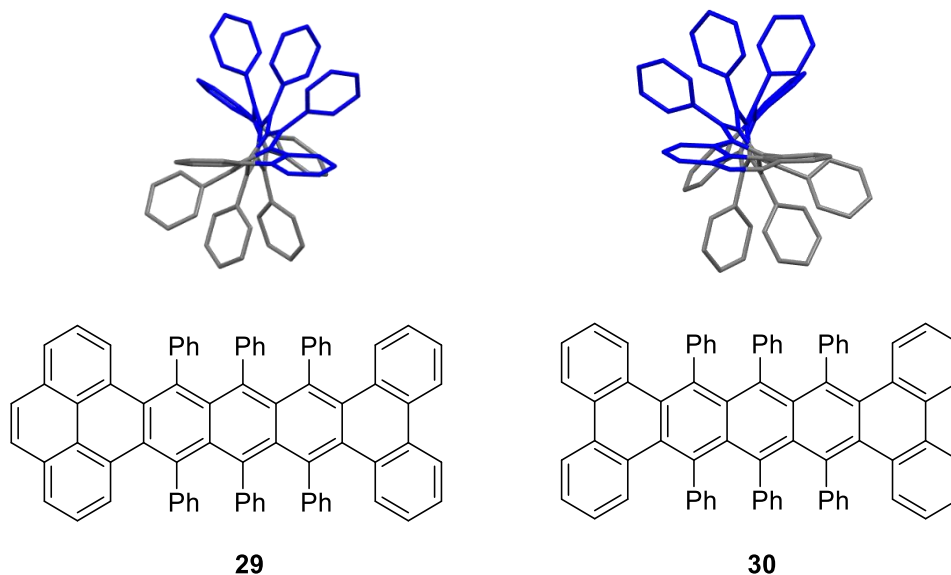


Figure 1.16. Pyrene capped hexacene **29** (135°) compared to phenanthrene capped pentacene **30** (144°).

Thus, in order to obtain even more twisted LTAs, the acene core needs to be fully phenylated and capped with phenanthrene end units. This substitution pattern has led to some of the largest twists reported for anthracene and tetracene derivatives. A similar pattern was observed for the pentacene. In fact, 9,10,11,12,21,22-hexaphenyltetrabenzo[*a,c,l,n*]pentacene (**30**) has a record-setting twist of 144° (Figure 1.16)^{28,43} and held the record from 2004 – 2018. It was expected that the addition of bulkier substituents, such as *m*-xylene **31** and 1-naphthyl **32** units, to pentacene **30** would further distort these compounds (Figure 1.17). Compounds **31**

and **32** have end-to-end twists of 148° and 141° , respectively.⁴² As expected, the *m*-xylene pentacene derivative results in a slightly more twisted structure. However, to our surprise, the 1-naphthyl derivative exhibits a slightly diminished twisted structure.

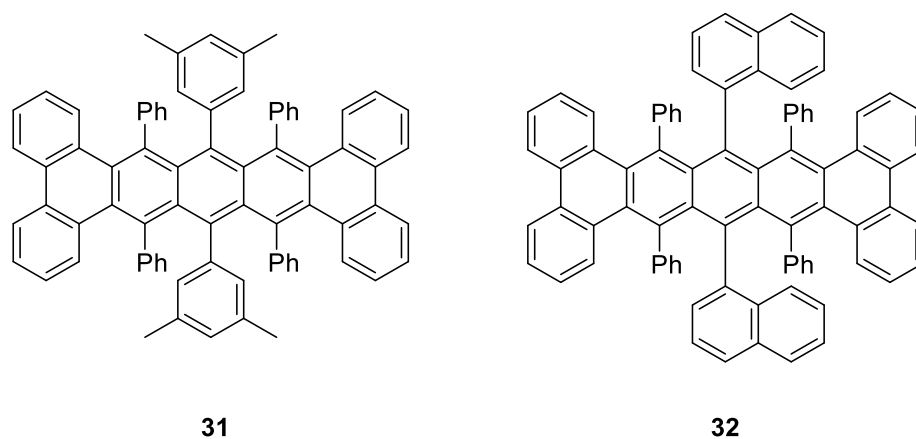
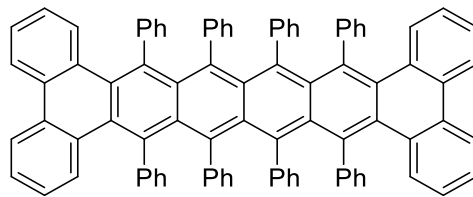


Figure 1.17. *M*-xylene substituted (**31**, 148°) and 1-naphthyl substituted (**32**, 141°) pentacenes.

Since neither of these compounds led to a large increase in the overall twist, Clevenger *et. al.* synthesized hexacene **14**, which was predicted by AM1 to have a twist of 182° .²⁹ The x-ray crystal structure of **14** exhibits a 184° end-to-end twist, in excellent agreement with the calculations, and to the best of our knowledge, represents the most twisted acene reported in the literature to date.²⁹ Based on the success of **14**, heptacene **33** was modelled by AM1 and predicted to be twisted 220° (Figure 1.18).²⁹



33

Figure 1.18. Heptacene **33**.

Synthesis

Several groups have pursued these synthetically challenging, yet aesthetically pleasing, compounds. This endeavor has led to a number of twisted acenes with lengths varying from naphthalene to dodecacene. These compounds are generally synthesized employing one of two approaches either the “benzyne” or “quinone” approach. For years, the synthesis and characterization of LTAs had been localized to the Pascal group.^{26-28,34-38} As such, their “benzyne” approach is the most often applied in the synthesis of these compounds.

Benzyne Approach

The general pathway to LTAs utilizing Pascal’s approach is depicted in Figure 1.19 and is consequently named the “benzyne” approach as it proceeds through a benzyne intermediate. The benzyne intermediate is generated in situ *via* diazotization of anthranilic acid **36**, which in the presence of cyclone **37**, yields 1,2,3,4,5,6,7,8,9,10-decaphenyl-9,10-dihydro-9,10-epoxyanthracene (**38**).³⁵ Cycloadduct **38** is then subsequently deoxygenated with activated Zn dust in refluxing acetic acid to yield **16** (3% yield).³⁵ The x-ray crystal structure

reveals **16** possesses C_2 symmetry in the solid state with an end-to-end twist of 63° and is the most twisted anthracene to date. A couple of examples of twistacenes generated from this approach are pictured along with their overall twist in Figure 1.20.³⁴⁻³⁸

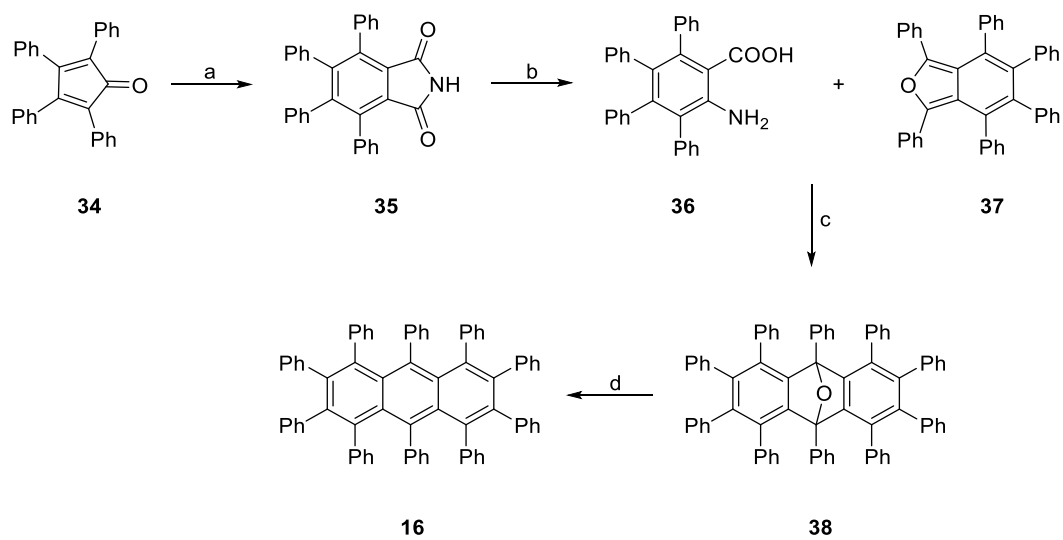


Figure 1.19. Pascal's decaphenylanthracene (**16**) synthesis.³⁴ (a) maleimide, nitrobenzene, reflux, 12 h, 69%; (b) i. NaOH, NaOCl, reflux, 10 min, ii. propanol, KOH, reflux 45 h, 61% (steps i and ii); (c) isoamyl nitrite, reflux, 10 min, 8%; (d) Zn, CH₃COOH, reflux, 9 h, 3%.

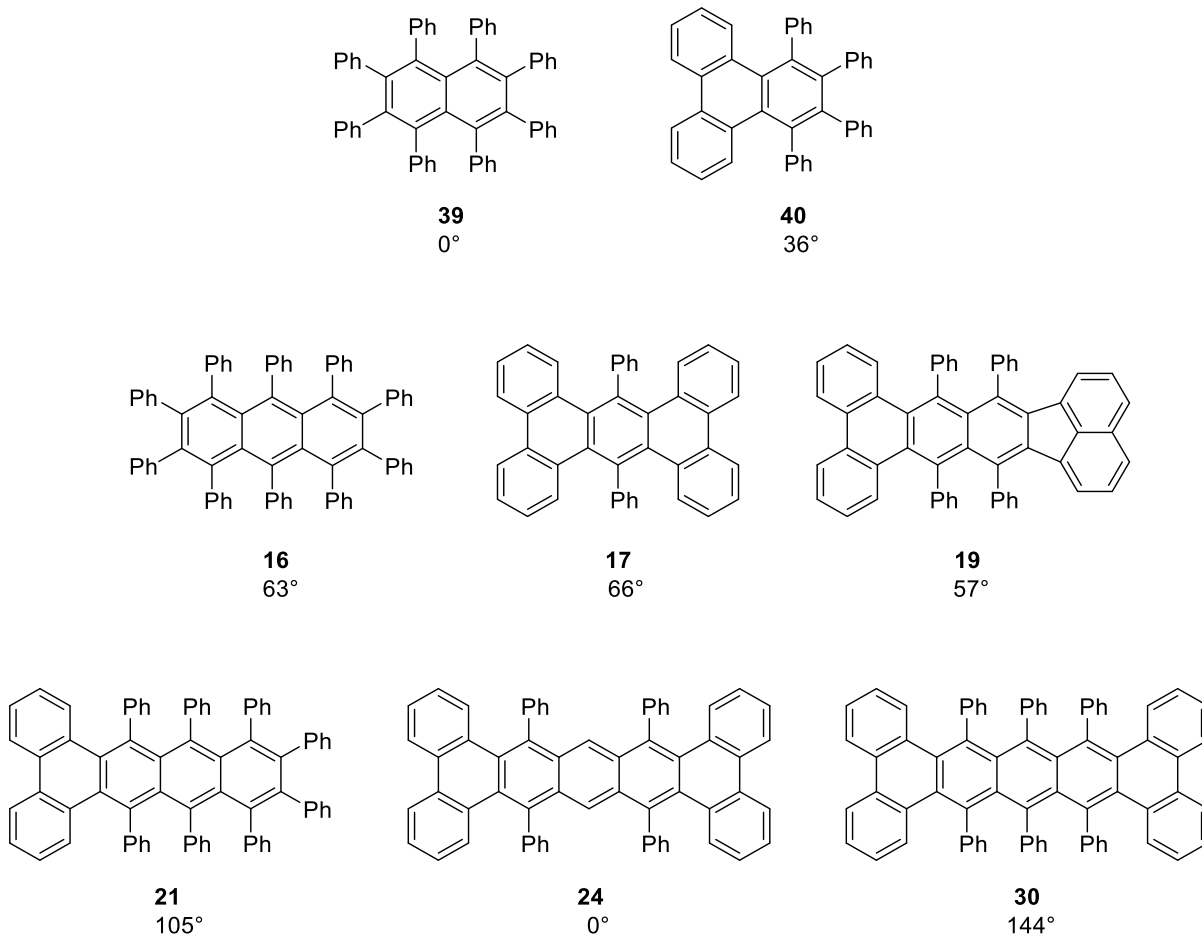


Figure 1.20. LTAs generated from the benzyne approach.

While successful, this approach is not without its limitations. The highly congested furan precursors inhibit the cycloaddition reaction with the aryne reducing yields.^{35,38,40} Steric bulk also affect the efficiency at which the epoxide is deoxygenated further decreasing overall yields and in the case of tetradecaphenylpentacene (**41**) has thus far proven unsuccessful.^{35,38}

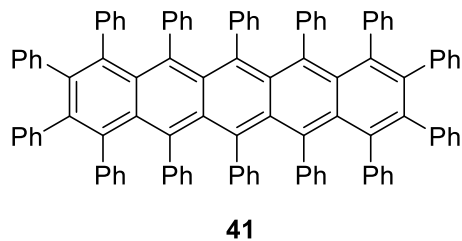


Figure 1.21. Fully phenylated pentacene **41**.

Quinone Approach

In comparison to Pascal's "benzyne" approach, our group utilizes what we have dubbed the "quinone" approach. The general pathway to LTAs is illustrated in Figure 1.22. *p*-Benzoquinone (**43**) is reacted with two equivalents of tetracyclone **42** to generate the quinone precursor **44**. Anthraquinone **44** was treated with phenyllithium to yield a diol intermediate **45**. Subsequent reduction of the diol intermediate with SnCl₂ yields decaphenylanthracene (**16**) in 52% yield.⁴⁴ As a result of this route, a significant improvement in the percent yield and a reduction in the number of steps required have been achieved when compared to Pascal's approach.⁴⁴

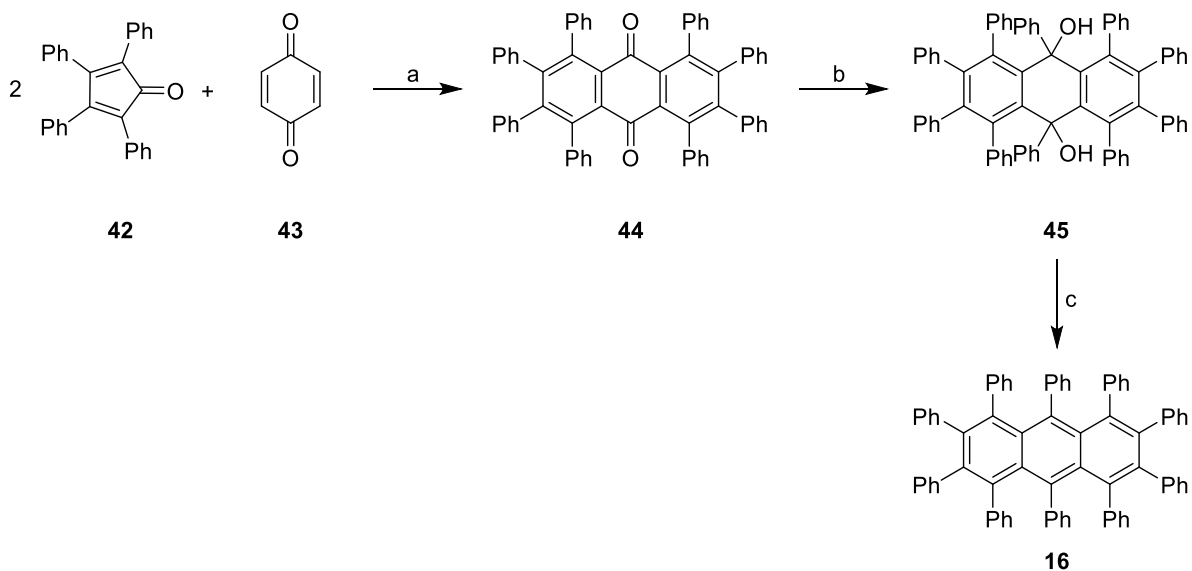


Figure 1.22. Kilway's decaphenylanthracene (**16**) synthesis.⁴³ (a) nitrobenzene, reflux, 23 h, 10%; (b) phenyllithium, benzene, rt, 17 h; (c) anhyd SnCl₂, HCl, THF, reflux, 1 h, 52% (steps b and c).

Furthermore, this method allows for variation of the position and type of substituent along the acene backbone, as well as, the addition of “caps”, such as phenanthrene or pyrene, to be placed at the ends. In addition, this strategy can be applied to an array of acene lengths. Utilizing this method, a library of well over 100 twisted acenes, both symmetrical and asymmetrical, with varying degrees of twist and length, have been synthesized including the most twisted acene to date with an overall twist of 184° (Figures 1.8 and 1.23).^{29,42,45}

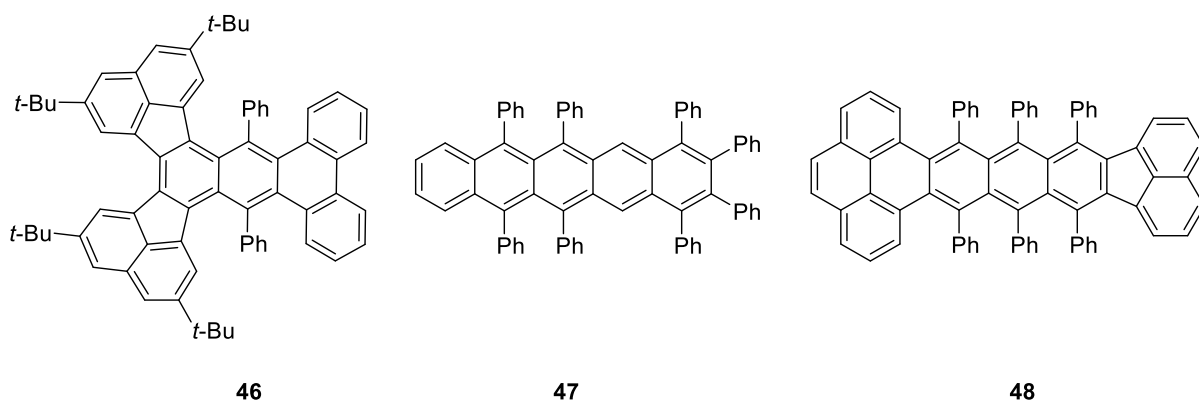


Figure 1.23. LTAs generated utilizing the “quinone” approach.

Chirality and Configurational Stability

Due to the adopted helical twist of these compounds, they exhibit conformational chirality, analogous to helicenes and binaphthyls. As such, they are designated as either *M* (minus) for a counterclockwise twist or *P* (plus) for a clockwise twist depending on the direction of the helical twist (Figure 1.24).⁴⁶ While these compounds are chiral, configurational stability has remained elusive. It is expected that these compounds racemize *via* multiple, shallow, nonplanar transition states and thus rapidly undergo racemization at room temperature making most LTAs nearly impossible to resolve.⁴⁴ By comparison, helicenes generally racemize through a single, high energy transition state and as a result have excellent configurational stability.^{47,48}

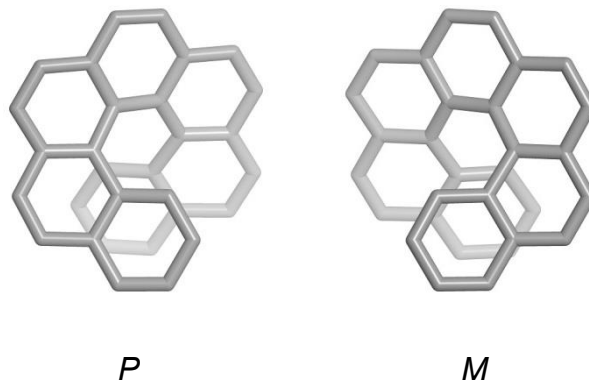
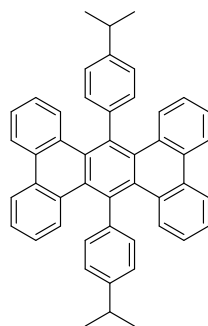


Figure 1.24. Designation of *P* (plus) and *M* (minus) enantiomer based on the conformational orientation.

Variable Temperature NMR Spectroscopy

In attempt to identify potentially configurationally stable LTAs prior to separation, variable-temperature nuclear magnetic resonance spectroscopy (VT NMR) has been employed on isopropyl LTA derivatives. Since these compounds are helically twisted, the methyl groups of the isopropyl substituent are diastereotopic, and consequently two sets of doublets should be observed in the ^1H NMR spectra. With increasing temperature, rapid interconversion occurs, and coalescence of the two doublets would be observed at which point the Gutowsky-Holm approximation can be employed to determine the barrier to enantiomerization. Utilizing this approach, the barrier for Pascal's 9,18-bis(4-isopropylphenyl)tetrabenz[*a,c,h,j*]anthracene (**49**) (Figure 1.25) was determined to be 16.7 kcal/mol, which is in good agreement with the B3LYP/6-31g(d) calculated barrier (18.2 kcal/mol).^{36,44} Although racemization was observable on the NMR time scale, the barrier was too low to allow for resolution at room temperature.



49

Figure 1.25. Pascal's isopropyl anthracene derivative **49**.

While VT NMR spectroscopy of compounds **50** and **51** was employed to determine this energy, these attempts proved to be unsuccessful over a 293-408 K temperature range. Instead, a minimum value of $\Delta G_{\text{rac}} \geq 24$ kcal/mol was determined for these compounds (Figure 1.26).⁴⁹ It was surprising that racemization of **50** was not observed considering its structural similarity and overall end-to-end twist in comparison to **49**. Whereas compound **51** is a much larger, more twisted LTA (126°), which one would expect to impart some configurational stability. These barriers should permit at least partial resolution at room temperature.

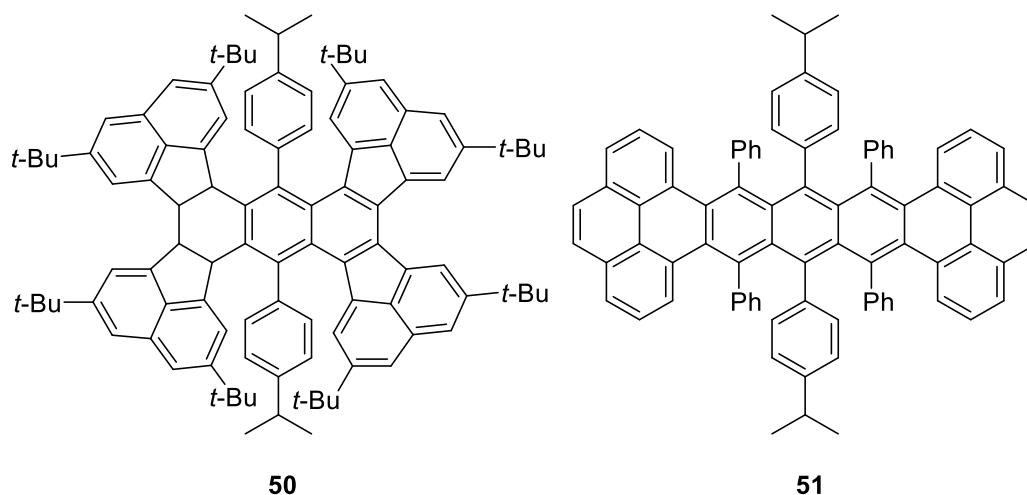


Figure 1.26. Miller's isopropyl substituted LTA derivatives **50** and **51**.

Chiral Resolution

Another method to determine the barriers to racemization is chiral resolution. This technique utilizes HPLC or SCF chromatography combined with a polysaccharide chiral stationary phase (CSP). The combination of HPLC with a polysaccharide CSP has led to the resolution of two closely related twisted pentacenes, 9,10,11,20,21,22-hexaphenyltetrabenzobenzopentacene (**30**) and 9,11,20,22-tetraphenyl-10,21di(p-tolyl)tetrabenzobenzopentacene (**52**) (Figure 1.27). They have barriers to racemization of 23.8 and 24 kcal/mol, respectively as determined by the monitoring the decay of the specific rotation.⁴³ This is an excellent agreement with the AM1 calculations in which **30** was found to proceed through a C_{2h} intermediate by means of a C_1 transition state which lies 23.0 kcal/mol above the D_2 ground state.⁴³ While AM1 indicated C_{2h} was a transition state, calculations at the B3LYP/6-31g(d) level revealed C_{2h} to be a shallow, second transition state connecting enantiomeric C_2 intermediates. At this level, ΔG_{rac} is calculated to be 33.2 kcal/mol,

significantly higher than the experimentally determined barrier to racemization (23.8 kcal/mol).⁴⁴

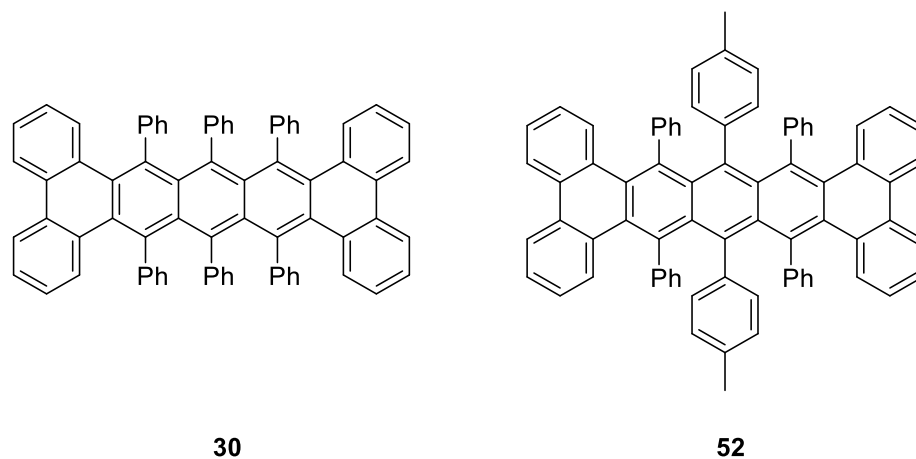


Figure 1.27. Successfully resolved pentacene derivatives **30** and **52**.

Pentacene **30** is highly twisted with an end-to-end twist of 144° and a specific rotation of $[\alpha]_D^{25} = +7400^\circ$, but only has a half-life of ~ 9 h.⁴³ These short half-lives not only make them difficult to study, but impractical for material applications. While the ΔG_{rac} is comparable to [5]helicene, the specific rotation is substantially larger. In fact it is more in line with [9]helicene (-7500) and among the largest specific rotation reported.^{49,50}

Table 1.1 Comparison of experimental and calculated ΔG_{rac} for LTAs and helicenes.

Compound	Experimental $\Delta G_{\text{rac}}^{\text{a}}$ (kcal/mol)	AM1 ΔG_{rac} (kcal/mol)	DFT ΔG_{rac} (kcal/mol)	$[\alpha]_{\text{D}}^{25}$
Anthracene 49	16.7 ³⁶	n/d	18.2	nd
[5]helicene	22.9 ⁵¹	22.9 ⁴⁷	25.65 ^{b,47}	-1670 ^{d,50}
Pentacene 30	23.8 ⁴³	23.0 ⁴³	33.2 ^{c,44}	+7400 ⁴³
[6]helicene	35.0 ⁵¹	31.4 ⁴⁷	38.16 ^{b,47}	3750 ⁵²
[9]helicene	41.7 ⁵¹	34.0 ⁴⁷	39.72 ^{b,47}	-7500 ⁵²

^aExperimental results. ^bB3LYP/3-21G. ^cB3LYP/6-31g(d). ^d26 °C, 578 nm. nd =not determined

Based on the successful resolution of **30**, it was thought that the pursuit of longer LTAs could be a route to configurational stability in these compounds. However, at this time, attempts to resolve hexacene **14** has proven unsuccessful. Therefore, alternative routes to enantiopure LTAs have been investigated.

Twist Bias

Pascal *et. al.* incorporated naphthyl substituents in a dissymmetric manner along the acene backbone in attempt to achieve configurational stability (Figure 1.28, **53**).⁵³ The naphthyl groups are essentially “frozen” in space due to the sterically crowded environment and inhibit the interconversion of enantiomers. Nevertheless, rapid inversion of the acene backbone still occurs. For the *cis* isomer, this inversion results in enantiomers. However, for the *trans* isomer, this gives rise to the interconversion of diastereomers of unequal energies imposing an energetically favored twist bias and thus “configurational stability.” Pascal demonstrated the success of this approach with 2,3-bis(1-naphthyl)-1,4-diphenyltriphenylene

(**53**), which has a calculated end-to end twist of 32° (B3LYP/6-31g(d)) and a specific rotation of $[\alpha]_{25D}$ of +320 and -330 for the *P* and *M* enantiomers, respectively.⁵³

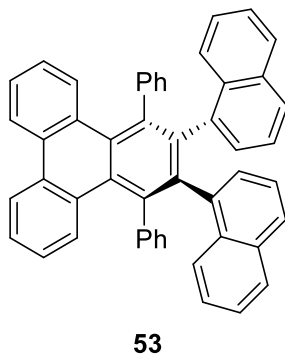
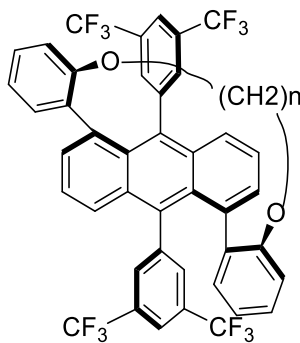


Figure 1.28. A route to configurationally stable LTAs through naphthyl substituted naphthalene **53**.

Alternative Routes to Configurationally Stable LTAs

Another approach to obtain enantiopure LTAs is by means of an ether “tether,” similar to the linkages in cyclophanes, connecting the 1 and 5 positions of a phenyl substituted anthracene (Figure 1.29, **54**).^{54,55} Covalently linking the ends of the twistacene restricts the backbone interconversion yielding stable *M* and *P* enantiomers. Unlike non-tethered LTAs, no noticeable conversion after prolonged heating was observed.^{36,54} In addition, the length of the “tether” can be modified to control the twist of the acene with overall twists between 23° and 38° obtained for $(\text{CH}_2)_6$ through $(\text{CH}_2)_3$ linkages, respectively.⁵⁴ Due to the configurational stability, the effect of twist on the optical and electronic properties could be systematically evaluated. A decrease in fluorescence quantum efficiency and optical band gap was found as

the end-to-end twist increases.^{54,55} Moreover, the tethered anthracene displays a bathochromic shift with the shortening of the ether linkage.^{54,55}



54

Figure 1.29. Controlled anthracene LTA through the use of an ether tether.

Prospective Applications

In order to take advantage of the improved stability of these twisted acenes for the aforementioned applications, they must retain the electronic and optical properties of the parent acene without exhibiting large variations from a change from planarity. A theoretical study at the B3LYP/6-31g(d) level correlating the changes in the HOMO-LUMO gap with the degree of twist for unsubstituted acenes has shown that the HOMO-LUMO gap for this series of acenes (tetracene through heptacene) remains relatively constant regardless of the degree of twist and decreases only slightly for anthracene.⁵⁸ Based on this study, the extent of the twist, especially in the larger acenes, has little effect on the electronic properties. Similar results have been attained with UV-vis spectroscopy and cyclic voltammetry.^{25,30,54}

Further confirmation of this principle can be seen with 6,8,15,17-tetraphenyl-1,18,4,5,9,10,13,14-tetrabenzoheptacene (Figure 1.13, **25**).²⁵ This compound orients itself in such a manner that the pyrene units align in the same plane in the solid state, resulting in an overall twist of 20.6°.^{25,33} The planarity of the pyrene units could allow for better stacking and π orbital overlap. With that being said, the twisted core prevents close π - π stacking and as such may alleviate aggregation issues that are common among their planar counterparts.

LTAs presumably interact through weak intramolecular forces, which are generally required for LEDs, making these compounds promising candidates for such applications.³⁰ This compound has been successfully employed as a dopant in combination with blue polyfluorene to construct a white light emitting diode (LED) with good luminescence efficiency and a low turn on voltage.^{25,33} Furthermore, these devices displayed limited emission color variation with change in voltage.

In contrast, Li *et al.* demonstrated the potential for near-planar LTAs to form strong intermolecular π - π stacking in the solid state.⁵⁶⁻⁵⁸ As mentioned previously, the twisted acene core generally prevents such strong π - π stacking interactions. This is further demonstrated with the highly twisted heptacene (Figure 1.30, **55**). Compound **55** exhibits an overall twist of 131° in the solid state and a hole mobility of $4.5 \times 10^{-4} \text{ cm}^2 \text{ V}^{-1} \text{ s}^{-1}$ after thermal annealing utilizing the space charge limited current (SCLC) method.⁵⁷ However, when examining the nearly planar (predicted B3LYP/6-31g(d) end-to-end twist of $\sim 2^\circ$) naphthalene derivative **56** after thermal annealing, Li *et al.* reported one of the highest SCLC hole mobilities for thin film semiconductors.⁵⁶

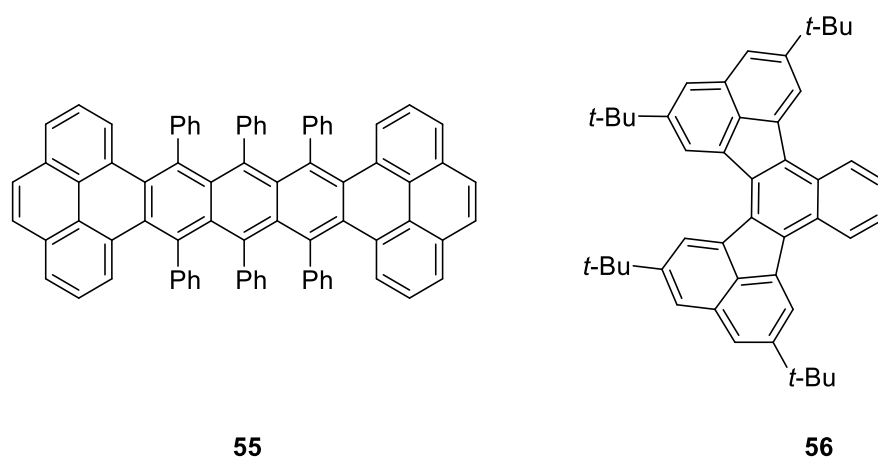


Figure 1.30. Structures of heptacene **55** and naphthalene **56**.

Summary

A diverse assortment of LTAs, varying in both length and end-to-end twist, have been synthesized including the most twisted LTA to date. While record setting, it is evident that simple expansion of the acene backbone will not necessarily result in an increased overall twist. However, strategic substitution and/or benzannulation can aid in the enhancing the overall twist. The substitution and resulting twist protect the highly reactive sites on the acene core while limiting the extent of π - π stacking. Thus, LTAs address a number of drawbacks in their planar counterparts, namely photooxidation and dimerization. While these compounds are highly twisted, they retain the electronic and optical properties of their planar counterpart. In addition, a number of routes to configurationally stable LTAs have been successfully demonstrated, facilitating the used of their chiroptical properties. As a result, these compounds have potential applications ranging from solar cells to OLEDs.

Results and Discussion

Prediction of the End-to-End twist of LTAs

Three common theoretical methods are molecular mechanics, and semiempirical and *ab initio* quantum mechanical treatments; each have distinct advantages and disadvantages. Molecular mechanics models the atoms as spheres and the bonds as springs in which classical mechanics can be applied to describe the bending, stretching, and twisting of the atoms.⁵⁹ Additionally, the constants used in this approach are provided by either experimental data or high level *ab initio* calculations. These methods are often employed for large molecules, such as proteins. Semiempirical calculations utilize Hartree-Fock approximations and are parameterized with empirical data to increase the computational efficiency.⁵⁹ On the other hand, *ab initio* methods do not utilize empirical data, but instead are derived from theoretical principles (as a goal to solve the Schrodinger equation).⁵⁹ As such, *ab initio* methods often provide more reliable results, but are quite expensive. For example, the total cpu time for the optimization and frequency calculations of **32** was approximately 9.5 days for DFT compared to 2 min for AM1 using the Lewis cluster.⁶⁰ For this study, semiempirical (AM1) and *ab initio* (DFT) methods were selected based on computing time and accuracy.

Historically, our group has been interested in the synthesis and design of highly twisted acene derivatives. This allure has been due in part to the synthetic challenge these compounds pose, as well as the pursuit of record-breaking LTAs. As such, we were interested in accurately predicting the end-to-end twist observed in LTAs so prospective compounds could be screened prior to synthesis. Therefore, the end-to-end twists were calculated at the AM1 and DFT

(B3LYP/6-31g(d)) levels of theory and compared to those obtained experimentally from the crystal structure (Figures 1.31 and 1.32). The results are listed in Table 1.2.

Semiempirical calculations at the AM1 level resulted in values that align well with the experimentally determined crystal structure values. For example, the calculated end-to-end twist of **14** was determined to be 182° compared to 184° for the crystal structure.²⁹ Similar results were observed for compounds **55** and **32** with differences of 3° and 4° , respectively.⁴² DFT calculations generated similar results, albeit with slightly larger differences (4° , 6° , and 1° , respectively).

When looking at asymmetrically capped LTAs (Figure 1.32), somewhat larger discrepancies were observed with the biggest disparity between experimental found for compound **48** with a difference of 16° . On the other hand, **57** and **29** both differed from the crystal structure by 6° .⁴² As observed in the symmetric molecules, DFT again overestimates the end-to-end twist with differences for 18° , 8° , 11° for **48**, **57**, **29**, respectively. With the exception of **48**, both AM1 and DFT calculations closely reproduced the experimentally observed crystal twist. Pascal *et. al.* reported similar success and trends with AM1 and DFT when investigating **30**, which was not the case for our **48**.²⁸ This difference **48** is attributed to crystal packing forces which were unaccounted for in this theoretical model.

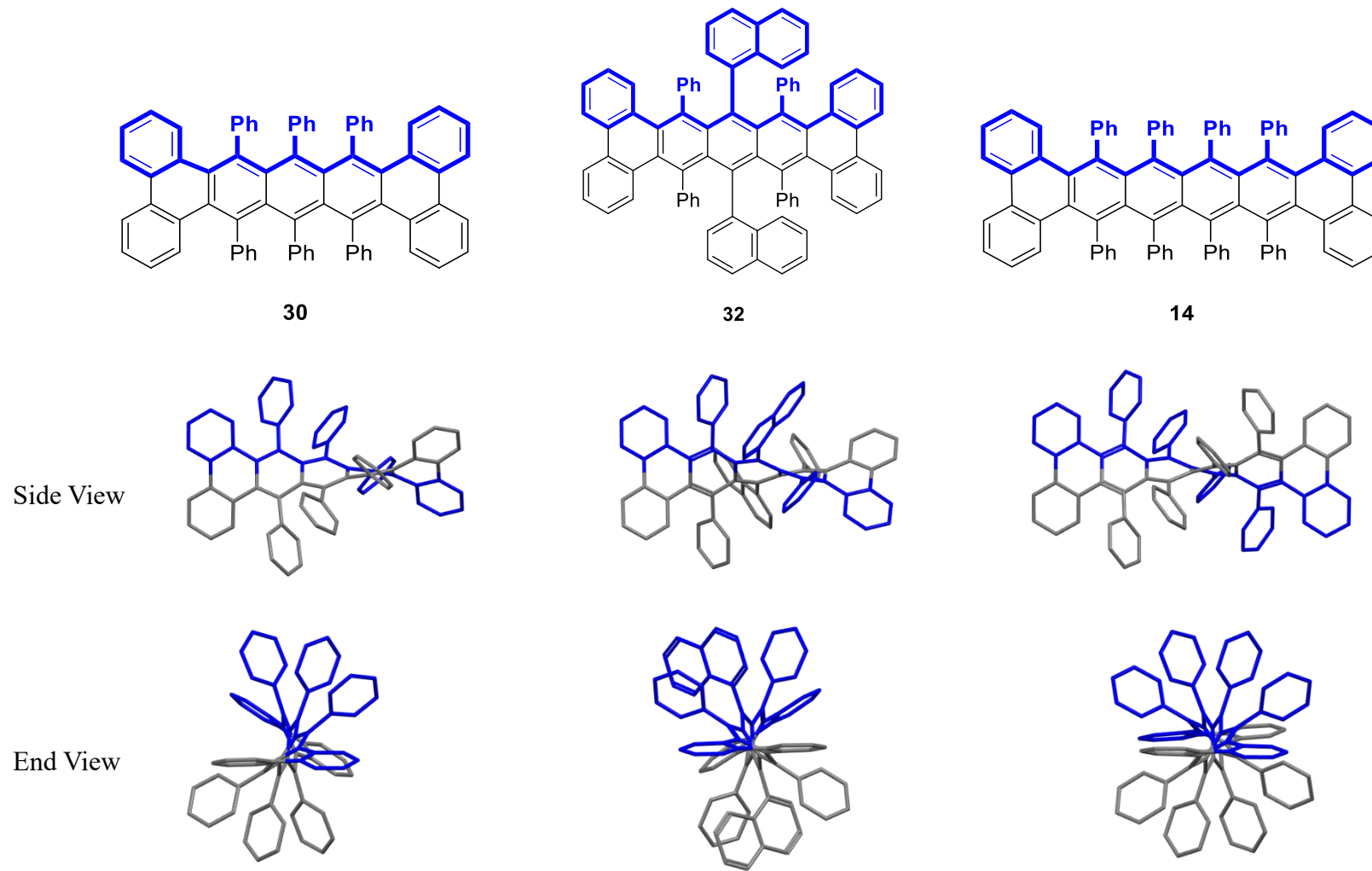
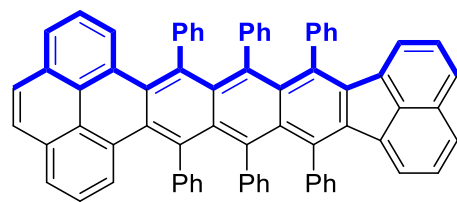
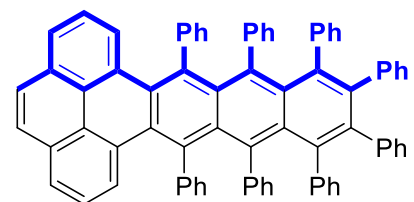


Figure 1.31. DFT B3LYP/6-31g(d) calculated twist of **30**, **32**, and **14**.



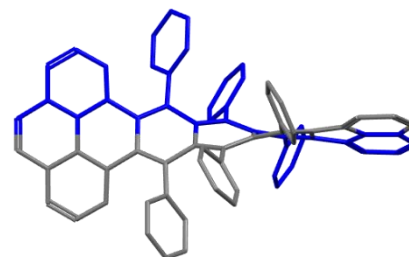
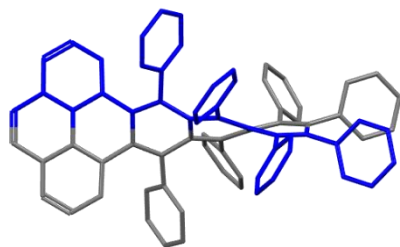
48



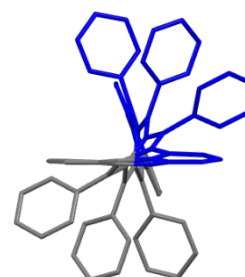
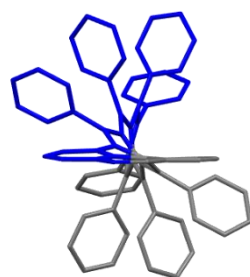
57

35

Side View



End View



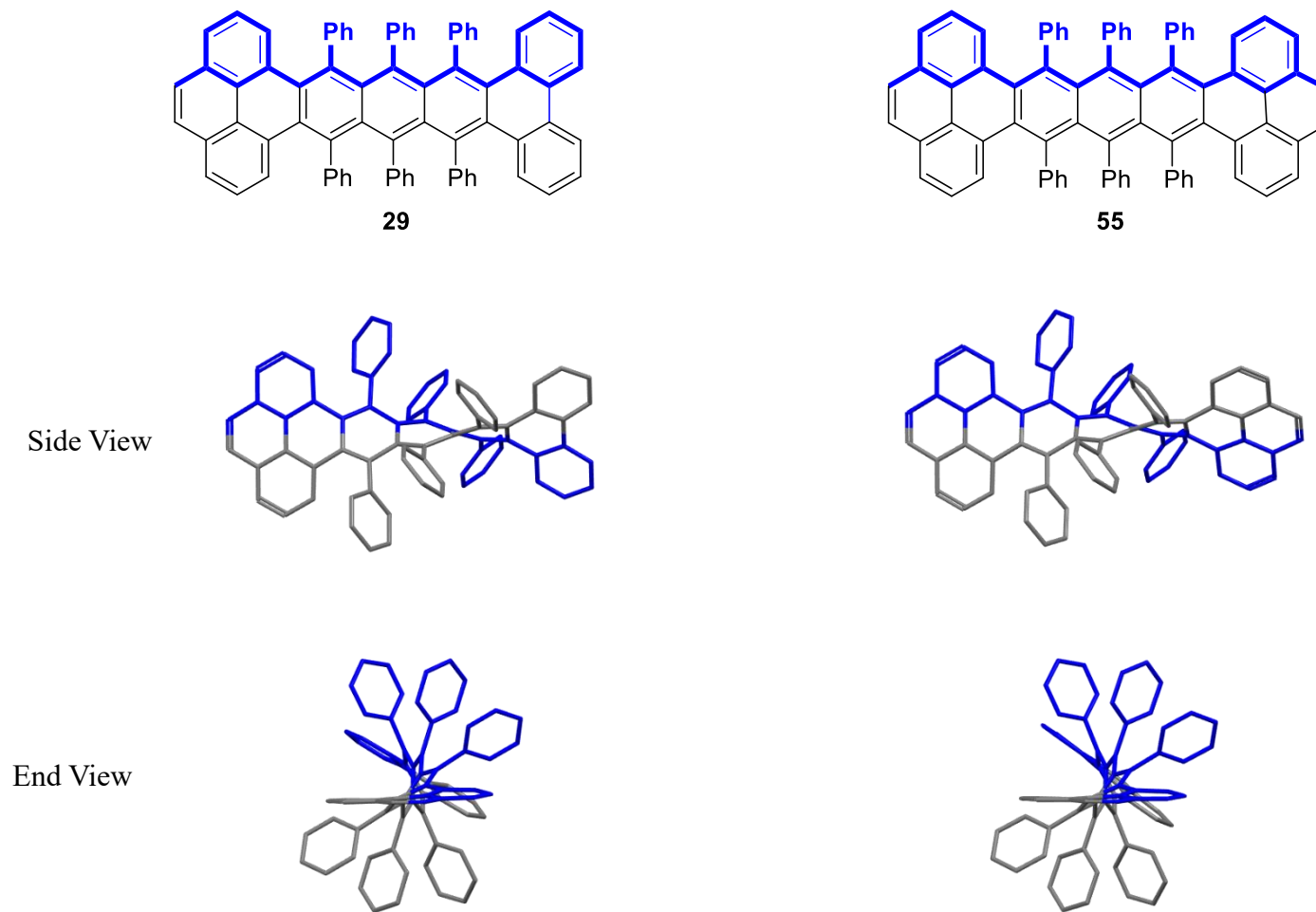


Figure 1.32. DFT B3LYP/6-31g(d) calculated twist of **48**, **57**, **29**, and **55**.

Table 1.2. Comparison of the theoretical and experimental end-to-end twists.

Compound	AM1	DFT/B3LYP6-31g(d)	Crystal Structure
29	141 ⁴²	146	135 ⁴²
57	104	106	98
48	103	105	87
55	139	144	143
14	178 → 182 ²⁹	171 → 188	176 → 184 ²⁹
32	144 ⁴²	147	141 ⁴²
30	143 ²⁸	149	144 ²⁸

These methods have been utilized in efforts to correlate substitution effects and guide the design of more twisted longitudinally twisted acenes.

Barriers to Enantiomerization

The compounds **62** and **63** were synthesized in our group using the aforementioned quinone approach. An example of this approach is outlined in Figure 1.33 for **58**. Thiophene **59** was reacted with *p*-benzoquinone **43** to generate the quinone precursor **60**. Anthraquinone **60** was treated with *n*-BuLi and 1-bromo-4-isopropylbenzene to yield the diol intermediate **61** and was immediately reduced with SnCl₂ yielding **58** with 0.7% yield.

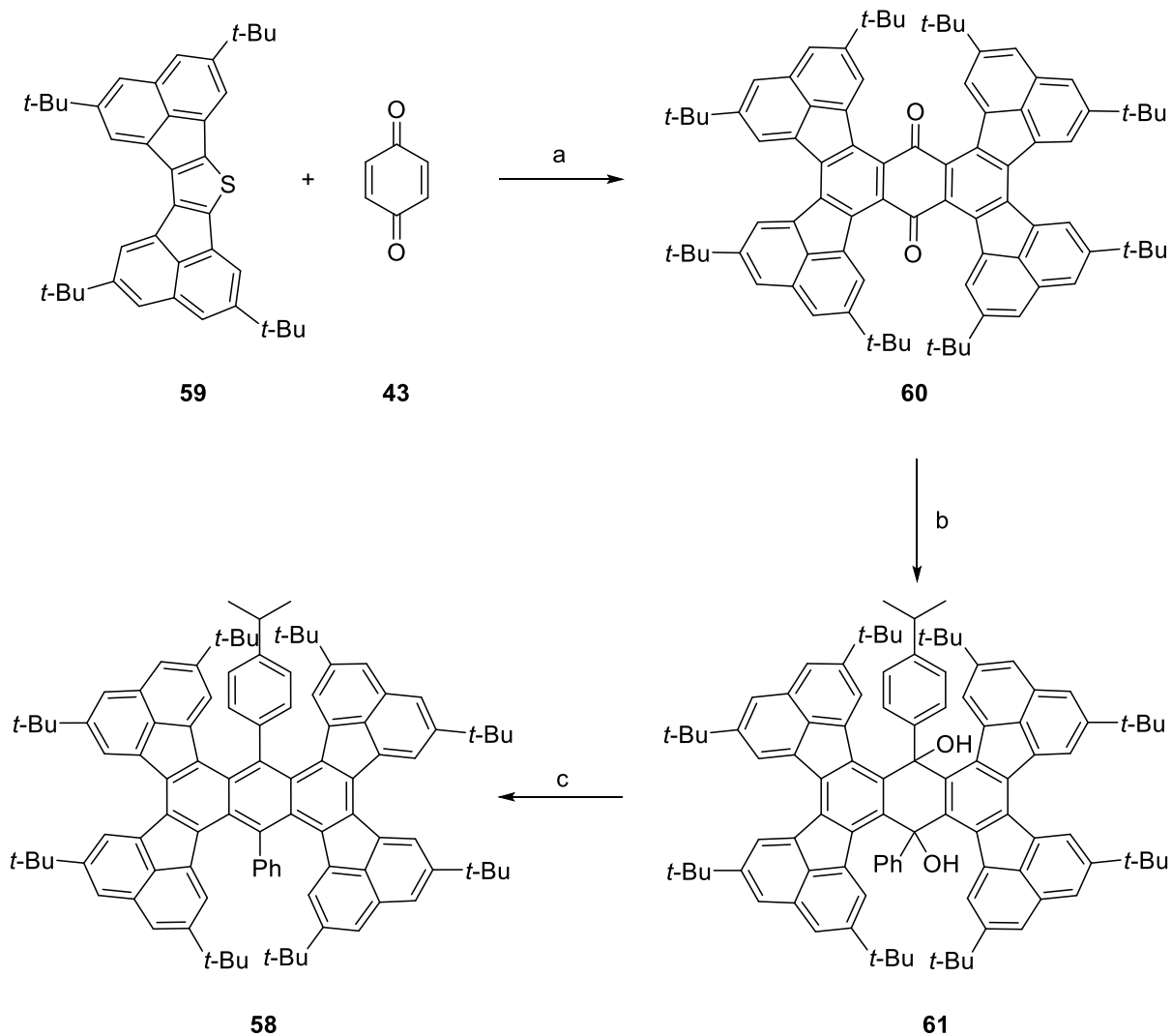


Figure 1.33. Synthetic route for the half-add isopropyl anthracene **58**. (a) nitrobenzene, reflux, 92 h; (b) *n*-BuLi, 1-bromo-4-isopropylbenzene, benzene, rt, 16 h; (c) anhyd SnCl₂, HCl, THF, reflux, 0.5 h.

As mentioned previously, variable-temperature nuclear magnetic resonance (VT NMR) spectroscopy is one method to quantify the barrier to racemization. This technique was applied for compounds **50** and **51** and has been successfully employed by the Pascal group for the isopropyl substituted anthracene **49**.^{36,49} Due to the chiral nature of these compounds,

the methyls of the isopropyl groups are diastereotopic. As such, these groups can serve as a "handle" that can be used to monitor the enantiomerization. This occurs as the methyl peaks present as a doublet of doublets due to the difference in environments (*M* vs. *P*) when the interconversion is slow and a doublet when rapid interconversion is occurring. Compounds **62** (Figure 1.34) and **63** (Figure 1.36) were dissolved in either CDCl₃ or 1,1,2,2-tetrachloroethane-*d*₂. This latter was selected due to its low melting point (-44 °C) and high boiling point (145-146 °C). ¹H NMR spectra were taken at 10 and 20 °C intervals for **63** and **62**, respectively. The resulting spectra are displayed in Figures 1.35 and 1.37.

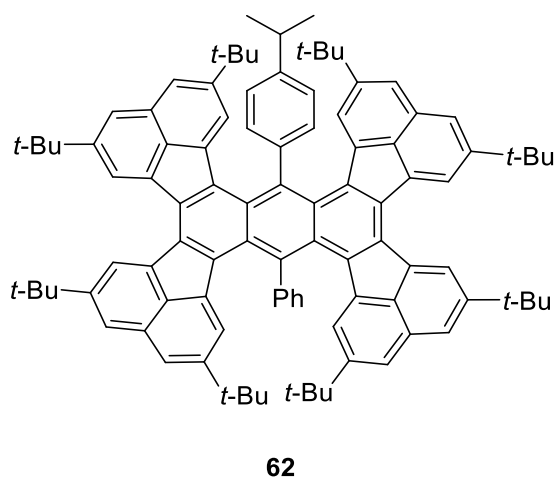


Figure 1.34. Half-add isopropyl anthracene **62**.

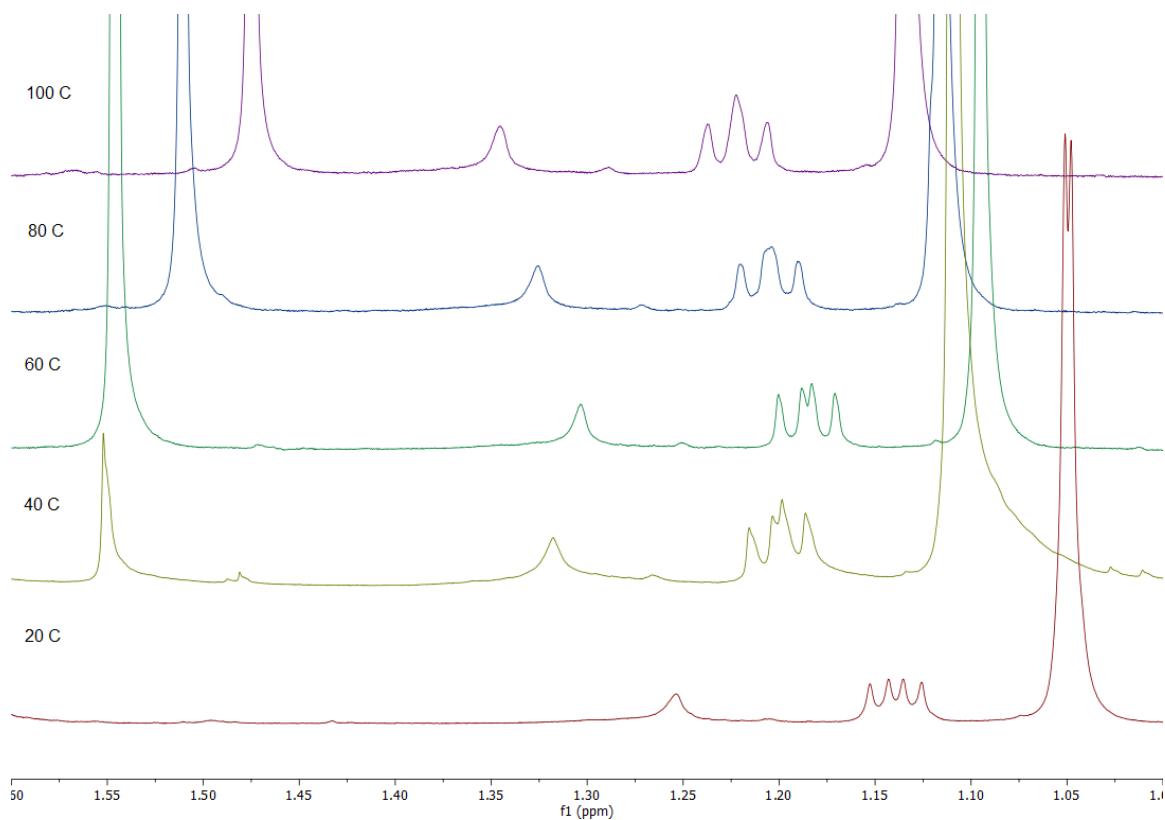
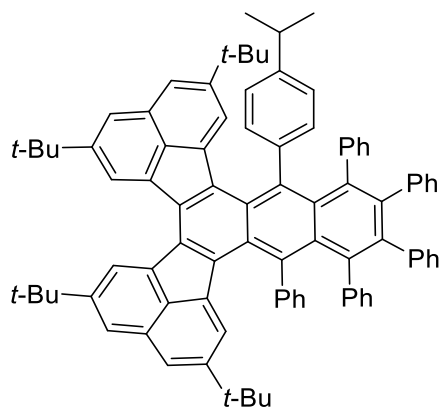


Figure 1.35. ^1H VT NMR spectra of **62** in 1,1,2,2-tetrachloroethane- d_2 .

As can be seen from the ^1H NMR spectra of **62**, coalescence was not observed, and the methyl groups were still clearly resolved at temperatures up to 100 °C. Similar to results observed for **50** by Miller, a temperature dependent shift was observed.⁴⁹ By comparison, **63** displays two distinct doublets in the ^1H NMR spectra. No temperature dependent shift was observed over the limited temperature range investigated.



63

Figure 1.36. Half-add phenylated isopropyl anthracene **63**.

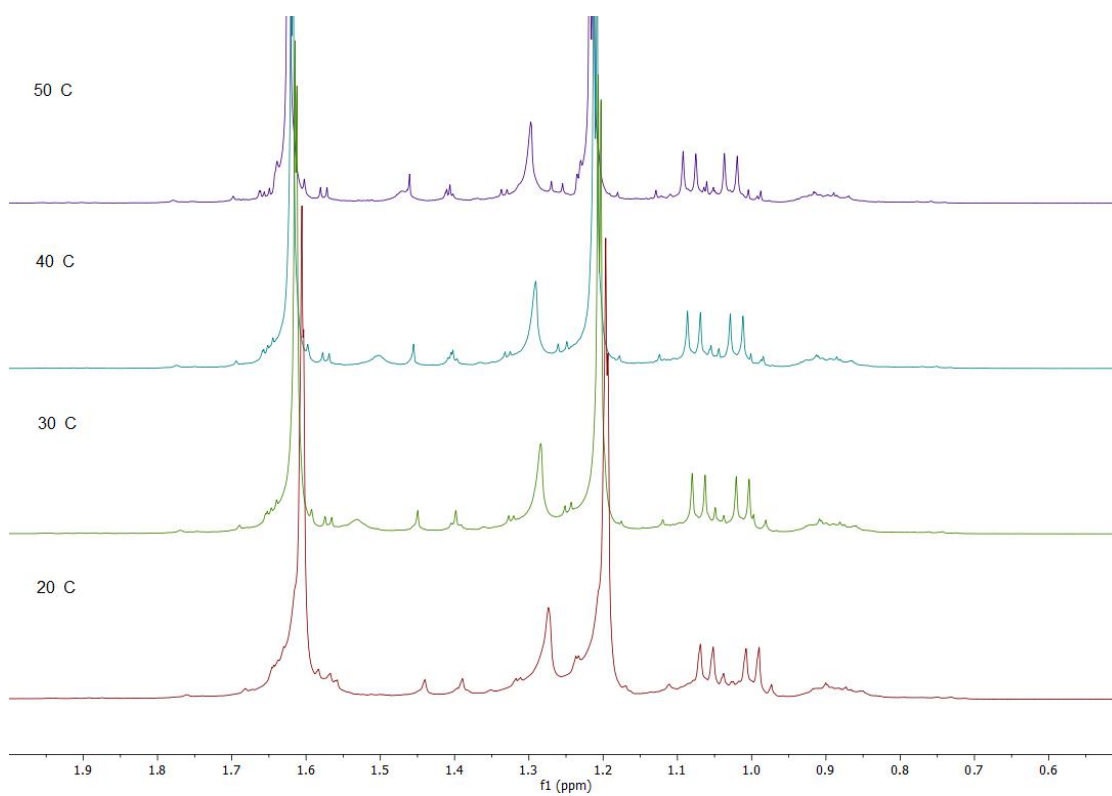


Figure 1.37. ^1H VT NMR spectra of **63** in CDCl_3 .

While we were unable to quantify the barrier to racemization, a lower limit of 20 kcal/mol was established based on the Gutowsky-Holm approximation. As **62** is structurally similar to **49**, it was expected that they would have comparable barriers to racemization. Therefore, in order to quantify the barrier to racemization of these two compounds, a wider temperature range (-35 to 135 °C) as well as different solvents need to be employed.

Twist Bias

As mentioned previously, these compounds may possess theoretically interesting chiroptical properties which could be utilized if they can be resolved. One approach is to pursue longer, more twisted acenes, but to date this route has proved unsuccessful. Another approach to configurationally stable LTAs is through the addition of naphthyl substituents in a dissymmetric fashion along the acene backbone.⁵³ The naphthyl groups rotate at a much slower rate than the acene core. For reference, Clough and Roberts found the barrier to rotation for 1,4,5,8-tetraphenylnaphthalene (**64**) to be 14.9 kcal/mol; thus rapid rotation occurs at room temperature (Figure 1.38).⁶¹ In more sterically congested environments, these barriers are higher as observed in **65** and **53** with ΔG_{rac} values of 33.1 and >39 kcal/mol, respectively.^{53,62}

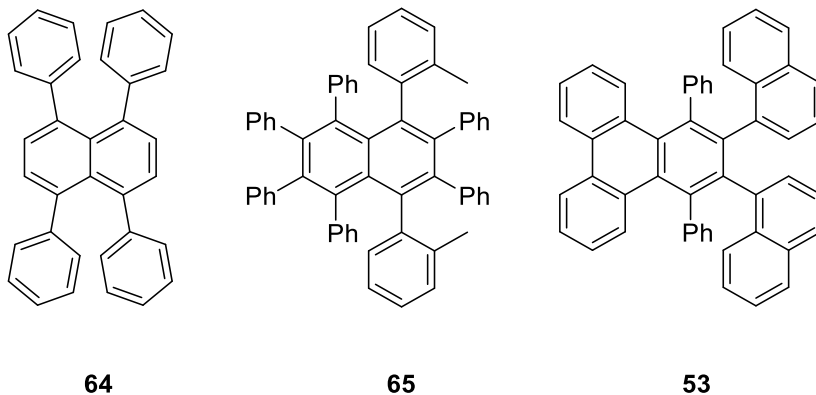


Figure 1.38. Structures with increasingly congested environments.

Therefore, the naphthyl groups should be, in essence, “frozen” in space, while the acene core is still free to rapidly racemize. The ability of the acene core to racemize interconverts diastereomers of different energies resulting in an energetically favored twist bias and thus, “configurational stability.” This interconversion of the acene backbone from the *P* enantiomer to the *M* enantiomer (blue) is illustrated in Figure 1.39. As can be seen in the figure, the naphthyl groups retain their clockwise orientation (red).

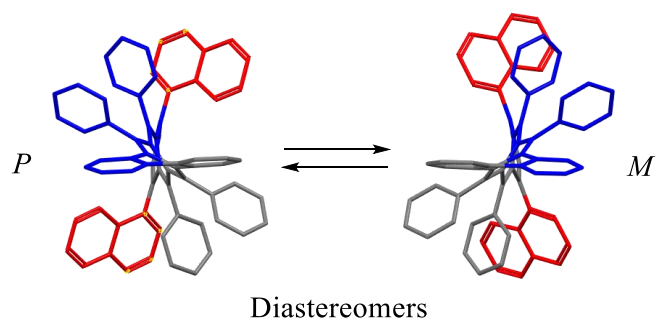


Figure 1.39. Example of interconversion from the *trans-P* to *trans-M* diastereomer.

Utilizing this approach, we have evaluated the effects of substitution on the twist bias for a series of tetracenes at the DFT level of theory. Due to the presence of diastereomers, six conformations exist for the naphthyl-substituted tetracene derivatives. The B3LYP/6-31g(d) optimized structures for compounds **66-70** and relative energies are displayed in Figures 1.40-1.44.

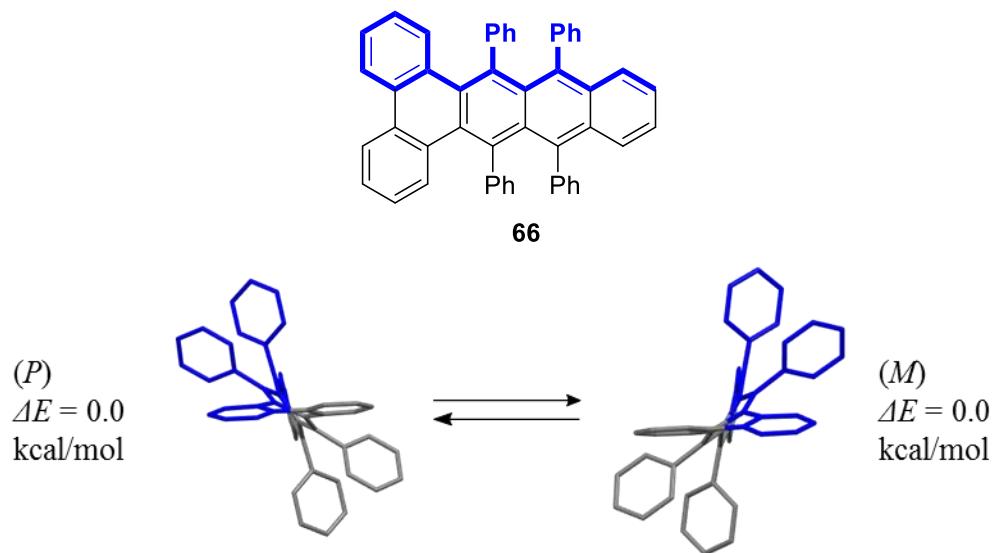


Figure 1.40. DFT B3LYP/6-31g(d) optimized structures and relative energies of the two conformations of **66**.

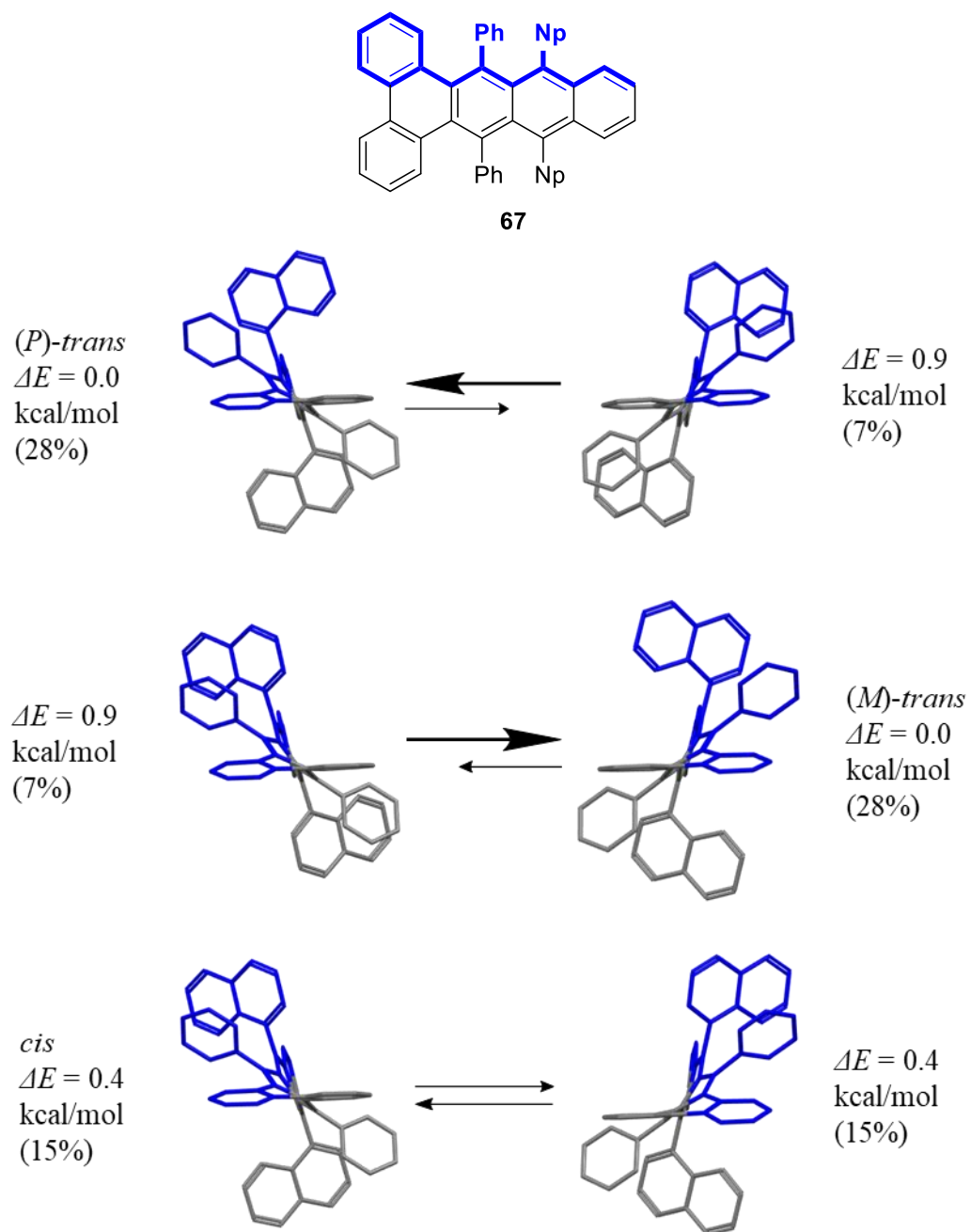


Figure 1.41. DFT B3LYP/6-31g(d) optimized structures and relative energies of the six conformations of **67**.

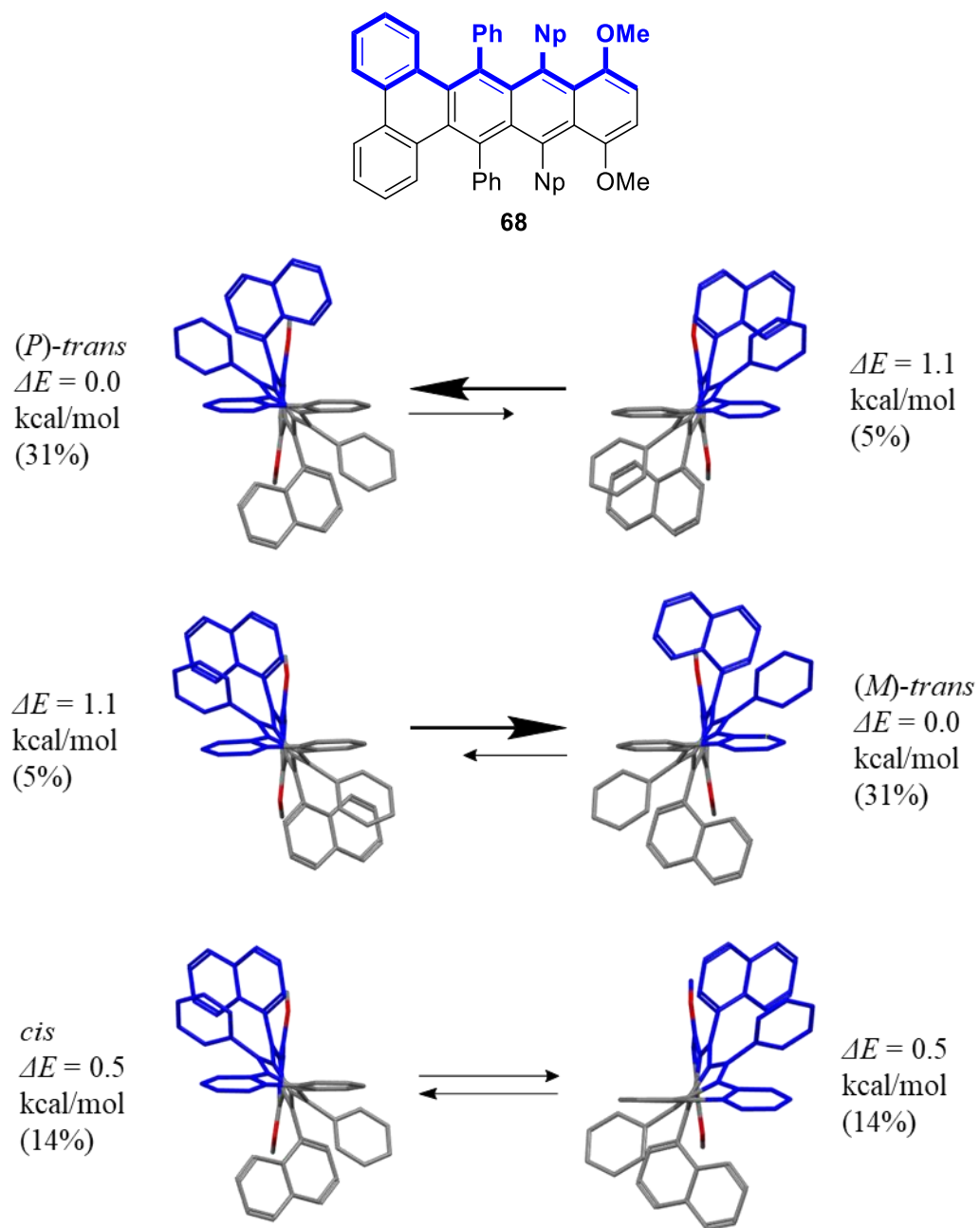


Figure 1.42. DFT B3LYP/6-31g(d) optimized structures and relative energies of the six conformations of **68**.

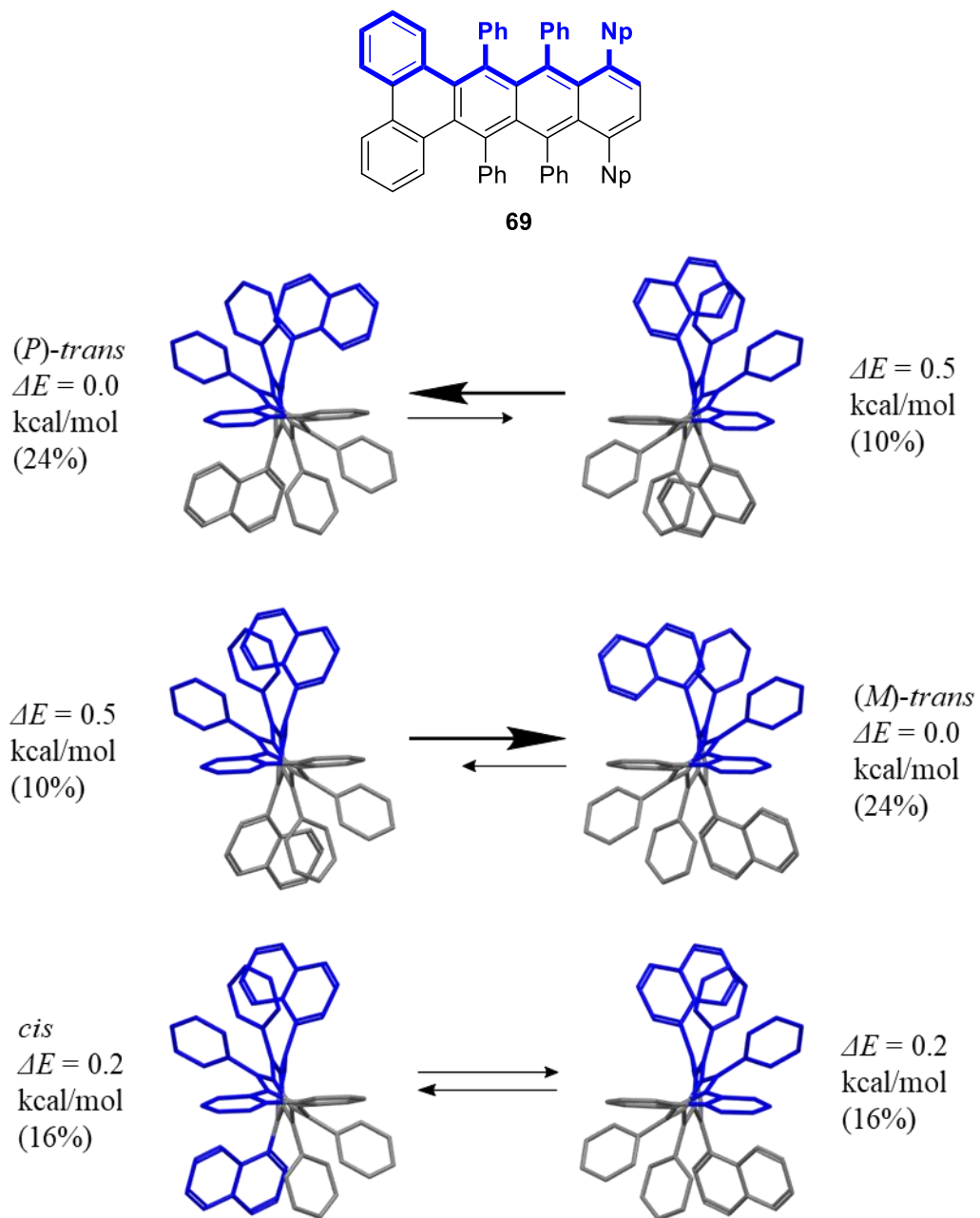


Figure 1.43. DFT B3LYP/6-31g(d) optimized structures and relative energies of the six conformations of **69**.

In all of the naphthyl-substituted derivatives, the lowest energy conformation was observed for the *trans* isomer with the smallest amount of overlap between the naphthyl group and the adjacent phenyl ring. The calculated overall twist along the tetracene unit, as well as the twist bias for compounds **66-70**, are compiled in Table 1.3. Twist biases were observed for compounds **67-70**.

Table 1.3. DFT B3LYP/6-31g(d) calculated overall twist and twist bias of **65-69** for the diastereomers.

Compound	Overall Twist ^a	Twist Bias (kcal/mol)	<i>Cis:trans</i> ^b	<i>Trans</i> ratio ^c
66	80°	0.0	0	0
67	81°	0.9	30:70	4:1
68	94°	1.1	28:72	6:1
69	103°	0.5	32:68	2:1
70	118°	0.7	30:70	3:1
53 ⁵⁴	~30°	0.8	28:72	4:1

^aDFT B3LYP/6-31g(d) calculated. ^bCalculated Boltzmann distribution at 298K.

^cBias toward energetically favored *trans* diastereomer.

The addition of methoxy groups at 11 and 14 positions produced the largest twist bias, with a calculated energy difference of 1.1 kcal/mol. The Boltzmann distribution for compound **68** at a temperature of 298 K predicted that it exists as a 72:28 mixture of *trans* and *cis* isomers. Moreover, the stable *trans* conformer was favored by approximately 6:1. This was a slight increase of 0.2 kcal/mol compared to the less sterically congested **67**, which exhibited a smaller energy difference and a 4:1 bias towards the lower energy conformer. Not surprisingly, when the naphthyl groups were moved to the 11 and 14 positions a smaller twist bias was obtained.

The extension the acene backbone from tetracene **67** to pentacene **70** yielded similar results in terms of the lowest energy conformer, with the most stable conformer favored by 3:1 (Figure 1.44). However, while the length increased by one unit, there was no increase in twist bias. In fact, a slight reduction in the energy differences (0.2 kcal/mol) was observed.

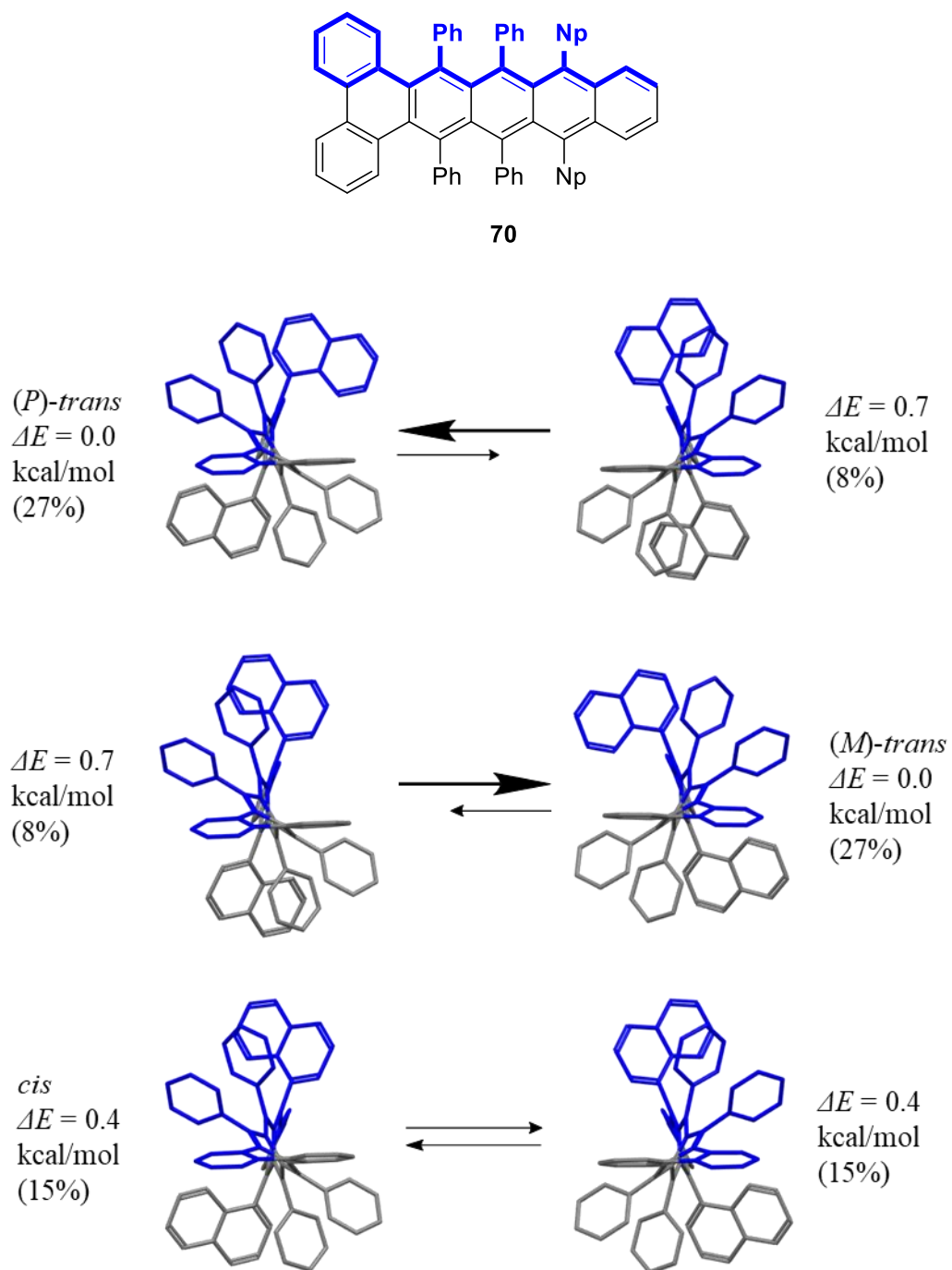


Figure 1.44. DFT B3LYP/6-31g(d) optimized structures and relative energies of the six conformations of **70**.

From this study, it is apparent that the twist bias is not directly proportional to the overall twist and is affected by many factors, including sterics. Furthermore, compounds **67**, **68**, and **70** have greater calculated end-to-end twists than Pascal's stable LTA (32°), yet they exhibit comparable twist biases.⁵⁴ Although the energy differences are quite low, they are comparable to Pascal's **53**. Based on the successful resolution of **53**, it is expected that resolution of compounds **67**, **68**, and **70** into their pure enantiomers should be obtainable.

In line with what was observed during our attempts to predict the helical twist, the DFT calculated twist along the tetracene backbone was in poor agreement with the solid state structure for compound **68**. The calculated structure exhibited a 12° higher twist (94°) than the crystal structure (81.7°).

Summary

The end-to-end twist of a series of LTAs were modelled at the AM1 and DFT levels of theory. Both methods were able to reproduce the experimentally derived values with the majority falling within 10° . The fast run times with AM1 provide a distinct advantage to DFT with results obtained within a few hours compared to a week or more for DFT calculations. For example, the total cpu time for **32** (optimization and frequency calculations) was approximately 9.5 days for DFT compared to 2 min for AM1 on the Lewis cluster. Based on the success of these comparisons, AM1 was used to predict what is expected to be the most twisted LTA to date, heptacene **33** (Figure 1.18). It was calculated to possess a twist of 220° , an increase of 36° as compared to its hexacene analogue.²⁹

To the same extent, theoretical methods can be employed to identify and design potential configurationally stable LTAs. As mentioned previously, these compounds may possess theoretically interesting chiroptical properties. In order to do so, the LTAs must have some degree of configurational stability. A successful approach to configurationally stable LTAs was demonstrated by Pascal *et. al.* in which the addition of bulky substituents, such as naphthyl groups, in an asymmetric fashion, induced a twist bias.⁵⁴ Twist biases were observed for all naphthyl substituted compounds **67-70**. Additionally, while **67**, **68**, and **70** have larger calculated end-to-end twists than Pascal's stable LTA (81°, 94°, and 118°, respectively compared to 32°), they exhibit comparable twist biases.⁵⁴ Based on the successful resolution of the Pascal's stable LTA and the comparable calculated twist biases, resolution of **67**, **68**, and **70** into their pure enantiomers should be obtainable.

Future Work

The future work on this project will focus on understanding what influences the acene distortion as it has been demonstrated that while sterics are a major component, it is not the sole contributor. For example, the naphthyl-substituted pentacene exhibits a slightly lower twist than the fully phenylated pentacene. In the former, it has been suggested that the naphthyl group may orient itself in such a manner that reduces the twist in order to increase the amount π - π overlap between the naphthyl group and the adjacent phenyl rings. The other potential is that the naphthyl group behaves as an electron withdrawing group. Thus, a system investigation of the effects of electron withdrawing and donating groups on the end-to-end twist should be undertaken.

Materials and Methods

Computational Methodology. Calculations were performed using AM1 and DFT at the B3LYP/6-31G(d) levels of theory as implemented in Gaussian 09.⁶³ Geometry optimizations were performed for all compounds followed by frequency calculations to verify the optimized structures correspond to a local minima. The AM1 structures were used as the starting geometry for all DFT calculations.

Variable Temperature NMR Measurements on Compounds 62 and 63. NMR studies of compounds **62** and **63** were carried out on a Varian AC 400 spectrometer. Compound **61** was dissolved in 1,1,2,2-tetrachloroethane-d₂, and ¹H NMR spectra were taken at 20 °C intervals. Compound **63** was dissolved in CDCl₃ and ¹H NMR spectra were taken in 10 °C intervals. Both samples were allowed to equilibrate for 20 minutes at each temperature prior to spectra acquisition.

References

1. Moss, G. P.; Smith, P. A. S.; Tavernier, D. *Pure Appl. Chem.* **1995**, *67*, 1307–1375.
2. Krüger, J.; García, F.; Eisenhut, F.; Skidin, D.; Alonso, J. M.; Guitián, E.; Pérez, D.; Cuniberti, G.; Moresco, F.; Peña, D. *Angew. Chem. Int. Ed.* **2017**, *56*, 11945–11948.
3. Tönshoff, C.; Bettinger, H. F. *Angew. Chem. Int. Ed.* **2010**, *49*, 4125–4128.
4. Mondal, R.; Shah, B. K.; Neckers, D. C. *J. Am. Chem. Soc.* **2006**, *128*, 9612–9613.
5. Anthony, J. E. *Angew. Chem. Int. Ed.* **2008**, *47*, 452–483.
6. Bettinger, H. F.; Tönshoff, C. *The Chemical Record* **2015**, *15*, 364–369.
7. Mondal, R.; Adhikari, R. M.; Shah, B. K.; Neckers, D. C. *Org. Lett.* **2007**, *9*, 2505–2508.
8. Strating, J.; Zwanenburg, B.; Wagenaar, A.; Udding, A. C. *Tetrahedron Lett.* **1969**, *10*, 125–128.
9. Einholz, R.; Fang, T.; Berger, R.; Grüniger, P.; Früh, A.; Chassé, T.; Fink, R. F.; Bettinger, H. F. *J. Am. Chem. Soc.* **2017**, *139*, 4435–4442.
10. Mondal, R.; Tönshoff, C.; Khon, D.; Neckers, D. C.; Bettinger, H. F. *J. Am. Chem. Soc.* **2009**, *131*, 14281–14289.
11. Zade, S. S.; Zamoshchik, N.; Reddy, A. R.; Fridman-Marueli, G.; Sheberla, D.; Bendikov, M. *J. Am. Chem. Soc.* **2011**, *133*, 10803–10816.
12. Aihara, J. *J. Phys. Chem. A* **1999**, *103*, 7487–7495.
13. Cheng, Y. C.; Silbey, R. J.; da Silva Filho, D. A.; Calbert, J. P.; Cornil, J.; Brudas, J. L., *J. Chem. Phys.* **2003**, *118*, 3764–3774.
14. Anthony, J. E. *Chem. Rev.* **2006**, *106*, 5028–5048.
15. Yoo, S.; Domercq, B.; Kippelen, B. *Appl. Phys. Lett.* **2004**, *85*, 5427–5429.
16. Kagan, C. R.; Afzali, A.; Graham, T. O. *Appl. Phys. Lett.* **2005**, *86*, 193505.
17. Tang, M. L.; Okamoto, T.; Bao, Z. *J. Am. Chem. Soc.* **2006**, *128*, 16002–16003.

18. Lin, Y.-Y.; Gundlach, D. J.; Nelson, S. F.; Jackson, T. N. *IEEE Trans. Electron Dev. Lett.* **1997**, *18*, 606–608.
19. Choi, H.; Kim, S.; Jang, J. *Adv. Mater.* **2004**, *16*, 732–736.
20. Kaur, I.; Jia, W.; Kopreski, R. P.; Selvarasah, S.; Dokmeci, M. R.; Pramanik, C.; McGruer, N. E.; Miller, G. P. *J. Am. Chem. Soc.* **2008**, *130*, 16274–16286.
21. Anthony, J. E.; Eaton, D. L.; Parkin, S. R. *Org. Lett.* **2002**, *4*, 15–18.
22. Allen, C. F. H.; Bell, A. *J. Am. Chem. Soc.* **1942**, *64*, 1253–1260.
23. Chen, Z.; Müller, P.; Swager, T. M. *Org. Lett.* **2006**, *8*, 273–276.
24. Maliakal, A.; Raghavachari, K.; Katz, H.; Chandross, E.; Siegrist, T. *Chem. Mater.* **2004**, *16*, 4980–4986.
25. Duong, H. M.; Bendikov, M.; Steiger, D.; Zhang, Q.; Sonmez, G.; Yamada, J.; Wudl, F. *Org. Lett.* **2003**, *5*, 4433–4436.
26. Pascal, R. A., Jr. *Chem. Rev.* **2006**, *106*, 4809–4819.
27. Xiao, J.; Duong, H. M.; Liu, Y.; Shi, W.; Ji, L.; Li, G.; Li, S.; Liu, X.-W.; Ma, J.; Wudl, F.; Zhang, Q. *Angew. Chem. Int. Ed.* **2012**, *51*, 6094–6098.
28. Lu, J.; Ho, D. M.; Vogelaar, N. J.; Kraml, C. M.; Pascal, R. A. *J. Am. Chem. Soc.* **2004**, *126*, 11168–11169.
29. Clevenger, R. G.; Kumar, B.; Menuey, E. M.; Kilway, K.V. *Chem. Eur. J.* **2018**, *24*, 3113–3116.
30. Paraskar, A. S.; Reddy, A. R.; Patra, A.; Wijsboom, Y. H.; Gidron, O.; Shimon, L. J. W.; Leitun, G.; Bendikov, M. *Chem. Eur. J.* **2008**, *14*, 10639–10647.
31. Huang, L.; Liao, Q.; Shi, Q.; Fu, H.; Ma, J.; Yao, J. CCDC 726175: Experimental Crystal Structure Determination, 2010, DOI: [10.5517/ccscn0s](https://doi.org/10.5517/ccscn0s)
32. Norton, J. E.; Houk, K. N. *J. Am. Chem. Soc.* **2005**, *127*, 4162–4163.
33. Xu, Q.; Duong, H. M.; Wudl, F.; Yang, Y. *Appl. Phys. Lett.* **2004**, *85*, 3357–3359.
34. Schuster, I. I.; Cracium, L.; Ho, D. M.; Pascal, R. A., Jr. *Tetrahedron* **2002**, *58*, 8875–8882.

35. Qiao, X.; Padula, M. A.; Ho, D. M.; Vogelaar, N. J.; Schutt, C. E.; Pascal, R. A. *J. Am. Chem. Soc.* **1996**, *118*, 741–745.
36. Pascal, R. A., Jr.; McMillian, W. D.; Van Engen, D.; Eason, R. G. *J. Am. Chem. Soc.* **1987**, *109*, 4660–4665.
37. Smyth, N.; Van Engen, D.; Pascal, R. A., Jr. *J. Org. Chem.* **1990**, *55*, 1937–1940.
38. Qiao, X.; Ho, D. M.; Pascal, R. A., Jr. *Angew. Chem. Int. Ed. Engl.* **1997**, *36*, 1531–1532.
39. Rodriguez-Lojo, D.; Perez, D.; Pena, D.; Guitian, E. *Chem. Comm.* **2013**, *49*, 6274–6276.
40. Xiao, Y.; Mague, J. T.; Schmehl, R. H.; Haque, F. M.; Pascal, R. A., Jr. *Angew. Chem. Int. Ed.* **2019**, *58*, 2831–2833.
41. Chen, W.; Li, X.; Long, G.; Li, Y.; Ganguly, R.; Zhang, M.; Aratani, N.; Yamada, H.; Liu, M.; Zhang, Q. *Angew. Chem.* **2018**, *130*, 13743–13747.
42. Clevenger, R. G.; Kumar, B.; Menuey, E. M.; Lee, G.-H.; Patterson, D.; Kilway, K. V. *Chem. Eur. J.* **2018**, *24*, 243–250.
43. Lu, J.; Ho, D. M.; Vogelaar, N. J.; Kraml, C. M.; Bernhard, S.; Byrne, L. R.; Pascal, R. A. *J. Am. Chem. Soc.* **2006**, *128*, 17043–17050.
44. Pascal, R. A.; Qin, Q. *Tetrahedron* **2008**, *64*, 8630–8637.
45. Clevenger, R. G. In Pursuit of Extraordinarily Twisted Acenes. Ph.D. Dissertation, University of Missouri – Kansas City, Kansas City, MO, 2014.
46. Cahn, R. S.; Ingold, C.; Prelog, V. *Angew. Chem. Int. Ed.* **1966**, *5*, 385–415.
47. Janke, R. H.; Haufe, G.; Wurthwien, E. U.; Borkent, J. H. *J. Am. Chem. Soc.* **1996**, *118*, 6031–6035.
48. Barroso, J.; Cabellos, J. L.; Pan, S.; Murillo, F.; Zarate, X.; Fernandez-Herrera, M. A.; Merino, G. *Chem. Comm.* **2018**, *54*, 188–191.
49. Miller, B. D. Synthesis and Analysis of Siloranes for Use as a Biomaterial and Extended Twisted Molecular Ribbons. Ph.D. Dissertation, University of Missouri – Kansas City, Kansas City, MO, 2013.

50. Goedicke, Ch.; Stegemeyer, H. *Tetrahedron Lett.* **1970**, *11*, 937–940.
51. Martin, R. H.; Marchant, M. J. *Tetrahedron* **1974**, *30*, 347–349.
52. Meurer, K. P.; Vögtle, F. *Top. Curr. Chem.* **1985**, *127*, 1–76.
53. Walters, R. S.; Kraml, C. M.; Byrne, N.; Ho, D. M.; Qin, Q.; Coughlin, F. J.; Bernhard, S.; Pascal, R. A., Jr. *J. Am. Chem. Soc.* **2008**, *130*, 16435–16441.
54. Bedi, A.; Shimon, L. J. W.; Gidron, O. *J. Am. Chem. Soc.* **2018**, *140*, 8086–8090.
55. Bedi, A.; Gidron, O. *Chem. Eur. J.* **2019**, *25*, 3279–3285.
56. Li Y.; Clevenger R. G.; Lu J.; Kilway, K. V.; Peng Z. *J. Phys. Chem. C* **2016**, *120*, 841–852.
57. Li Y.; Clevenger R. G.; Lu J.; Kilway, K. V.; Peng Z. *J. Mater. Chem. C* **2014**, *2*, 7180–7183.
58. Li, Y.; Scheel, K. R.; Clevenger, R. G.; Shou, W.; Pan, H.; Kilway, K. V.; Peng, Z. *Adv. Energy Mater.* **2018**, *8*, 1801248.
59. Jensen, F. *Introduction to Computational Chemistry*. John Wiley & Sons, Inc., USA, 2006.
60. The computation for this work was performed on the high performance computing infrastructure provided by Research Computing Support Services and in part by the National Science Foundation under grant number CNS-1429294 at the University of Missouri, Columbia Mo.
61. Clough, R. L.; Roberts, J. D. *J. Org. Chem.*, **1978**, *43*, 1328–1331.
62. Qiao, X.; Pelczer, I.; Pascal, R. A. *Chirality*, **1998**, *10*, 154–158.
63. Gaussian 09, Revision D.01, M. J. Frisch, G. W. Trucks, H. B. Schlegel, G. E. Scuseria, M. A. Robb, J. R. Cheeseman, G. Scalmani, V. Barone, G. A. Petersson, H. Nakatsuji, X. Li, M. Caricato, A. Marenich, J. Bloino, B. G. Janesko, R. Gomperts, B. Mennucci, H. P. Hratchian, J. V. Ortiz, A. F. Izmaylov, J. L. Sonnenberg, D. Williams-Young, F. Ding, F. Lipparini, F. Egidi, J. Goings, B. Peng, A. Petrone, T. Henderson, D. Ranasinghe, V. G. Zakrzewski, J. Gao, N. Rega, G. Zheng, W. Liang, M. Hada, M. Ehara, K. Toyota, R. Fukuda, J. Hasegawa, M. Ishida, T. Nakajima, Y. Honda, O. Kitao, H. Nakai, T. Vreven, K. Throssell, J. A. Montgomery, Jr., J. E. Peralta, F. Ogliaro, M. Bearpark, J. J. Heyd, E. Brothers, K. N. Kudin, V. N. Staroverov, T. Keith, R. Kobayashi, J. Normand, K.

Raghavachari, A. Rendell, J. C. Burant, S. S. Iyengar, J. Tomasi, M. Cossi, J. M. Millam, M. Klene, C. Adamo, R. Cammi, J. W. Ochterski, R. L. Martin, K. Morokuma, O. Farkas, J. B. Foresman, and D. J. Fox, Gaussian, Inc., Wallingford CT, 2016.

Development of a Silorane-Based Biomaterial for Use as an Antimicrobial Delivery Device

CHAPTER 2

DEVELOPMENT OF A SILORANE-BASED BIOMATERIAL

Introduction

In order to alleviate pain and improve the patient's quality of life, total joint replacements (TJR) are performed on all major joints: shoulder, hip, knee, and ankle. Of these surgeries, hip and knee replacements are the most prevalent and approximately one million procedures are performed each year in the United States alone.¹ By 2030, total hip and knee surgeries are on the rise and predicted to reach nearly 572,000 and 3.48 million, respectively.² Unfortunately, this trend is not limited to these replacements. In 2010, Day *et. al.* studied the prevalence of upper extremity arthroplasties (shoulder and elbow) in the US and concluded: "the growth rates of upper extremity arthroplasty were comparable to or higher than rates for total hip and knee procedures."¹ While in general these procedures were often utilized in patients that were 65 years or older, but there is a growing trend for these surgeries (specifically, hip, knee, shoulder and elbow) in younger patients.²⁻⁴ This change in patient demographics further expands the demand for TJA procedures, and the number of revisions is expected to rise as well. This increase is a result of a number of factors, including younger patients, an aging population, and extended lifespans.

Most joint replacement surgeries use commercially available bone cement to stabilize the implant in the marrow space. These bone cements are primarily comprised of poly(methyl methacrylate) (PMMA). Since it was first introduced for use in orthopaedics by Sir John Charnley in 1960, PMMA has been the "gold standard" for prosthesis fixation due to its ability

to disperse the weight of the body over a large area of bone and its good compressive strength.^{5,6} In addition to joint replacements, bone cements have been employed in numerous other applications, such as kyphoplasties and antibiotic spacers/beads.

Commercial PMMA-Based Bone Cement

Commercially available bone cements have remained largely unchanged since their inception in the late 1950s.⁷⁻⁹ Although the FDA has approved over 30 different PMMA-based bone cements; their compositions are notably similar.^{7,10,11} These cements are manufactured as a two-component system, a powder and liquid monomer. The powder is composed of pre-polymerized PMMA, a radio-opacifier (barium sulfate or zirconium oxide), and an initiator (benzoyl peroxide). The liquid monomer consists of methyl methacrylate (MMA) monomer, N,N-dimethyl-*p*-toluidine (activator) and hydroquinone (inhibitor) (Figure 2.1).⁸ In these systems, the tertiary amine reacts with benzoyl peroxide to generate a peroxide free radical, which are used to initiate the polymerization reaction. This general pathway is illustrated in Figure 2.2.

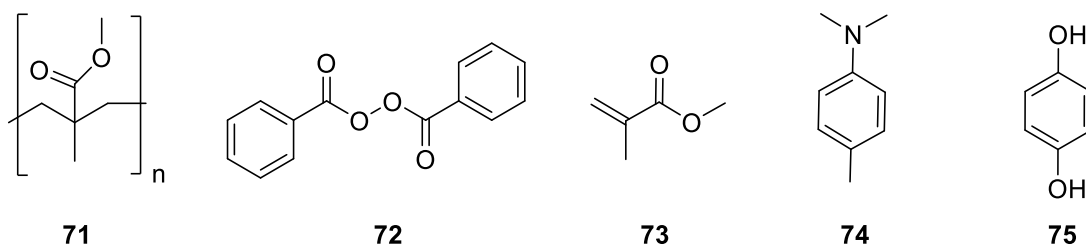


Figure 2.1. Structures of bone cement components: PMMA (**71**), benzoyl peroxide (**72**), methyl methacrylate (**73**), N,N-dimethyl-*p*-toluidine (**74**), and hydroquinone (**75**).

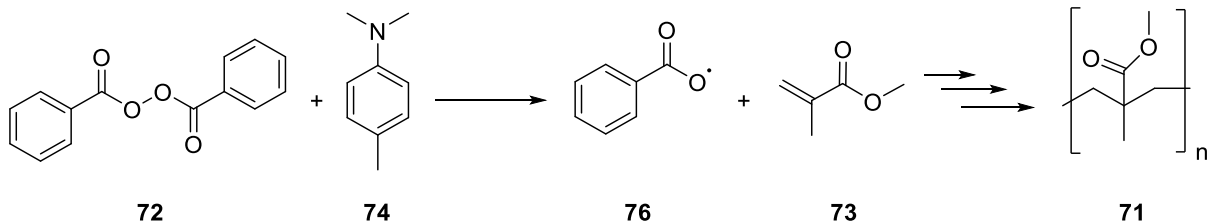


Figure 2.2. General reaction scheme of commercial bone cement polymerization.

While these formulations have ideal mechanical and handling properties, they still have several drawbacks. For example, PMMA polymerization is an exothermic process with average temperatures in the range of 70-100 °C *in vitro*.^{8,12} These temperatures are approximately 2-2.5 times higher than the average body temperature (37 °C) and as such, can cause cell death and damage to the surrounding tissues. However, *in vivo* studies have shown the temperature to be much lower for this polymerization (between 40-47 °C). This is likely due to heat transfer to the implant and continuous blood circulation.¹³ In addition to the high curing temperature, the monomer of PMMA, methyl methacrylate (MMA), is highly volatile and toxic. Therefore, it poses a health hazard to both patients and healthcare personnel alike, as unpolymerized monomer leaks from the preparation.¹⁴⁻¹⁶ Furthermore, shrinkage is an inevitable by-product of a polymerization reaction. In PMMA-based cements, the MMA polymerization corresponds to a 6-7% theoretical reduction in volume.¹³ However, in practice the amount of shrinkage may lower, due to incomplete monomer consumption, water absorption, and inclusion of air pockets.^{17,18} The contraction of the bone cement during curing and cooling can result in small gaps at the cement/bone or cement/prosthesis interfaces, which

may result in premature failure due to aseptic loosening.¹⁹ In an attempt to address these limitations, a number of alternatives have been investigated.

Alternative Bone Cements

The majority of investigations into alternative bone cements have followed one of two routes. The first is to utilize components similar to the existing PMMA based systems (i.e., Bis-GMA) to address specific drawbacks such as toxicity, heat generation, or inertness. Vallo and Schroeder demonstrated that the incorporation of 2,2-bis[4(2-hydroxy-3-methacryloyloxypropoxy)] (Bis-GMA) in place of MMA reduces the maximum exotherm and amount of polymerization shrinkage.²⁰ In addition, an increase in compressive strength and flexural modulus was observed. Others have explored alternative activators, reduced benzoyl peroxide formulations, modified monomers, and incorporation of bioactive fillers, to name a few.⁸ However, these alternatives often only address a few of the drawbacks typical of PMMA-based cements.

The second approach is the development of a new base material to replace existing PMMA cements. An example of this approach is calcium phosphate-based bone cements. These cements have good biocompatibility, small heat generation, and minimal shrinkage.²¹ However, these materials exhibit reduced compressive strength compared to PMMA-based cements and slowly degrade over time.²¹ Therefore, calcium phosphate-based cements are not suited for implant fixation. Another alternative are silorane resin composites which were initially developed to address the shortcomings present in methacrylate-based dental cements. While silorane-based materials have been used previously for dental applications, these

materials have not seen prior use in orthopaedic applications.²² Silorane is a term coined to describe compounds that possess a mixture of siloxane **77** and oxirane **78** moieties (Figure 2.3).²³

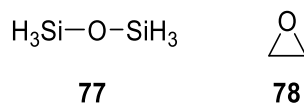


Figure 2.3. Examples of a siloxane **77** and an oxirane **78**.

The advantage of these compounds is the non-toxic nature of siloxanes in combination with the slight expansion upon polymerization of the oxiranes.²³⁻²⁵ As mentioned earlier, all polymerizations suffer from polymerization shrinkage. However, silorane composites have been demonstrated to exhibit less polymerization shrinkage on the order of 1-1.5% compared to 6-7% for PMMA bone cements.^{13,23,25-27} The difference in polymerization shrinkage is associated with the cationic ring-opening of the oxirane moiety. In addition to the reduced polymerization shrinkage, these composites are non-toxic and display similar mechanical properties to methacrylate-based composites.^{24,25,28-30}

Silorane-Based Bone Cement

Composition

Our group has developed a silorane-based biomaterial in order to take advantage of the promising potential of silorane materials and address the aforementioned PMMA limitations.

This biomaterial utilizes a silorane resin (SilMix) comprised of 2,4,6,8-tetrakis(2-(7-oxabicyclo[4.1.0]heptan-3-yl)ethyl)-2,4,6,8-tetramethyl-1,3,5,7,2,4,6,8-tetraoxatetrasilocane (CYGEP, **79**)³⁷ and bis[2-(3{7-oxabicyclo[4.1.0]heptyl})ethyl] methylphenyl silane (PHEPSI, **80**)³⁸ in a 1:1 ratio by weight (Figure 2.4) both of which have previously received FDA approval for use in dental composites. Although these monomers had been mass-produced for sale in Filtek™ P90, they were not commercially available. Therefore, a route to the large-scale production of the monomers was needed. In the end, adapted procedures based on Crivello and Aoki's previous work were developed.^{31,32} The scale-up and optimization of the monomer synthesis was investigated by Dr. Bradley Miller, a former group member.³³ The adapted synthetic routes to CYGEP and PHEPSI are depicted in Figures 2.5 and 2.6, respectively. CYGEP and PHEPSI are both generated *via* a hydrosilylation reaction using a precious metal catalyst.

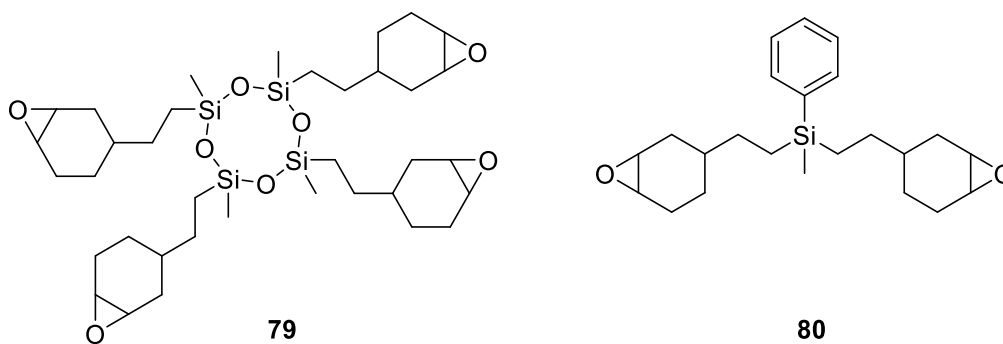


Figure 2.4. Structures of CYGEP (**79**) and PHEPSI (**80**) monomers.

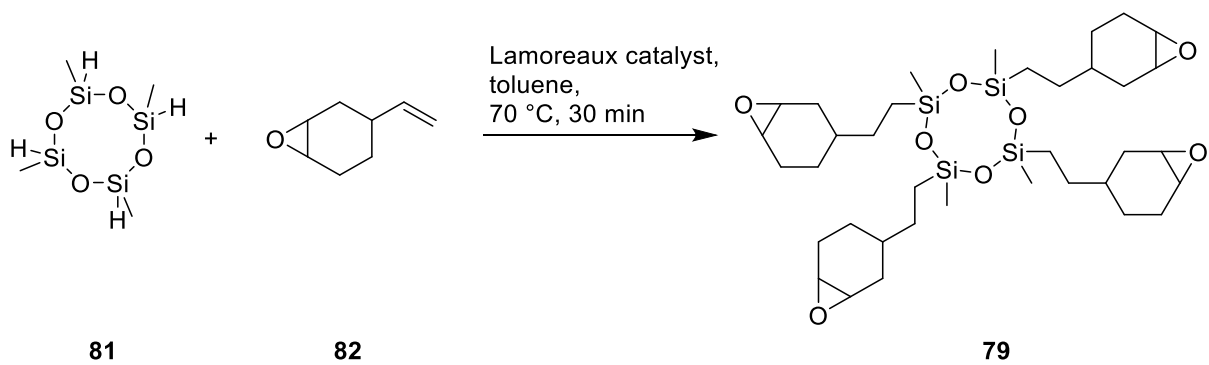


Figure 2.5. Synthesis of CYGEP (**79**).

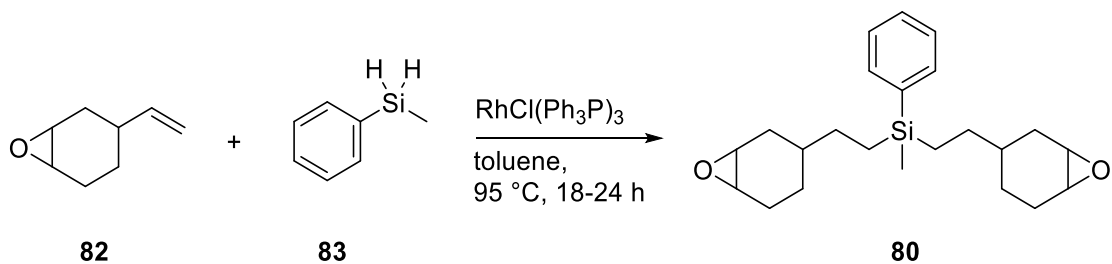


Figure 2.6. Synthesis of PHEPSI (**80**).

In addition to the silorane resin, surface-modified and unmodified baria and yttria silicate glasses were added to the SilMix resin in an attempt to achieve mechanical properties comparable to PMMA-based bone cements. These glass fillers not only offer improved strength, but aid in dispersion wetting and particle-matrix adhesion.³⁹ The inclusion of barium and yttrium oxides in the glass filler itself provides an additional benefit as both serve as radio-opacifiers, therefore eliminating the need to incorporate a radio-opacifier in addition to the filler. The two glass fillers were altered with one of the following surface modifications: (2-(7-oxabicyclo[4.1.0]heptan-3-yl)ethyl)trimethoxysilane (ECHE, **84**), ((9,9-diethyl-1,5,7,11-tetraoxaspiro[5.5]undec-3-yl)methyl)trimethoxysilane (1TOSU, **85**), or (3-(9,9-diethyl-

1,5,7,11-tetraoxaspiro[5.5]undec-3-yl)propyl)trimethoxysilane (3TOSU, **86**) (Figure 2.7). These modifications were selected in part for their similarity to the SilMix monomers in order to obtain better interaction between the filler and resin. Furthermore, the bicyclic substructure has been shown to reduce polymerization stress due to decreased contraction or even slight expansion upon polymerization.³⁴⁻³⁶ The addition of these surface-modified fillers resulted in enhanced mechanical properties and reduced polymerization stress which will be discussed later. Each glass filler and subsequent modification was tested for polymerization in the SilMix system using the Gillmore Needle Test (GNT). All samples passed the polymerization test. Dr. Rachel Weiler's, another former group member, investigated the effects of these fillers on the material properties.³⁷

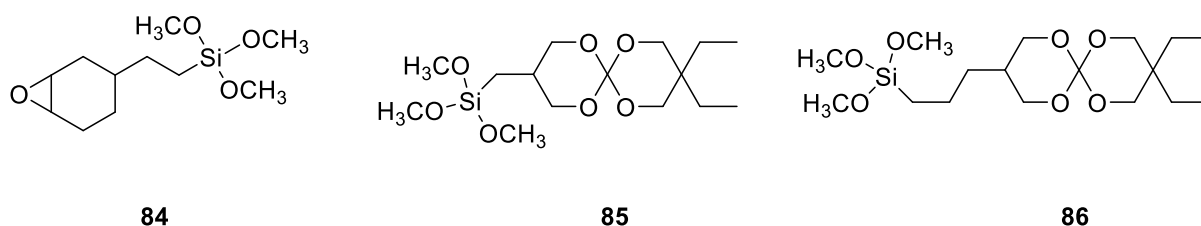


Figure 2.7. Structures of glass filler modifications: ECHC (**84**), 1TOSU (**85**), and 3TOSU (**86**).

The final component of the silorane-based biomaterial is the initiation system. Filtek™ P90 utilized a three-component initiation system comprised of a photoinitiator, iodonium salt **87**, a photosensitizer, camphorquinone (**88**), and an electron donor (e.g., tertiary amine **89**) in their Filtek™ P90 dental cement.³⁸

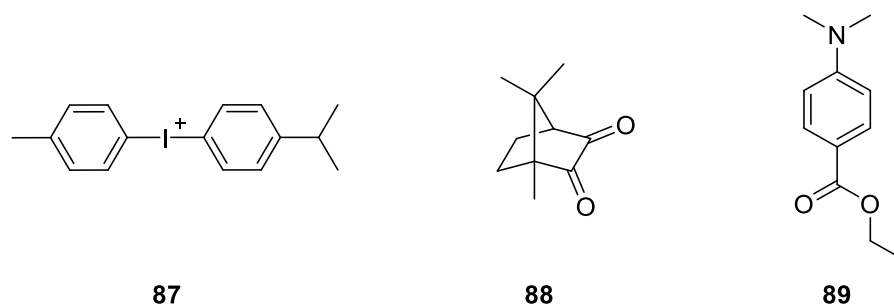


Figure 2.8. Chemical components of Filtek™ P90 light initiation system.

Onium salts are common photoinitiators in cationic polymerizations due in part to their high quantum yields and thermal stability.³⁹⁻⁴¹ However, a photosensitizer is required for visible-light-induced polymerization as their absorption maxima lie between 220-360 nm.^{39,42} Camphorquinone (CPQ) is a standard photosensitizer in these systems as its peak absorbance, 468 nm, falls well within the range of most dental light-curing units (400-540 nm).^{43,44} The CPQ and amine form an exciplex, which can then react with the iodonium salt to generate the reactive cationic species.⁴⁴⁻⁴⁶ While this system is effective for dental purposes, light-initiated systems are impractical for orthopaedic applications. Therefore, an alternative initiation system needed to be developed. Several chemical initiations systems were investigated including strong acids. Of the strong acids tested, hexafluorophosphoric acid was the only one to polymerize within the one hour timeframe.³⁷ This chemical initiation system was associated with short handling times and increased acidity. As a result, mixed initiation systems were investigated and ultimately a dual, chemical and light, cured system was selected. This system utilizes a chemical cure, Lamoreaux catalyst (LMC, **90**), in combination with a light initiation system (1.19 wt.% *p*-(octyloxyphenyl)phenyliodonium hexafluoroantimonate)(PIH, **91**), 0.40

wt.% camphorquinone (CPQ, **88**), and 0.06 wt.% ethyl *p*-dimethylamino benzoate (EDMAB, **89**)).

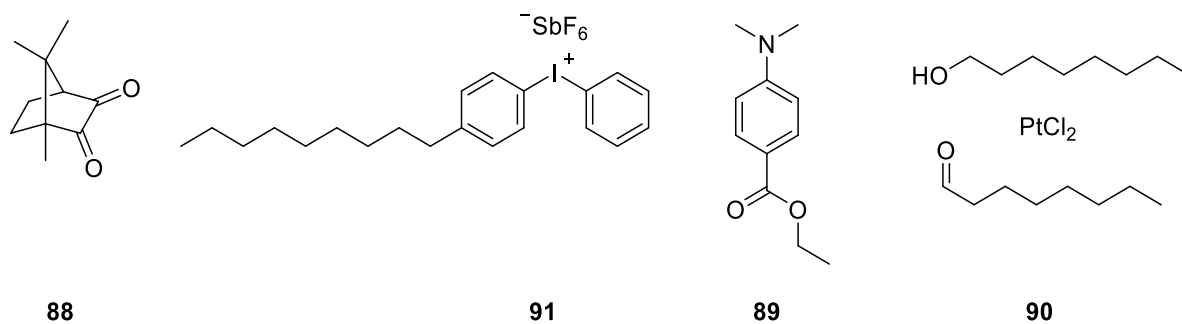


Figure 2.9. Composition of the silorane dual-cured initiation system: CPQ (**88**), PIH (**91**), EDMAB (**89**), and LMC (**90**).

Through the employment of this mixed system, a high degree of cure and reasonable handling times have been achieved. A detailed description of the investigation of chemical and mixed initiation systems investigated can be found in Dr. Rachel Weiler's dissertation.³⁷ A side-by-side comparison of the compositions of silorane and PMMA bone cements and their role is given in Table 2.1.

Table 2.1. Comparison of the chemical composition of PMMA and silorane bone cements.

PMMA	Component	Silorane
Methyl methacrylate	Resin	CYGEP and PHEPSI
Pre-polymerized poly(methyl methacrylate) (PMMA) beads	Filler	DY5 and M12 modified glass fillers
Barium sulfate/Zirconium oxide	Radiopacifier	
Benzoyl peroxide	Initiator	Lamoreaux's Catalyst, CPQ (PS), PIH (PI), and EDMAB (CI)
N,N-dimethyl- <i>p</i> -toluidine	Activator	

Biocompatibility

Earlier work with the SilMix resin demonstrated that the light-cured silorane material is non-toxic.⁷ The next step was to evaluate the dual-cured, filled silorane material for toxicity. This was accomplished using the trypan blue assay and MLO-A5 bone cells and compared to light-cured silorane and three commercial bone cements, Osteobond, Palacos, and Simplex™ P (Figure 2.10a and 2.10b).³⁷ All of the silorane formulations, regardless of the type of glass or filler modification, were shown to be non-toxic. By comparison, toxicity was observed in each of the commercial bone cements. The DY5-1TOSU silorane bone cement exhibited less than 5% dead cells, while each of the commercial bone cements had greater than 14% dead cells. A statistically significant decrease in cell number was observed for the silorane-based bone cements compared to control; however, this trend was not observed in the percent dead cells ($p < 0.05$). This result likely arises due to a lack of cell adherence to the bone cement surface. Additionally, silorane bone cement may support bone formation as evident by *in vitro* alkaline phosphatase activity and mineralization.²⁸

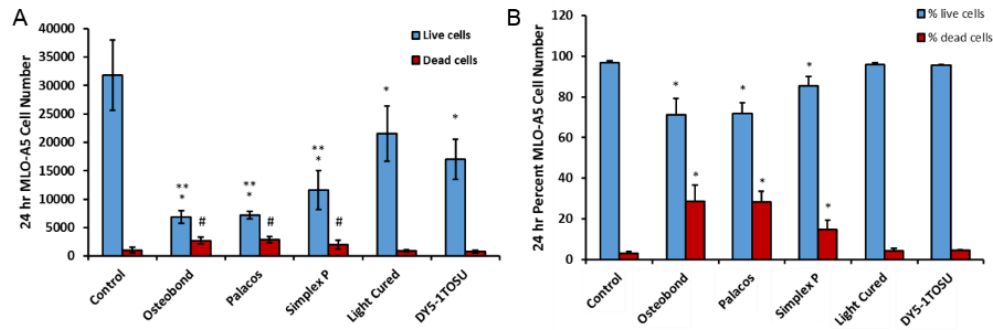


Figure 2.10. Biocompatibility of DY5-1TOSU silorane bone cement *in vitro*. (A) Effect of bone cements on cell number (*p<0.01 vs control; **p<0.05 vs silorane bone cements; # p<0.05 vs control and silorane bone cements). (B) Effect of bone cements on percent live and dead cells (*p<0.05 vs control and silorane bone cements).

Mechanical Properties

As this material is intended for use in weight-bearing applications (i.e., anchoring knee implants), it must possess appropriate strength to withstand the stresses exerted on the joint during normal use. Minimum thresholds have been set by the International Standard Organization (ISO 5833, Implants for surgery — Acrylic resin cements) for the following static tests: flexural strength, flexural modulus, and compressive strength. Since no toxicity was observed in any of the filler formulations, mechanical testing commenced. The results are summarized in Table 2.2.

Table 2.2 Summary of the effects of the surface modified glass fillers on the material properties of the silorane bone cement. The ISO 5833 standard is given as a reference.³⁷

	ISO 5833 Standard ⁴⁷	M12-3TOSU	M12-ECHE	DY5-3TOSU	DY5-ECHE	DY5-1TOSU	Simplex™ P
Exothermicity (°C)	≤90	26 ± 0.5	26 ± 0.5	26 ± 0.5	26 ± 0.5	26 ± 0.5	61.6 ± 3.7
Handling time (mins)	3-15	8-10	8-10	8-10	8-10	8-10	6-10
Flexural modulus (GPa)	≥1.8	4.3 ± 0.2 ^b (n=4)	3.1 ± 0.09 (n=3)	3.3 ± 0.4 ^c (n=7)	3.0 ± 0.2 (n=6)	3.3 ± 0.2 (n=2)	2.4 ± 0.2 (n=10)
Flexural strength (MPa)	≥50	46 ± 4 ^b (n=4)	41 ± 4 (n=3)	37 ± 8 ^c (n=7)	36 ± 5 (n=6)	59.5 ± 0.1 (n=2)	61 ± 3 (n=10)
Compressive strength (MPa) ^a	≥70	92 ± 7 (n=9)	83 ± 18 (n=4)	88 ± 15 (n=10)	91 ± 8 (n=7)	85 ± 4 (n=10)	72 ± 4 (n=8)
Cytotoxicity (% cell death)	n/a	<5%	<5%	<5%	<5%	<5%	15%

^aMaximum Compressive Strength. ^b0.56%LMC, 59.99% filled. ^c0.61%LMC, 60% filled.

Pullout Strength

In addition to assessing the flexural and compressive strengths, the strength of the bone-cement interface was evaluated using a pullout method. The cements were evaluated both in a mimic system and *ex vivo*. For the mimic system, no differences were observed for any of the silorane cement formulations (Figure 2.11).³⁷

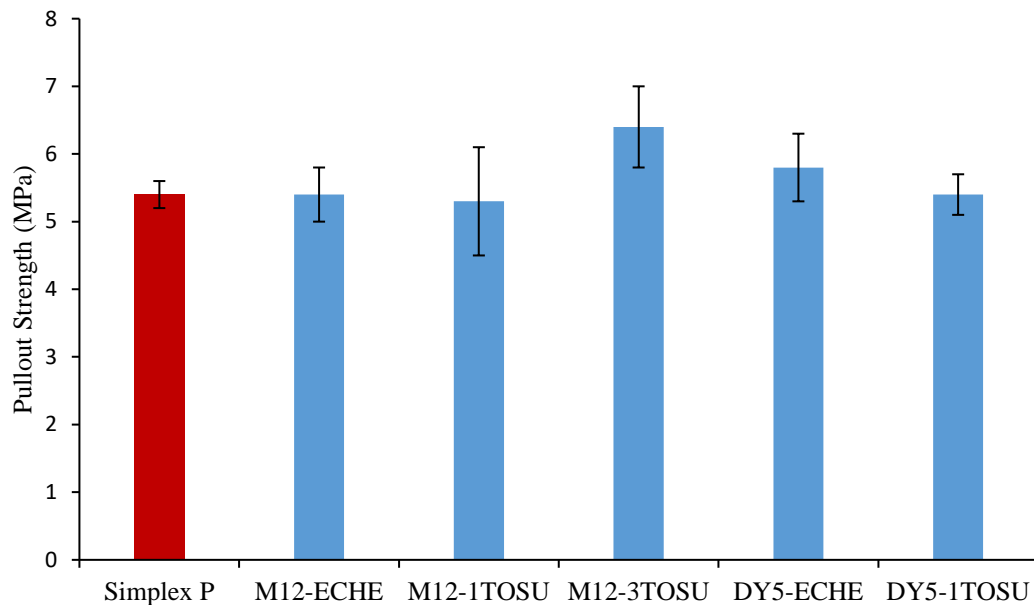


Figure 2.11. Mimic pullout strengths of different glass-filled silorane formulations.

While the silorane formulations displayed ideal pullout strengths *in vitro*, a substantial decrease in strength was observed *ex vivo*. The results are shown in Figure 2.12. The pullout strength was significantly reduced for four out of the five tested silorane cement formulations ($p < 0.05$). This was the first indication that moisture negatively impacts the material's mechanical properties.

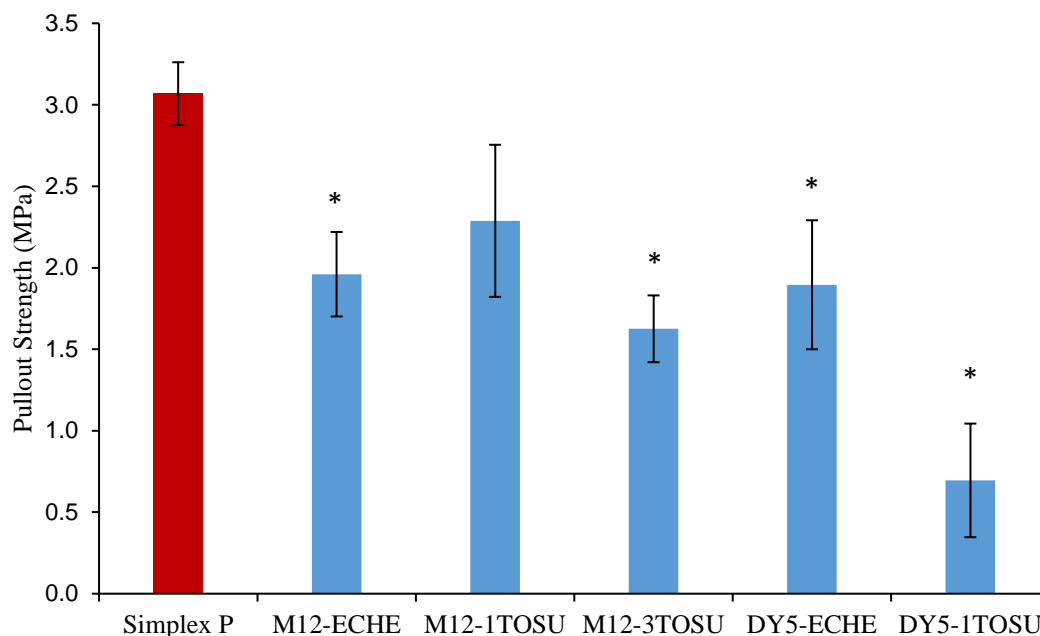


Figure 2.12. *Ex vivo* pullout strength of silorane formulations compared to Simplex™ P (* $p < 0.05$).

Silorane Moisture Investigation – Drying

In order to understand the effect of moisture on this system, the mechanical strength was evaluated for SilMix with varying concentrations of water. The water content was determined by Dr. Thomas Schuman using a Karl-Fischer titration. The saturated material was associated with reduced mechanical strength, slower polymerization and a decreased degree of cure.⁴⁸ Therefore, SilMix was dried *via* an azeotropic distillation (toluene-water). The dried samples yielded higher degrees of curing and improved mechanical strength. However, some water in the system is required for an improved degree of conversion in cationic polymerizations.^{48,49} This was apparent in the differences in the degree of cure between the dried and ultra-dried samples, although the dried sample did display slightly lower mechanical

strength than the ultra-dried samples. Therefore, the ideal water concentration was determined to be ~0.03%.⁴⁸ It was water concentration in the as-synthesized SilMix resin (0.18%) was close to the saturation point (0.19%).⁴⁸ Ultimately, 9,9-diethyl-1,5,7,11-tetraoxaspiro[5.5]undec-3-yl)methyl]trimethoxysilane (TOSU, **81**) surface-modified yttrium aluminosilicate (DY5) glass filler, was chosen based on the cement’s biocompatibility and similar mechanical properties to PMMA-based cement.

In Vivo Pullout Testing

Based on the findings from Dr. Schuman and favorable *ex vivo* results, three DY5-1TOSU silorane cement formulations, DY5-1TOSU (60% filled), DY5-1TOSU dried (60% filled), and DY5-1TOSU 65% dried (65% filled), were investigated *in vivo*. The percent filled is with respect to filler volume and dried is in reference to the water content (~0.03%) of the SilMix prior to mixing. The composition of these three formulations is listed in Table 2.3.

Table 2.3. Composition of silorane formulations tested *in vivo*.

	%LCSM	%LMC	%Filler
DY5-1TOSU (60% filled)	39.68	0.32	60.00
DY5-1TOSU dried (60% filled)	39.68	0.32	60.00
DY5-1TOSU 65% dried (65% filled)	34.60	0.40	65.00

Additionally, a 65% dried, dipped sample was included in attempts to improve the rod-cement interface. Previously we have shown that drying the resin results in improved mechanical properties.^{39,40} Fifteen thirteen-month-old rats were operated on under aseptic conditions and

a dried titanium rod (1.5 x 22 mm) was inserted into each cement-filled femur (n=3/formulation). One-week post-operation, the animals were sacrificed and the femurs harvested and tested using an Instron 5967. The dried formulations showed improved pullout strength compared to the as-synthesized formulations (Figure 2.13). Furthermore, increasing the filler content to 65% resulted in comparable pullout strength to commercial Simplex™ P bone cement (4.4 ± 0.9 MPa and 4.1 ± 1.3 MPa, respectively).³⁷

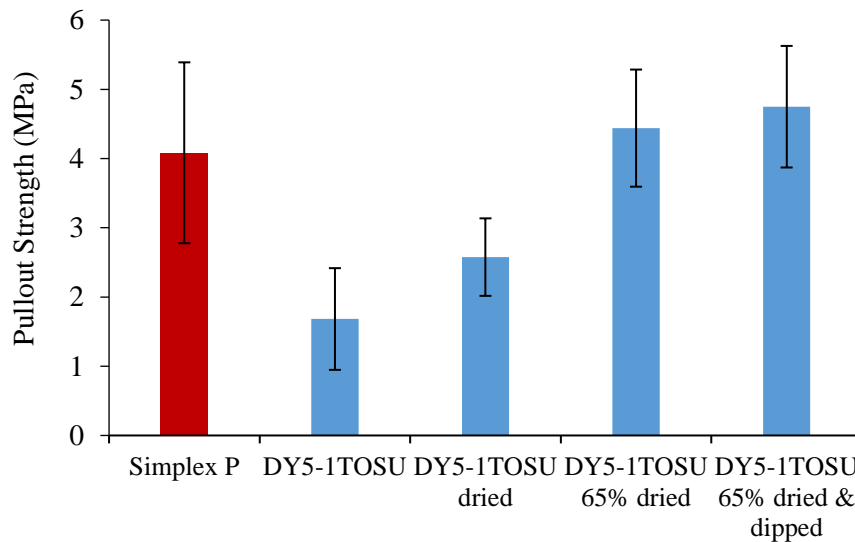


Figure 2.13. Effects of moisture and percent filler on pullout strengths of dried DY5-1TOSU bone cement one-week PO.

While drying the resin prior to use led to improved pullout strengths, no difference was observed between the dried and dried, dipped 65% DY5-1TOSU filled materials (4.4 ± 0.8 MPa and 4.7 ± 0.9 MPa, respectively). Since no enhancement in the cement-rod interface was observed with the dry, dipped material, the decision was made to move forward with the dried,

65% filled material. The next step was to evaluate the material over an eight-week period and the surgeries were performed as described above. It was found that the silorane formulation exhibited comparable pullout strength to Simplex™ P (Figure 2.14 and Table 2.4).

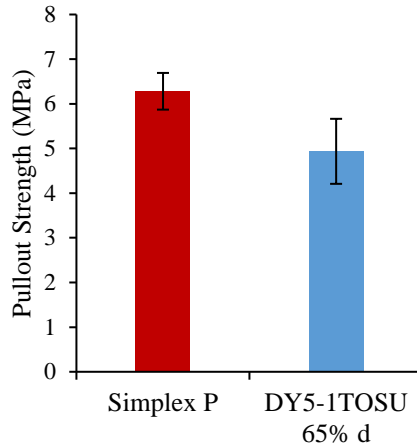


Figure 2.14. Pullout strength of dried 65% DY5-1TOSU silorane and Simplex™ P bone cements eight-week PO.

Table 2.4. Average *in vivo* rat pullout strength – 8 wk PO.

	Average Pullout Strength (MPa)
Simplex™ P	6.3 ± 0.4
Dry, 65% DY5-1TOSU Silorane	4.9 ± 0.7

Summary

Commercial PMMA-based bone cements are the “gold standard” for fixing and anchoring implants in joint replacements. Although these cements are mechanically sound, they have several limitations. These include high curing temperatures, monomer toxicity, and

a lack of biocompatibility to name a few. As a result, alternative bone cements have been developed.

We have developed a silorane-based biomaterial that demonstrates none of the drawbacks typical of commercial bone cements, such as a high exotherm and monomer toxicity. Furthermore, the silorane biomaterial has been shown to have improved biocompatibility and less shrinkage in comparison to commercial PMMA bone cements.^{7,9} Of the compositions tested, the dried, 65% DY5-1TOSU filled formulation was identified as an appropriate alternative to PMMA-based bone cements based on its mechanical strength. The next step was to investigate this material in a large animal model. As this would require large amounts of material, the issues with the production of SilMix needed to be addressed first.

Results and Discussion

Synthesis and Optimization

While the silorane biomaterial has shown promise as an alternative to PMMA-based bone cements, improvements in the synthesis and purification of the silorane monomers are still required for large scale applications. Synthesis and purification of the PHEPSI monomer are relatively straight forward with yields averaging between 40-50%. As a result, our efforts were focused on the CYGEP monomer. CYGEP production has been challenging due to low monomer yields (10-20%), a time-intensive purification process (>36 h), and slight variations between batches.

As mentioned previously, CYGEP was synthesized using an adapted procedure from Aoki.³¹ However, in contrast to Crivello's reported synthesis, our CYGEP monomer routinely

had, extraneous peaks present at 4.6 and 0.15 ppm in the ^1H NMR spectrum, which we assumed to be an impurity.⁵⁰ This impurity was determined to be a small amount of byproduct, either the di- or tri-substituted CYGEP monomer (Figure 2.15).³³ Therefore, attempts to synthesize the pure tetrasubstituted CYGEP were made. The concentration and preparation (commercial vs. in-house) of Lamoreaux's catalyst were altered in an effort to push the reaction to completion, thus eliminating the Si-H peak (Figure 2.16). The results are provided in Table 2.5. For each of the samples tested, the catalyst was added until an exothermic reaction occurred.

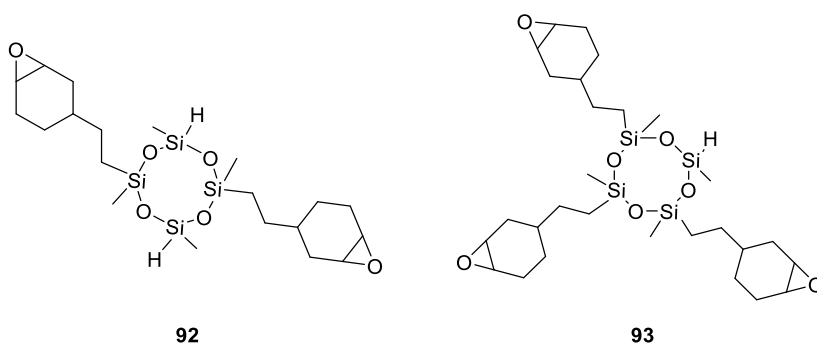


Figure 2.15. Proposed by-products of the CYGEP synthesis.

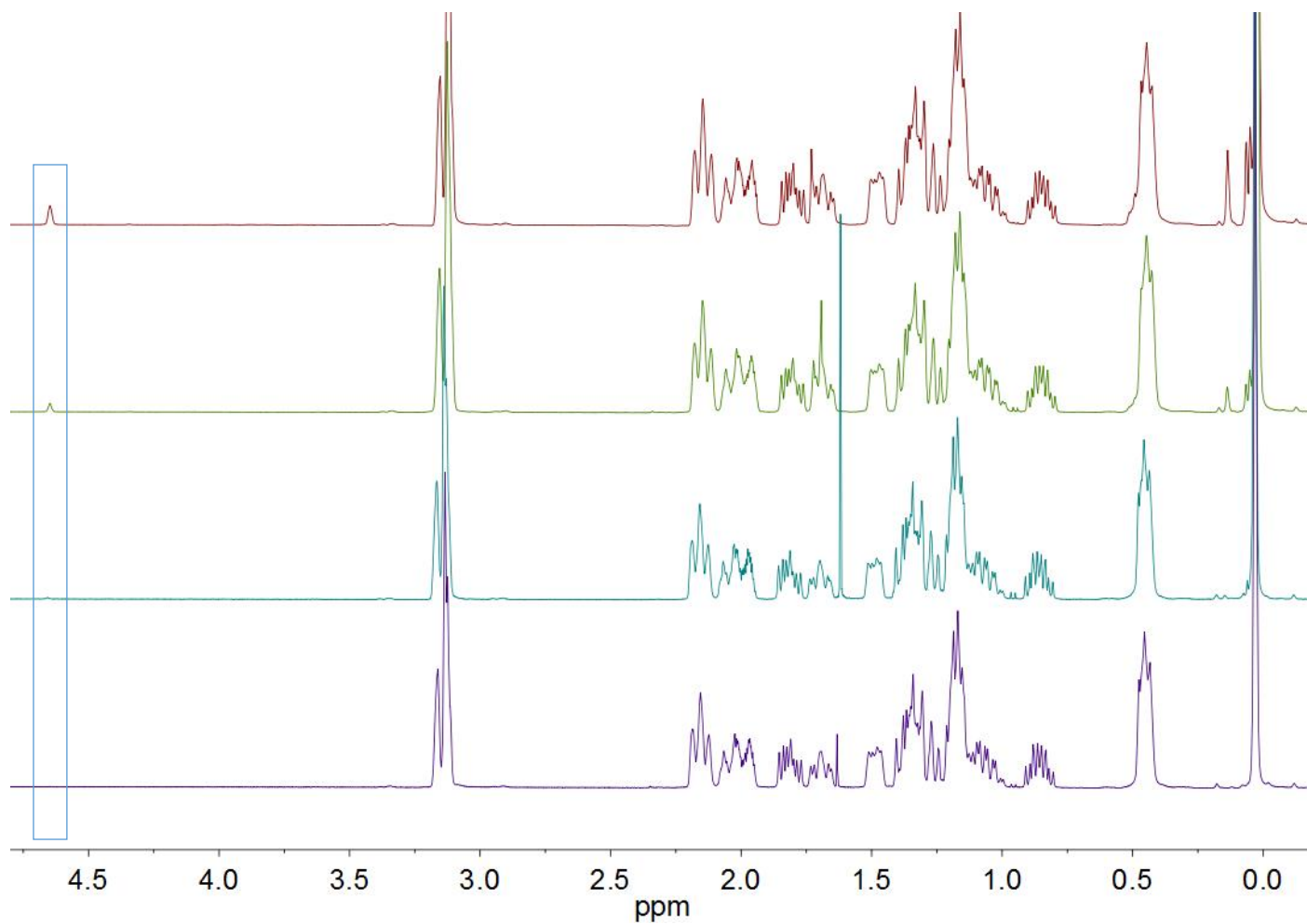


Figure 2.16. ^1H NMR spectra of our attempts to eliminate the di- and tri-substituted CYGEP byproducts. The Si-H peak (4.6 ppm) is highlighted in the blue box.

Table 2.5. Attempts to obtain pure tetrasubstituted CYGEP.

Trial	Lamoreaux's Catalyst	Conc.	Volume LMC (mL)	4.6 peak present	Polym.
1	Gelest	0.79 w/v%	1.3	Y	N
2	Gelest	1 v/v%	1.5	Y	N
3	Gelest	2 v/v%	0.75	N	N
4	Gelest	Conc.	0.07	N	N
5	In-house	0.5 w/v%	0.24	N	N
6	In-house	0.79 w/v%	0.21	N	N

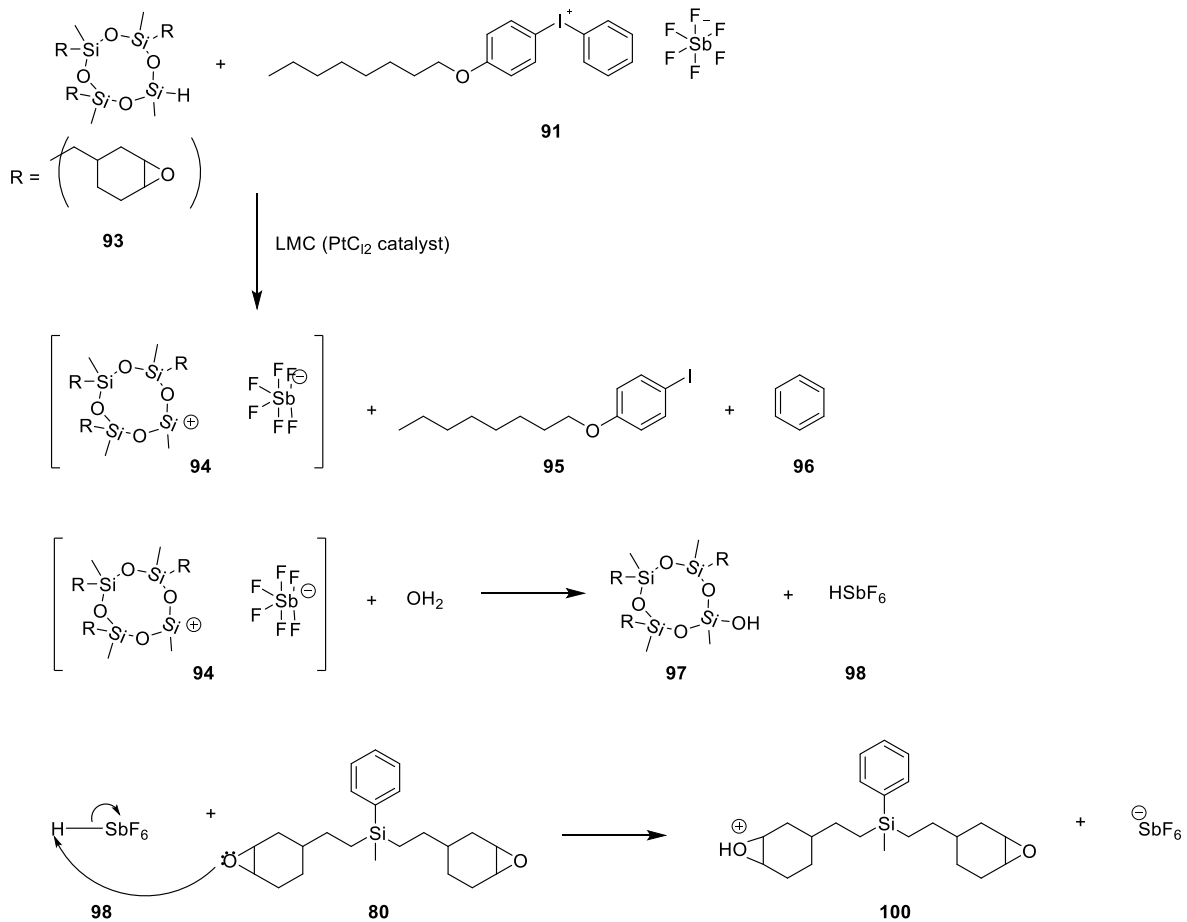
*Polymerization was defined as passing the Gillmore Needle Test at 1 h.

Increasing the catalyst concentration when using the commercial catalyst produced the desired tetra-substituted CYGEP monomer as judged by ^1H NMR spectroscopy, whereas similar results were observed with lower concentrations of the in-house catalyst. As expected, running the reaction to completion led to an improvement in the average overall yields, which were up to ~31% from ~15%. In addition, the use of in-house catalyst led to several differences as compared to the commercial Gelest samples including fewer byproducts (1 vs. 3) and less catalyst required for the reaction to proceed. These differences can be explained by the difference in Pt concentration between the two samples. Despite the fact the Pt concentration of our in-house catalyst has not been determined, a comparison can still be made between the concentrations of the two. The Gelest LMC (2-2.5% Pt) is a light yellow, whereas the in-house LMC is a dark black/brown suggesting it is more concentrated than its commercial counterpart. Surprisingly, once the tetra-substituted monomer was obtained, the samples failed to polymerize. This phenomenon was not limited to samples in which no Si-H peak was present. Therefore, we set out to identify the cause of this polymerization inhibition.

Investigation of the Role of Si-H in Polymerization

Each of the CYGEP monomers was tested with the same PHEPSI monomer, which had successfully passed the Gillmore Needle Test. The light initiation system and catalyst were tested with a good SilMix and polymerization occurred without an issue. After verifying the polymerization failure was not a result of the light initiation system or PHEPSI monomer, our attention turned to the role the Pt catalyst plays in the curing mechanism. While the exact mechanism has not been determined, Crivello had proposed that a small amount of Si-H is necessary for polymerization to occur *via* a platinum catalyst.⁵¹ It was proposed that the Pt catalyst reacts with the hydrogen on the silane to reduce the phenyliodonium salt and form silicenium ions.⁵¹ The latter then reacts with water present in the monomer to generate a Bronstead acid, which is then available to attack the epoxide to start the cationic ring-opening polymerization (Figures 2.17 and 2.18).⁵¹

Initiation



Propagation

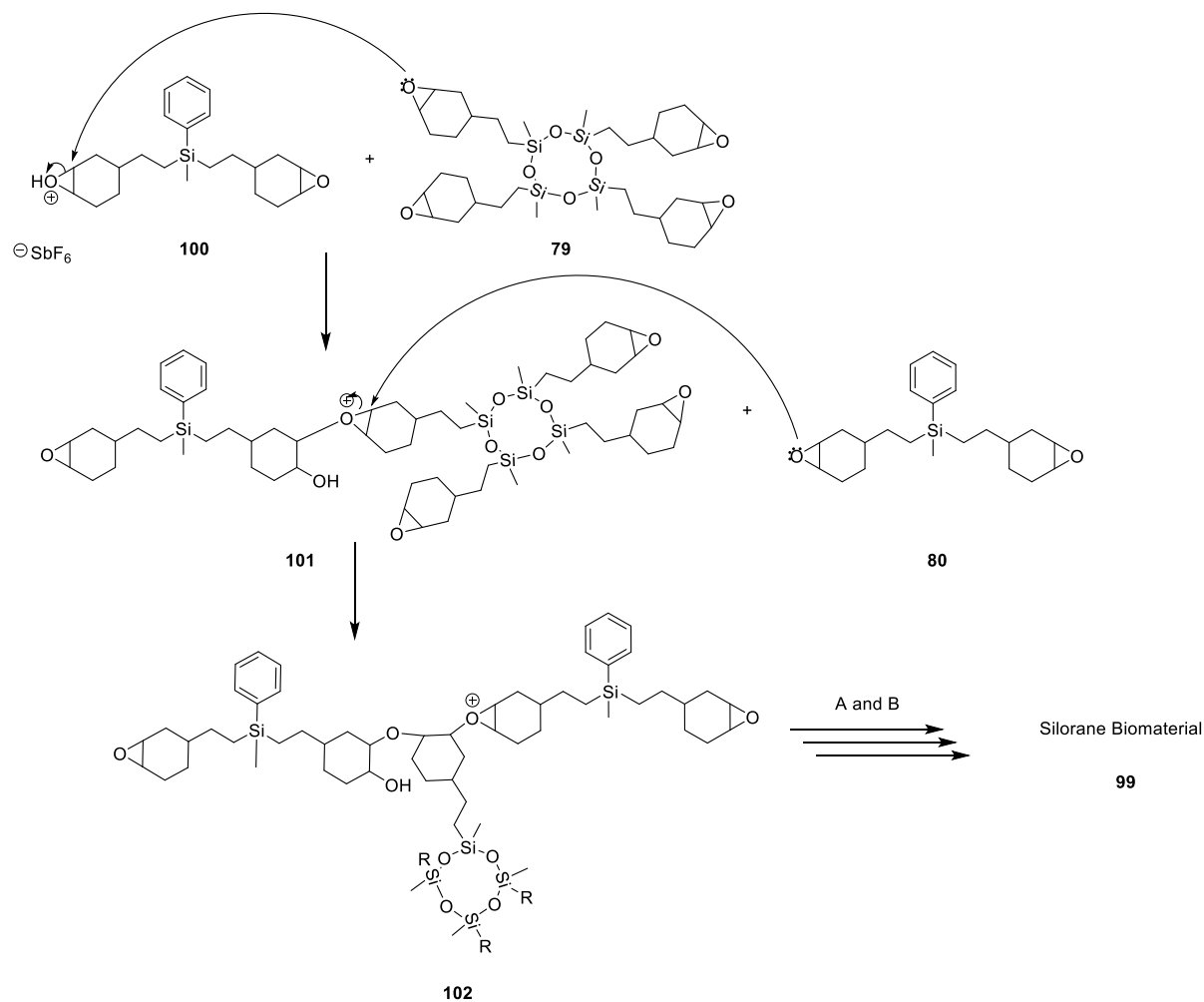


Figure 2.18. Proposed silane reduction of the phenyliodonium salt in our monomer system.

In order to investigate the role Si-H plays in the polymerization of our dual-cured system, the amount of Si-H present was determined by the ratio of Si-H (4.6 ppm) to the epoxide (3.16/3.12) and methyl (0.03) peaks obtained from the ^1H NMR spectra. This ratio was then used to see if a general trend could be found between the ratio of Si-H present in the CYGEP monomer and its likelihood of polymerizing within the h cutoff. These results can be found in Table 2.6. With a few exceptions, a general trend was observed in which samples with

a ratio of Si-H:epoxide \geq 1:250 polymerized. The time to polymerization was not affected for samples that fell within this ratio, whereas it was delayed for those that fell outside. To maintain uniformity, a maximum Si-H:epoxide threshold of 1:80 was set.

Table 2.6. Integration of CYGEP ^1H NMR spectra with respect to the Si-H peak.

CYGEP Batch	4.6 ppm	3.16/3.12 ppm	0.03 ppm	Polym.*	LMC Batch
111	-	1	1.44	Y	21
114	-	1	1.5	Y	21
115	-	1	1.41	Y	22
116	-	1	1.44	Y	22
125	-	1	1.43	Y	22
133	-	1	1.16	Y	24, 22
136	-	1	1.22	N	22
138	-	1	1.29	N	22
139	-	1	1.26	N	25, 22
3M	-	1	1.48	N	13
UN59	-	1	1.29	N	29
UN60	-	1	1.29	N	29
70	1	1582.04	1966.72	N	14 sv
72	1	1476.03	1863.84	N	14 sv
UN63	1	1315.63	1624.53	N	33
UN83	1	1092.21	1340.64	N	33
67	1	1073.97	1342.45	N	14 sv
UN91	1	983.64	1256.14	N	33
140	1	752.18	934.59	N	22
148	1	750.23	913.82	N	33
148-D	1	699.12	885.17	N	33
UN90	1	557.72	717.92	N	37
UN84	1	548.39	696.5	N	33
UN77	1	538.24	683.53	N	33
UN87	1	502.1	631.13	N	33
142	1	471.95	571.56	Y	22
107	1	371.28	543.78	Y	21
UN65	1	340.13	404.1	Y	33
109	1	335.88	483.49	Y	21

80	1	331.28	431.5	Y	19
108	1	324.59	468.68	Y	21
UN88	1	303.46	385.87	N	33
110	1	287.21	416.39	Y	21
112	1	285.42	362.91	N	22, 21
150	1	247.37	299.28	N	33
153	1	242.11	304.86	N	33,34
84	1	232.96	293.25	Y	19
UN80	1	222.7	28.17	Y	33
UN82	1	222.14	280.9	Y	33
UN76	1	216.57	264.52	Y	33
151	1	187.54	225.96	Y	33
85	1	184.29	231.36	Y	19
141	1	179.57	217.77	Y	22
113	1	174.81	220.96	N	21
UN86	1	157.97	200.15	Y	34
UN67	1	154.15	184.75	Y	33
UN-73	1	145.46	175.58	Y	33
UN-74	1	144.74	180.89	Y	33
UN-66	1	138.45	163.13	Y	33
126	1	130.75	195.1	Y	22
87	1	103.2	129.91	Y	19
UN-68	1	101.54	121.3	Y	33
147	1	97.19	115.83	Y	33
143	1	92.83	114.03	Y	24,29
CUN69	1	88.44	101.82	Y	33
CUN75	1	84.9	107.1	Y	33
83	1	83.6	105.2	Y	19
145	1	80.98	95.93	Y	29
88	1	76.15	94.19	Y	19
61/62/64	1	74.26	88.89	Y	29
UN57	1	70.59	95.41	Y	29
81	1	69.48	85.64	Y	19
58	1	67.43	79.4	Y	13,14,29
UN78	1	64.1	80.58	Y	33
146	1	57.67	67.57	Y	29
UN85	1	56.84	72.23	Y	34
86	1	55.91	69.94	Y	19
82	1	54.16	66.58	Y	19
79	1	47.82	58.71	Y	19

UN81	1	42.65	54.17	Y	33
UN79	1	34.96	44.35	Y	33
UN70	1	33.26	35.55	Y	33
63	1	20.21	24.99	Y	33

*Polymerization was assessed using the Gillmore Needle Test.

This analysis also exposed differences between in-house catalyst samples. Darker (black), more viscous in-house samples were able to catalyze samples with a lower Si:H:epoxide than those that were lighter (brown) and less viscous. This was attributed to the presumably higher Pt concentrations in the darker samples. To further verify that a lower Pt concentration increases the polymerization time, a side-by-side comparison of in-house and commercial (2-2.5% Pt) LMCs was performed (Table 2.7).

Table 2.7. In-house and commercial LMC polymerization results.

LMC	% LCSM	% Filler	% LMC	Polymerization time
In-house	39.68	60.00	0.32	45 min
Commercial (Gelest)	39.68	60.00	0.32	>20 h

No change in consistency was observed for the commercial LMC sample until after 20 h. This is in stark contrast to the in-house sample, which polymerized in 45 min. These findings support the differences found between in-house LMC samples.

Furthermore, since it was proposed that the hydrogenated silicon only contributes to the chemical cure portion of our initiation system, monomers that failed to polymerize utilizing our dual-cure system were rerun using the light cure system to ensure there were no underlying

polymerization problems with the monomers. As expected, these samples polymerized without issue.

CYGEP Optimization

Once the polymerization issues were resolved, our focus turned to improving the overall yield, which was approximately 15%, on average, for acceptable samples. Attempts to optimize the purification step proved futile. Therefore, our efforts turned to improving the efficiency of the reaction. First, the effects of the reaction time on the percent yield were investigated. The results are given in Table 2.8. It was found that increasing the reaction time improved yields, albeit only slightly. Granted, some of the increase may stem from improved purification between batches. Ultimately, the reaction time was increased to one h due to the improved yields and shorter reaction time.

Table 2.8. Effects of reaction time on CYGEP yield.

Entry	Heating before LMC addition	Heating after LMC addition	% Yield
1	30 min	15 min	19.3
2	30 min	45 min	14.5
3	30 min	1 h	25.5
4	30 min	1.5 h	17.6
5	30 min	2.5 h	21.4
6	30 min	12 h	28.7

Despite the increase in reaction time, only slight improvements in the overall yield were observed. Since the catalyst concentration had already been optimized, 0.79 w/v%, the effects

of hydrous versus anhydrous toluene for the dilution of the commercial LMC was examined (Table 2.9). The use of hydrous toluene led to a two-fold increase in the average yield (20.2% vs. 40.2%). This was a welcomed advance. The last reaction condition to be examined was the rate of catalyst addition. No standard rate had been determined and as such varied among reactions. Three different rates of addition were evaluated based on our previous experience. Increasing the rate to 0.5 mL every 5 sec resulted in a ~1.5 times increase in percent yield compared to the previously used 0.2 mL per 5 sec (Table 2.10). Interestingly, introducing the catalyst all at once resulted in comparable yields to 0.5 mL samples.

Table 2.9. Effect of solvent on CYGEP synthesis.

<u>Toluene</u>	<u>Average %yield</u>
Anhydrous	20.2
Hydrous	40.2

*All samples passed polymerization.

Table 2.10. Optimization of the rate of LMC addition.

<u>Rate of LMC Addition</u>	<u>Average %yield</u>
0.2 mL/5 sec	26.8
0.5 mL/5 sec	39.7
1 mL/2 min	37.8

*All samples passed polymerization.

Summary

With few exceptions, the tetrasubstituted CYGEP monomer samples failed to polymerize. Upon closer inspection, it was found that a minimum threshold of silane was

necessary in order for polymerization to occur using the dual-cured system. However, the absence of silane had no effect on the light initiation system.

An optimized procedure for the production of CYGEP was identified, which consisted of changing the carrier solvent and rate of addition of the catalyst. First, the impact of the solvent carrier on the efficiency of the catalyst was investigated. The use of hydrous rather than anhydrous toluene resulted in an increased yield of 20%. Second, the addition of the catalyst at a rate of 0.5 mL every 5 sec until an exothermic reaction was observed increased the overall yield 1.5-fold. This combination generated a two-fold increase in the overall percent yield for CYGEP. Therefore, we were able to increase CYGEP production to approximately 30 g of dried SilMix per month. With the issues in SilMix production addressed, the next step was to assess the material in a large animal model.

In Vivo Animal Studies

After identifying an ideal silorane formulation (33.94% LCSM, 0.40% LMC, 63.77% DY5-1TOSU filler) was identified and successfully demonstrated in a small animal model (rats), the next step was to test this formulation in a large animal model. For this, a swine model was chosen due to their anatomical and physiological similarity to humans. The study was run for eight weeks in order to provide a more accurate depiction of how the material would act *in situ* as well as the effects of the cements on osteogenesis. For this study, fourteen female Landrace pigs were used. Either Simplex™ P (n=7) or the silorane cement (n=7) was injected into the right femoral intramedullary canal and a titanium rod (100 mm x 6.5 mm) inserted. These surgeries were performed at the National Swine Resource and Research Center in

Colombia, MO by Dr. Donna Pacicca. The pigs were sacrificed eight weeks post-operation (PO). The operated and non-operated femurs were harvested and histological samples were taken from each of the major organs as well as from the femurs. Simplex™ P was used per the manufacturer's directions.

While we had extensive experience using these materials both *in vitro* and *in vivo*, in a small animal model, we had never worked with the material on the scale required for the pig studies (Table 2.11).

Table 2.11. Amount of silorane material required per animal.

Animal Model	SM/animal
Rat	4 g
Pig	50 g

Based on our previous experience and quality control testing, it was known that larger quantities of the silorane biomaterial polymerize faster. However, during our preliminary testing, this was not an issue, and the material routinely polymerized in 15-30 min. The next modification was the development of a delivery device. For the rat studies, a dental syringe was used, but this was impractical for pigs due to the size difference.

A variety of delivery devices were explored in conjunction with the surgeon. Ultimately, a 30 mL luer lock syringe was identified as a possible delivery device. The luer lock was removed and a 145 mm of Tygon tubing was attached based on the diameter for extrusion and the ability to deliver the cement into the marrow cavity. While test trials had been performed prior to surgery without issue, there were problems encountered during

surgery. There was one failed silorane delivery due to premature polymerization of the cement in the syringe. This failure was attributed to the pressure exerted on the cement as it was being extruded. Therefore, care was taken for the addition and mixing of the cement as well as the delivery for other silorane samples.

Complications were not only observed for the silorane formulations, but were also observed in the PMMA samples. In one of the Simplex™ P pigs, the anesthesiologist first noticed the blood pressure plummeted followed by the bluish hue of the tongue (a likely sign of hypoxia) and suspended the surgery until the pig was stabilized. Consequently, no Ti rod was inserted as the cement had begun to set by time the pig was stable, but the pig survived. Although PMMA-based bone cements are commonplace in TJA procedures, rare complications such as bone cement implantation syndrome or BCIS have been reported.^{52,53} BCIS, as defined by Donaldson *et. al.*, “is characterized by hypoxia, hypotension or both and/or unexpected loss of consciousness occurring around the time of cementation, prosthesis insertion, reduction of the joint or, occasionally, limb tourniquet deflation in a patient undergoing cemented bone surgery.”⁵³ While the cause of BCIS has not been identified, it has been proposed that it arises as a result of emboli (bone, marrow, or fat), displaced by the high pressure generated upon cement injection and implant insertion, traveling to the lungs and heart.^{53,54} As all of our previous *in vivo* studies had utilized rats and the blood pressure was not monitored, we had never experienced this complication. Increased pressure has been implicated in BCIS, it was only detected in the one Simplex™ P sample even though the same delivery device setup and surgical technique were utilized for both cements.

Over the eight-week period, four animals died or were sacrificed. Two were sacrificed shortly after surgery due to cement being found outside the marrow cavity, one was sacrificed after breaking its non-operated femur, and one died coming out of anesthesia following the alizarin red injection. The latter two were lost a week before the end of the study, so it was decided to include them in the pullout testing. Due to the problems that arose during surgery and the animals lost over the course of the study, the sample size was reduced for both Simplex™ P (n=5) and silorane (n=7).

Histology

After sacrificing the animals, the vital organs (kidneys, liver, lungs, and heart) were visually inspected by a veterinarian for any pathological changes. There were no noticeable changes observed. Histological samples confirmed the visual observations with no toxicity reported in any of the silorane or Simplex™ P specimens. Furthermore, an increase in mineralization rate was observed for silorane samples compared to Simplex™ P, similar to the results observed in the rat model.

Pullout Testing

Pullout testing was to be performed using the same method employed for the rat model in which the distal end (knee) of the femur would be removed to expose the titanium rod. However, while preparing the first few femurs, we realized that the rods were deeper than expected and a substantial portion of the condyles would need to be removed in order to expose the Ti rod for pullout testing. This resulted in the loosening of the rod prior to testing.

Therefore, the decision was made to expose the Ti rod from the mid-shaft as it was expected that the bulk of the strength would come from bone regrowth and the potential osseointegration. The bone growth was anticipated to be near the growth plate (distal end of the femur). Due to the change in femur preparation and the rods not being perfectly centered in the marrow space, the original pullout apparatus could no longer be used, so a new pullout device was developed with the help of Dr. McIff at KUMC and Dr. Schumann at Missouri Science and Technology. A side-by-side comparison of the old and new pullout apparatuses is illustrated in Figure 2.19. As a result of this modification, the condyles had to be trimmed to fit within the cylindrical base. The detailed updated femoral preparation and pullout procedures can be found in the Materials and Methods section. The final sample size was three and four for silorane and Simplex™ P, respectively.

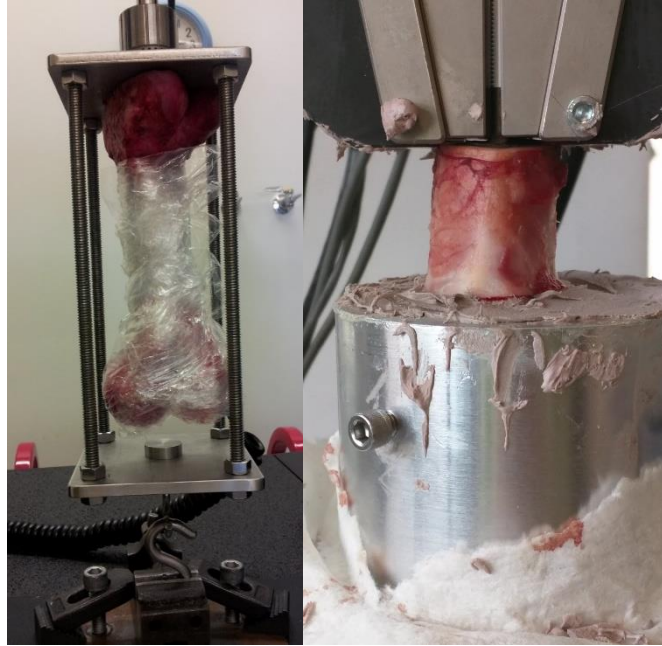


Figure 2.19. Side-by-side comparison of the old and new pig pullout apparatuses.

Once the Ti rods were exposed, the pullout tests were performed. All of the Simplex™ P samples failed at the rod/cement interface. By comparison, one of the silorane samples failed at the rod/cement interface and the other two failed at the cement/bone interface. While there was some variability between the pullout strengths of Simplex™ P and silorane samples, no significant differences were found ($p > 0.05$, Tables 2.12 and 2.13).

Table 2.12. Pig pullout strength.

Pig ID	Cement	Failure ^a	Force (N)
1	Silorane	C/B	508
2	Silorane	R/C ^b	432
3	Silorane	C/B	405
4	Simplex TM P	R/C ^b	770
5	Simplex TM P	R/C	602
6	Simplex TM P	R/C	444
7	Simplex TM P	R/C	412

^aR – rod, C – cement, B – bone. ^bEstimated location of failure.

Table 2.13. Average pig pullout strength.

Cement	Average Force (N)
Silorane	448 ± 53
Simplex TM P	557 ± 164

It was observed that the cement did not uniformly fill the marrow space and thus, the surface area of the rod in contact with the cement varied both within and between cement groups. This variation was first evident in the x-rays of the harvested femurs and was further confirmed after a closer look at the marrow space surrounding the Ti rod (Figures 2.20-2.22). This also explains the rod loosening observed in the first few samples (exposure from the distal end). These discrepancies are not uncommon as it is difficult to consistently fill the marrow space due to the spongy nature of the marrow space and size. By comparison, the entire marrow space was reamed and irrigated allowing for more consistent cement filling in the rat femur.



Figure 2.20. X-rays of Simplex™ P (top) and silorane (bottom) pig femurs. The arrows indicate cement location.

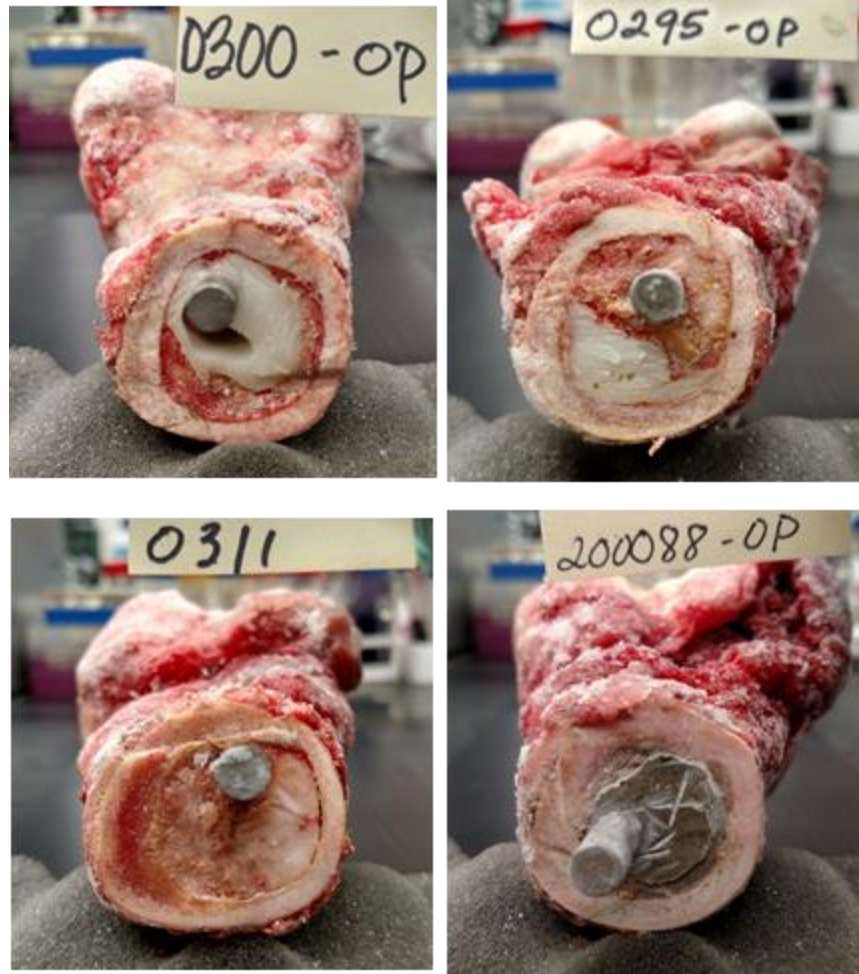


Figure 2.21. Photographs of the titanium rod exposure at the midshaft illustrating the variability in filling the marrow cavity within and between Simplex™ P (top) and silorane (bottom) samples.



Figure 2.22. Longitudinally cut femurs displaying differences in cement filling between silorane (left) and Simplex™ P (right).

Summary

The 65% DY5-1TOSU silorane-based cement was found to be a suitable alternative to the commercial PMMA-based bone cement, Simplex™ P. Despite the lack of uniform cement of filling, comparable pullout strength *in vivo* was obtained. This material also demonstrated no toxicity systemically or locally. Furthermore, in agreement with the small animal model, the silorane-based cement shows signs of osteogenic potential. Based on the success of these trials and the difference in chemistry, it was anticipated that this material would be an ideal candidate for antimicrobial-laden bone cement applications. These applications and the investigation of our silorane biomaterial as an antimicrobial delivery device are discussed in the next chapter.

Materials and Methods

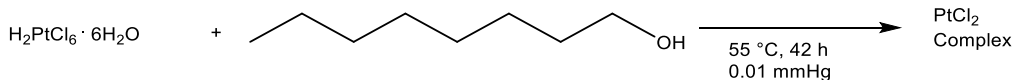
General Experimental Details. ^1H and ^{13}C NMR spectra were recorded on a Varian AC 400 NMR spectrometer operating at 400 MHz and 100 MHz, respectively. Column chromatography was performed with irregular 60 Å silica gel (20-45 μm ; Silicycle Inc.). TLC was performed on plastic backed silica gel 60 Å with F254 indicator. Spots were visualized with UV light (254 nm, PHEPSI) and iodine (CYGEP). Solvents, hexanes ($\geq 98.5\%$; Fisher Scientific), ethyl acetate ($\geq 99.5\%$; Fisher Scientific), acetonitrile ($>95\%$; Alfa Aesar), methanol ($>99.8\%$; Alfa Aesar), and anhydrous toluene (99.8%; Sigma Aldrich), were used as supplied. 1-Octanol ($\geq 99\%$; Sigma Aldrich), 4-vinyl-1-cyclohexene 1,2-epoxide (98%; Sigma Aldrich), chloroplatinic acid hexahydrate ((38-40% Pt) (99.9%-Pt); STREM), phenylmethylsilane ($>95\%$; Gelest), and 2,4,6,8-tetramethylcyclotetrasiloxane (99%; Alfa Aesar) were used without further purification. Wilkinson's catalyst (99%; STREM), platinum-octanal/octanol complex (2-2.5% Pt in octanol; Gelest), *p*-(octyloxyphenyl)phenyliodonium hexafluoroantimonate ($\geq 95\%$; Gelest), camphorquinone (97%; Sigma Aldrich), ethyl *p*-dimethylaminobenzoate ($>99\%$; Acros), α,α -diphenyl- β -picrylhydrazyl (DPPH) (95%; Alfa Aesar), ascorbic acid ($\geq 99\%$; Fisher), hydroquinone (99%; Alfa Aesar), and 1-methylpiperazine ($>98\%$; Alfa Aesar) were used as received. CDCl_3 and $\text{DMSO-}d_6$ were purchased from Cambridge Isotope Laboratories. SpeedMixersTM (DAC 150FV and DAC 150FVZ-K) were purchased from FlackTek Inc. Rifampin, amphotericin B, and vancomycin, and SmartSetTM were purchased through KUMC. SimplexTM P was purchased from Truman Medical Center. SimplexTM P and SmartSetTM commercial bone cements were prepared according to the manufacturer's instructions.

Synthesis of 2,4,6,8-tetrakis(2-(7-oxabicyclo[4.1.0]heptan-3-yl)ethyl)-2,4,6,8-tetramethyl-1,3,5,7,2,4,6,8-tetraoxatetrasiloxane (CYGEP, 79). CYGEP was synthesized using a modified procedure by Aoki.³¹ A solution of anhydrous toluene (21 mL), 2,4,6,8-tetramethylcyclotetrasiloxane (12.1 mL, 49.9 mmol), 4-vinyl-1-cyclohexene 1,2-epoxide (31.0 mL, 237.7 mmol), and acetonitrile (0.54 mL) were heated at 70 ± 2 °C for 30 min. Commercial Lamoreaux's catalyst (0.79 w/v% in toluene) was added at a rate of 0.5 mL/5 s until an exothermic reaction (~ 135 °C) occurred (approximately 1.5 – 2.0 mL). The reaction was heated for an additional h and then stirred at RT overnight (12 h). Residual solvent and starting materials were removed under reduced pressure. A yellow solution was obtained and subjected to column chromatography (silica gel; eluent: hexanes, followed by 2%, 6%, 8%, and 10% ethyl acetate:hexanes). The appropriate fractions were combined and reduced under vacuum to obtain pure CYGEP as a colorless oil (16.46 g, 22.3 mmol, 45%). ¹H NMR (400 MHz, CDCl₃) δ 0.3 (s, 12H), 0.46 (m, 8H), 0.85-2.16 (m, 36H), 3.13-3.17 (m, 8H) ppm; ¹³C NMR (100 MHz, CDCl₃) δ -0.8, 13.9, 14.0, 14.1, 23.6, 24.0, 24.1, 26.8, 29.3, 29.8, 30.4, 31.5, 31.6, 32.0, 32.1, 35.1, 35.2, 51.9, 52.7, 53.2 ppm.

Synthesis of bis[2-(3{7-oxabicyclo[4.1.0]heptyl})ethyl]methylphenyl silane (PHEPSI, 80). PHEPSI was synthesized from an adapted procedure by Crivello.³² A solution of anhydrous toluene (80 mL), Wilkinson's catalyst (0.04 g, 0.04 mmol), and phenylmethylsilane (11.0 mL, 80.0 mmol) was stirred for 10 min under argon. After which, 4-vinyl-1-cyclohexene 1,2-epoxide (25.2 mL, 193.2 mmol) was added and the solution heated for 24 h at 90 – 95 °C. The reaction mixture was cooled to RT; and the residual solvent and starting materials were

removed under reduced pressure. A dark orange/maroon solution was obtained and subjected to column chromatography (silica gel; eluent: hexanes, followed by 5%, and 10% ethyl acetate:hexanes). The appropriate fractions were combined and reduced under vacuum to obtain pure PHEPSI as faint yellow oil (14.90 g, 40.2 mmol, 50.2%). ^1H NMR (400 MHz, CDCl_3) δ 0.20 (s, 3H), 0.67-0.73 (m, 4H), 3.13-3.17 (m, 4H), 7.32-7.35 (m, 3H), 7.44-7.46 (m, 2H) ppm; ^{13}C NMR (100 MHz, CDCl_3) δ -5.4, 10.6, 10.8, 23.6, 23.9, 25.3, 26.7, 30.1, 30.3, 30.6, 31.5, 32.5, 35.5, 51.9, 52.0, 52.7, 53.3, 127.7, 128.8, 133.7, 138.2 ppm.

Lamoreaux's Catalyst (LMC, 90). Lamoreaux's catalyst (LMC) was prepared using adapted procedure from Lamoreaux and subjected to quality control prior to use.⁵⁵ The reaction scheme is provided below.



Quality Control. ^1H NMR spectroscopy was employed to ensure monomers met or exceeded set purity standards (95.8%). Each monomer was visually inspected for films or color prior to testing. A small sample (~0.8 g) of SilMix containing the monomer to be tested and a corresponding control was mixed for 15 min in a SpeedMixer™. SilMix sample was combined with *p*-(octyloxyphenyl)phenyliodonium hexafluoroantimonate (1.19 wt.%), camphorquinone (0.40 wt.%), and ethyl *p*-dimethylamino benzoate (0.06 wt.%) in a SpeedMixer™ for 15 min. Once the sample was cooled to RT, the DY5-1TOSU filler was added. The filled material was mixed for another 20 min in a SpeedMixer™ and then allowed to cool to RT. At which point,

Lamoreaux's catalyst was added, by weight, with a syringe and hand mixed for approximately 45 s. A small portion of the sample was placed in a Delrin® acetal washer secured to a glass slide with lab tape and the polymerization was evaluated using the Gillmore Needle test. The final composition of quality control sample: 39.68% LCSM, 0.32% LMC, and 60.00% DY5-1TOSU filler.

Gillmore Needle Test. The Gillmore Needle test was performed in 15 min intervals for one h. A ¼ lb needle was gently placed on the sample. If the sample gave under the weight of the needle or if the needle left an indent, the sample was considered to “fail” and was retested 15 min later. Once the sample supported the weight of the ¼ lb needle, a one lb needle was placed on the sample and the sample was assessed in the same manner as the ¼ lb needle. Samples that supported the weight of the one lb needle at or before the h mark were considered to pass.

SilMix Drying. The silorane resin was dried as described by Ranaweera *et. al.*³⁹ NMR tubes and pipettes were dried for 1 h at 200 °C prior to testing. Two large drops of the dried SilMix were added to a clean, dry NMR tube and DMSO-*d*₆ (0.6 mL) was added. The samples were then shaken vigorously until the material was in solution. For each test, a baseline sample of DMSO-*d*₆ (0.6 mL) was prepared simultaneously with the dried sample. ¹H NMR spectrum was taken for each sample and the spectra referenced to DMSO. The DMSO, H₂O, and -CH₂O- peaks were integrated and a ratio of H₂O:SM was determined. The water in the baseline sample was subtracted from the dried SM sample to determine the percent water present in the SilMix sample.

Silorane Pig Sample Preparation. CYGEP and PHEPSI were prepared as previously described. The monomers were combined in a 1:1 ratio by weight (SilMix) and mixed in a SpeedMixer™ for 15 min. Once mixed, SilMix was dried as described by Ranaweera *et. al.*³⁹ A photoinitiation system comprised of *p*-(octyloxyphenyl)phenyliodonium hexafluoroantimonate) (1.19 wt.%), camphorquinone (0.40 wt%), and ethyl *p*-dimethylamino-benzoate) (0.06 wt.%) was combined with dried SilMix in a SpeedMixer™ for 20 min. DY5-1TOSU modified filler was added to the light-cured SilMix (LCSM) and mixed for an additional 20 min in a SpeedMixer™. Lamoreaux's catalyst (LMC) was added with a syringe by weight and hand mixed for approximately 45 s. The material was transferred to a 30 mL syringe and injected into the right femoral cavity of the pig. The final composition of the silorane biomaterial was: 34.60% LCSM, 0.40% LMC, and 65.00% DY5-1TOSU filler.

Femur Preparation for *In Vivo* Pullout Testing. X-rays were used to identify the orientation of the rod and to determine the depth at which to cut the bone. The femurs were removed from the freezer and were cut above the rod at the midshaft. A handsaw and oscillating saw were used to expose approximately 12 mm of the Ti rod from the proximal end. The bone and cement were carefully removed until the desired rod length was exposed with care taken not to damage the rod. After exposing the rod, a cutting guide was secured to the rod using a chuck. The handsaw was then used to produce a level cut perpendicular to the rod. Once the cut was level, the guide was removed and the femur was returned to the freezer. Additionally, the end section of the midshaft was cut in half, placed in PBS solution, and saved for histology.

***In Vivo* Pullout Testing.** The femurs were removed from thawed and brought to RT prior to potting. The condyles were trimmed to size using the pullout fixture as a guide. Any remaining tissue was removed prior to potting and a line at ~5.5 cm from the surgical implant site was drawn around the bone shaft to indicate the potting depth. The remaining bone surface was covered with a paper towel to ensure no Bondo attached to the bone surface in order to obtain preserve histological samples. Bondo was prepared according to the manufacturer's directions (~300 g per sample) and added to the fixture up to the 5.5 cm line. Flat screws were hand tightened to further secure the Bondo and bone in place. Pullout testing was performed 40 mins after potting for each sample. The samples were run on a MTS 858 Mini Bionix II with a 14 kN load cell. The failure detector, sampling frequency, load rate, and displacement limit were set as follows: 25% F_{max} , 100 HZ, 0.25 mm/sec, and 5 mm, respectively.

Statistical Analysis. Statistical analysis was performed using either Student's t-test or one-way ANOVA and Tukey HSD post-hoc. A p-value of <0.05 was considered significant.

CHAPTER 3

SILORANE-BASED BIOMATERIAL AS AN ANTIMICROBIAL DELIVERY DEVICE

Introduction

As mentioned previously, TJAs are on the rise worldwide. In addition to the vast number of TJAs performed each year, the number of revision surgeries is expected to rise. Kurtz *et. al.* predicted a 137% and 601% increase in hip and knee revisions by 2030.⁵⁶ This growth is due in part to an increase in demand from younger patients (<65 years), an aging population, and a finite implant lifetime (on average 10-15 years).⁵⁷⁻⁵⁹ As with any surgery, serious complications, such as prosthetic joint infections (PJIs) or an infection of the bone, implant, or surrounding tissues, can occur. These risks are further compounded when the patient presents with additional risk factors including previous joint replacement surgeries, age (<65), obesity, immune deficiencies, and diabetes.^{57,60-65} PJIs have a relatively low incidence rate in primary joint arthroplasties of 1-4%.^{60,61,66-70} For context, this will equate to more than 40,000 cases of PJI in the United States alone by the year 2030 and is likely grossly underestimated as it does not account for the total ankle, elbow, and shoulder arthroplasties.

These infections can lead to devastating complications, including amputation and death^{71,72} For example, the five-year mortality rates for PJIs of TKA and THA are 28% and 33%, respectively.⁷³ PJIs account for the first and third most common reason for revision in total knee and total hip arthroplasties, respectively.^{74,75} Moreover, the risk of PJIs has not changed over time.⁷³ Thus, PJI cases are expected proportionally with the number of TJA

procedures.^{60,73} To further complicate matters, the risk of contracting a PJI jumps from 1-4% for primary arthroplasties to 4-15.8% for multiple revisions.^{76,77}

These infections not only drastically affect the patient's quality of life, but are an economic burden on the healthcare system with costs expected to exceed \$1.62 billion by 2020.⁵⁹ Furthermore, the actual economic effect is likely more substantial as this estimate only includes direct hospital costs and does not take into account the cost for surgeons, specialists, pharmaceutical treatment, physical therapy, or home care. These costs are further increased when antibiotic-resistant strains are present.⁷⁸

Pathogeneses of PJIs

PJIs can occur at any point over the lifetime of the implant and are designated as either acute (<90 days) or chronic (>90 days) depending on when the symptoms present.⁷⁹ Acute infections are generally associated with highly virulent organisms (e.g., *Staphylococcus aureus*) likely the result of perioperative contamination or a hematogenous infection.⁸⁰ Chronic infections, on the other hand, arise due to less virulent species, such as coagulase-negative *staphylococci* and *propionibacterium acnes*.⁸⁰⁻⁸² Numerous microorganisms, both bacterial and fungal, have been implicated in PJIs. The prevalent causative microorganisms in prosthetic hip and knee infections are depicted in Figure 3.1.⁸³ Similar pathogens are often implicated in shoulder and ankle PJIs, although the distribution differs. For example, *P. acnes* is the most frequently identified causative organism in prosthetic shoulder infections accounting for 39-70% of positive cultures.^{84,85}

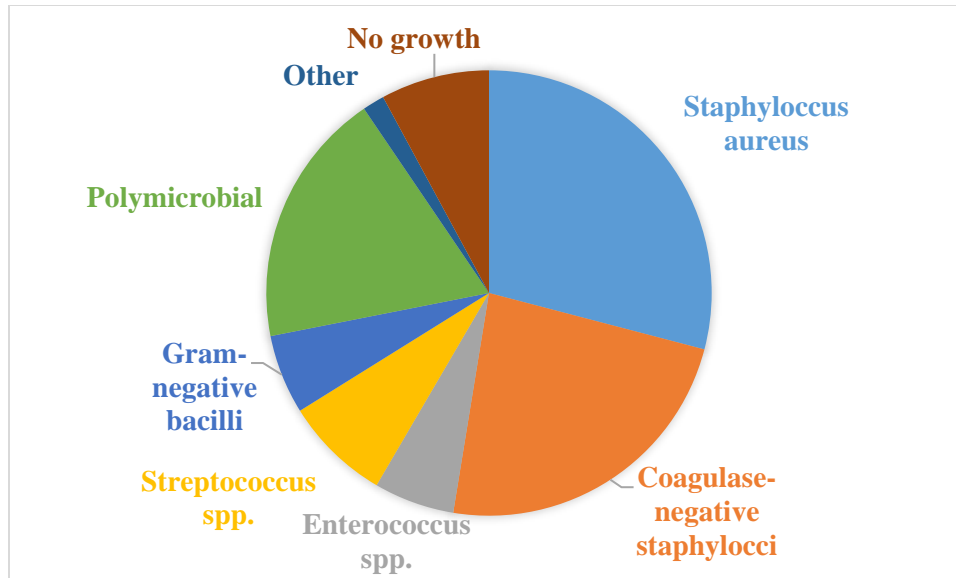


Figure 3.1. Common pathogens associated with prosthetic joint infections.

Fungal PJIs are extremely rare, accounting for approximately 1% of all PJIs with a recurrence rate up to 25%.^{86,87} *Candida albicans* was the most common pathogen identified accounting for 46% of fungal PJIs.⁸⁷

Further complicating treatment, foreign objects, such as implants and bone cement, can serve as a breeding ground for both bacterial and fungal biofilms. Biofilms produce an extracellular matrix which provides protection from antimicrobials and the host immune system.⁸⁸⁻⁹¹ Biofilm formation occurs in the following manner: reversible attachment, irreversible attachment, maturation, and dispersion.⁹² Reversible adhesion is mediated through a variety of physiochemical forces between the substrate and microbial surface.⁹³ Once the cells have entered the irreversible attachment phase, it is challenging to dislodge them. Thus, antimicrobial tolerance increases as the biofilm ages.^{83,88,89} It has also been suggested that a phenotypic shift in cell behavior occurs during biofilm growth in which a small subpopulation

of the bacteria (~1%) develop into persister cells.^{93,94} These cells are not genetically mutated, but instead are thought to lie dormant. Their dormant nature leads to increased antimicrobial tolerance due to the mode of action for most antimicrobials.^{89,93,94} These protective measures result in increased MICs, often 10-100x times higher than their planktonic equivalents. The presence of persister cells, along with the presence of multispecies biofilms, may contribute to the increase in recurrent infections seen in PJI patients.⁹³⁻⁹⁵

Treatment of PJIs

PJIs are often difficult to treat as systemic antibiotic or antifungal treatments are often ineffective on their own due to challenges in reaching the minimum inhibitory concentration (MIC) at the site of the infection without causing adverse effects.⁷ Therefore, surgical intervention is often necessary in addition to systemic antimicrobials. A general outline for the selection of treatment options is illustrated in Figure 3.2.⁹⁶

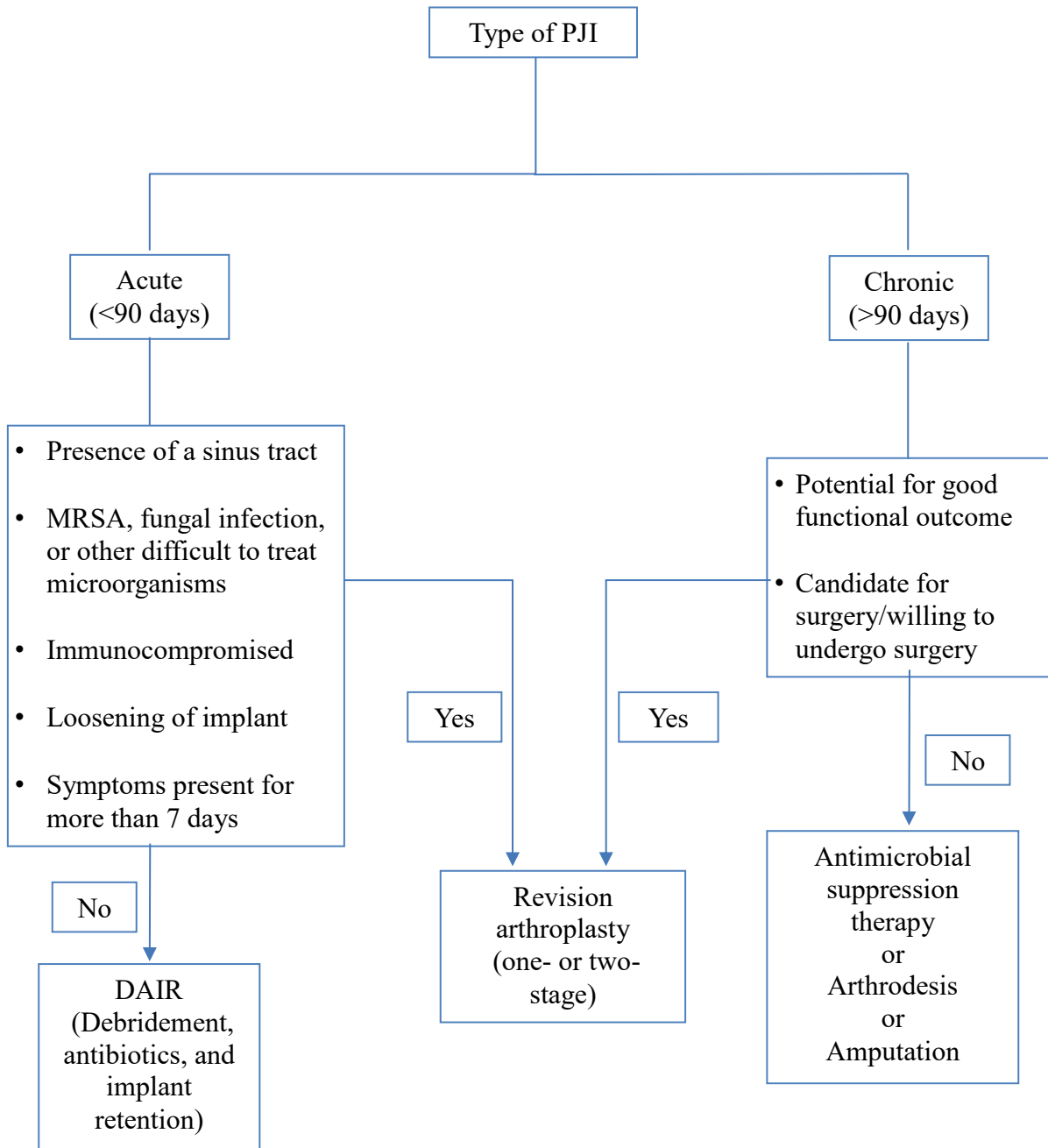


Figure 3.2. Schematic of treatment options for PJIs.

In the case of acute and hematogenous acute infections, debridement, antibiotics, and implant retention (DAIR) is often utilized. However, the success of this technique is reliant on several factors including, but not limited to, the duration of infection, causative organisms, presence of a sinus tract, and antibiotic duration.^{79,97} As a result, DAIR has a large variability in success rates ranging from 18-100%, with the lower range being attributed to component retention and highly virulent or resistant organisms.⁹⁷ Chronic infections are more challenging to treat due to more mature biofilm formation as such thorough debridement and complete removal of the prosthesis is required. These types of infections are often treated through either a one- or two-stage revision. In the case of a two-stage revision, this process involves thorough debridement, resection of the infected implant, insertion of a temporary antibiotic-laden spacer, followed by the insertion of permanent implant once the infection has been cleared and has a success rate between 75-90%.^{16,98-101} The antibiotic-laden spacer often serves a dual purpose. The first is to maintain high antibiotic concentrations to eradicate the infection without causing adverse effects systemically. The second is to preserve mobility and ligament contraction as these spacers can remain in place from anywhere to a few weeks to months.^{102,103} In addition to surgical treatment (DAIR, one-, or two-stage procedures), four to six weeks of systemic antimicrobial therapy is employed.

Antimicrobial-Laden Bone Cements

In order to treat and/or prevent PJIs, antibiotics or antifungals are incorporated into commercial PMMA bone cements and labeled antimicrobial-loaded commercial bone cement or ALBCs. They are inserted at the site of the infection in the form of spacers and/or beads,

which allows for the MIC to be reached while keeping systemic concentrations below toxic levels.^{7,64} ALBC beads can be used for a variety of ailments, including soft tissue infections/traumas. The use of ALBCs prophylactically has been shown in THAs to be comparable to the use of systemic antibiotics and the combination of ALBCs and systemic antibiotics reduced the rate of infection by 50%.¹⁶ Antibiotic elution occurs *via* a bulk diffusion model. There is a massive initial release of antibiotics, which is attributed to a surface phenomenon followed by continued elution over the course of several days.¹⁰²

Antimicrobial Selection

Antimicrobial coverage is an important factor when treating a joint infection, but further consideration must be taken when choosing which antibiotics or antifungals to incorporate. These factors address issues, such as chemical and thermal stability, sensitizing potential, elution profile, and effect on mechanical strength, to name a few.¹³ In order to effectively treat PJIs, antimicrobial selection should be based on its effectiveness against the causative organism. In cases in which a causative organism has not been identified, surgeons generally opt for broad-spectrum antimicrobial coverage against the most commonly observed or suspected pathogens. This is accomplished through the incorporation of a single antimicrobial or a mixture of antimicrobials, such as vancomycin and gentamicin.^{104–106} In addition to selecting the appropriate antimicrobial coverage, the available form needs to be taken into consideration as well. Studies have shown that the incorporation of liquid forms into PMMA cements significantly reduces the mechanical strength of the resultant cement.^{107–109}

The antimicrobials must be water-soluble as they are eluted from the cement *via* diffusion.^{13,110} Thus solubility and pore size affect the elution rate and overall concentration.

Furthermore, selection and dosage should be application-specific as it is well established that the mechanical strength is affected by the type and volume of antibiotic(s) incorporated.^{111,112} Additionally, the chemical and thermal stability needs to be considered as current commercial bone cements are limited in terms of which antibiotics or antifungals can be incorporated and eluted due to the chemical composition and nature of PMMA polymerization. As mentioned previously, PMMA polymerization occurs *via* an exothermic free radical mechanism with average temperatures in the range of 70-100 °C.^{8,9,12,113} Therefore, the antimicrobial must be thermally stable in order to survive the high temperatures present during the curing process. Due to the nature of polymerization, the antimicrobial chemical structure should be examined for any potential free radical scavenging activity, which could result in delayed curing times and reduced bioactivity of the antimicrobial. As a result, only a select number of antibiotics and antifungals can successfully be incorporated into and eluted from commercial PMMA cements.

Current ALBCs

Currently, only three (gentamicin, tobramycin, and vancomycin) antibiotics have been approved by the FDA for use in commercially available ALBCs in the United States. These three antibiotics have the most broad-spectrum applicability. Gentamicin and tobramycin are both broad-spectrum aminoglycosides that are effective against gram-negative bacteria, whereas vancomycin is a broad spectrum glycopeptide and is effective against gram-positive

bacteria. In the United States, ALBCs have been restricted to revision surgeries and in the low dose form (2.4% or 1 g of antibiotic per 40 g of cement) only. The addition of antibiotics at this dosage has no adverse effects on the mechanical strength. As such, surgeons often use them routinely in primary TJAS and high-risk patients. While prophylactic use of ALBCs has been effective in reducing infection rates, there is concern about the emergence of antimicrobial resistance due to the extended elution of sub-inhibitory concentrations of antibiotics.¹⁶ This concern is realized with the emergence of vancomycin-resistant *S. aureus*, gentamicin resistant coagulase-negative *staphylococci*, and fluconazole-resistant *Candida*.^{16,114,115} As such, it is pertinent to evaluate the usage of ALBCs for primary TJAs and to further expand the number of antimicrobials that can be incorporated into and eluted from commercial bone cements.

While ALBCs are recommended for revision surgeries, in the case of PJIs, most surgeons prefer a higher dosage, often between 8-17%.^{16,116} The rationale for a higher antibiotic content is to ensure MICs can be maintained over a sufficient period to completely eradicate the infection and limit the development of resistant strains.^{16,116} This need, along with the desire for higher antimicrobial load rates, has led surgeons to incorporate greater concentrations of both approved antibiotics and other antimicrobials into PMMA-based bone cements "off label."^{16,117}

Several antibiotics, in addition to the FDA-approved selections, can be incorporated into PMMA bone cements at a low dose without consequence. However, the usage of "off label" antimicrobial-laden bone cement could have undesired effects, including decreased mechanical strength, delayed setting times, or little to no antimicrobial release. A list of

compatible and incompatible antimicrobials and their target organism(s) is given in Table 3.1.

This list is by no means exhaustive.

Table 3.1 PMMA-compatible antimicrobials.¹¹⁸⁻¹²⁴

Gentamicin	Penicillin	Kanamycin	Cefazolin	Ciprofloxacin
Clindamycin	Tobramycin	Vancomycin	Amikacin	Ampicillin
Cefuroxim	Daptomycin	Oxacillin	Teicoplanin	Synercid

One example of these unforeseen complications is rifampin, a broad-spectrum antibiotic effective against biofilms. Rifampin-incorporated PMMA bone cement exhibits significantly delayed polymerization and dramatically reduced mechanical properties.^{123,125,126} These changes result in a cement that is no longer suitable for weight-bearing applications, but could perhaps be utilized for ALBC beads. Based on the delayed polymerization, it was suggested that rifampin might act as a free radical scavenger, thus inhibiting PMMA polymerization.¹²⁵ It is possible to overcome the deleterious effects of rifampin incorporation on PMMA through the encapsulation of rifampin. Sanz-Ruiz *et. al.* were able to overcome the deleterious effects of rifampin incorporation on PMMA through the encapsulation of rifampin which enabled the release of rifampin while conserving the mechanical properties.¹²⁷

The other significant risk in using "off label" ALBCs and perhaps the most important is the potential for limited antimicrobial elution from the PMMA-matrix. While amphotericin B can be incorporated into PMMA-based cements, it displays limited elution. The total amount released varies from <0.01-0.20% for load rate ranging from 0.3%-7.5%.¹²⁸⁻¹³² The compressive strength increased following the incorporation of amphotericin B.¹²⁸ This increase

was attributed to the potential interaction of the polyene backbone of amphotericin B with a free radical during PMMA polymerization. Although limited amphotericin B elution has been observed *in vitro*, Marra *et. al.* were the first to report the use of amphotericin B-laden bone cement (750 mg in 160 g cement) for the treatment of a *candida albicans* hip infection.¹³³ A peak amphotericin B concentration of 3.2 mg/L was obtained from the wound drainage 50 h after insertion.¹³³ Moreover, the blood and wound drainage antifungal concentrations remained above the MIC.

Attempts have been made to improve PMMA's ability to elute antimicrobials through the addition of poragens (soluble materials, i.e., cefazolin, that increase the porosity of the resultant cement), modified mixing techniques, or antimicrobial encapsulation.^{127,129,134} While the addition of poragens improves elution from ALBCs, they often adversely affect the mechanical strength especially as the concentration of poragens increases.^{129,135} Enhanced elution was reported by Cunningham *et. al.* for the liposomal amphotericin B formulation compared to the deoxycholate formulation.¹³¹ However, the liposomal formulation was associated with reduced compressive strength likely due to a poragen effect that arises from the volume difference between the two formulations. Kweon *et. al.* noted that the addition of a poragen (cefazolin) increased elution, but as the antifungal was eluted the compressive strength fell below the threshold set by ISO 5833 for weight bearing applications.¹²⁹

Alternatives to PMMA-Based ALBCs

Due to the limitations of acrylic bone cements for antimicrobial delivery mentioned above, a great deal of research has been done in an attempt to identify alternatives that address

these shortcomings. PMMA is a non-degradable polymer and as such, a second surgery is required to remove the beads and/or spacer. The necessity of a second surgery further increases the chance of infection as well as increases treatment costs. Therefore, several biodegradable options have been investigated. These materials can incorporate a wider breadth of antimicrobials than PMMA and have success rates of $\geq 80\%$.^{136,137} As the name suggests, these materials are subsequently degraded by the body over a few weeks to a few months, depending on the composition and formulation.^{138,139} The degradation of these compounds is expected to further improve the release of antibiotics. However, the rate at which the antibiotics are released varies depending on the composite and the nature of the material (e.g., collagen vs. PLGA).^{136,137,140} For example, collagen sponges release a large bolus of antibiotics on day 1 with complete elution achieved after day 4.¹⁴¹ By comparison, a poly lactic-co-glycolic acid had sustained release for 14 days.¹³⁷ In addition to improved elution profiles, these materials are biocompatible and can be osteogenic (e.g., calcium sulfate and bioactive glass).^{140,142,143} Synthetic polymers such as poly lactic-co-glycolic acid (PLGA) show great promise as the elution kinetics and mechanical properties can be tailored based on the formulation.^{136,137,139,144} While biodegradable materials have several advantages, they are not without their limitations. The majority of these materials have been developed for non-weight-bearing applications and as such, they are not suitable replacements for PMMA in ALBC spacers.

Summary

Prosthetic joint infections are a growing concern due to the increasing number of total joint arthroplasty procedures and the prevalence of comorbidities in these patients.

Furthermore, with the number of antimicrobial-resistant pathogens on the rise, it is pertinent to expand the number of antimicrobials that can be incorporated into and eluted from bone cement. However, due to the chemical composition and nature of PMMA polymerization, only a few select heat and chemically stable antibiotics and antifungals can be incorporated into and eluted from current commercially available bone cements. Attempts to address these shortcomings have been made with a focus on biodegradable materials. These materials are able to incorporate a more comprehensive array of antimicrobials and exhibit improved elution profiles. Nevertheless, these alternatives are not without their limitations and many do not possess sufficient mechanical strength for weight-bearing applications. Therefore, there is still a need to identify a suitable weight-bearing alternative to PMMA-based ALBCs.

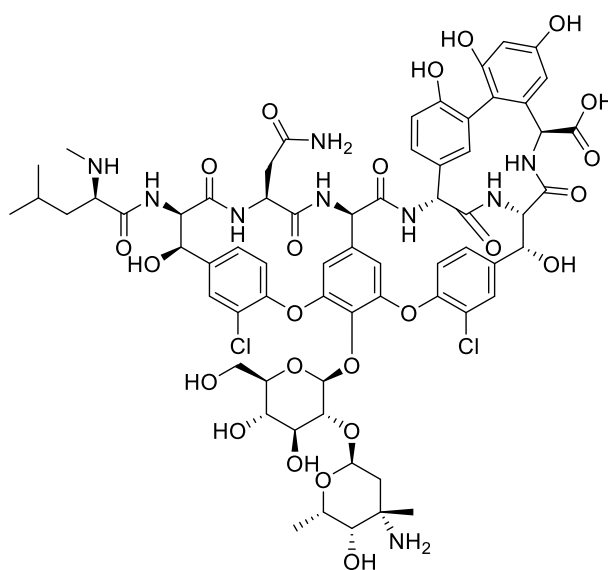
Results and Discussion

Our silorane-based bone cement has the potential to address the limitations that have often precluded a large arsenal of antibiotics and antifungals from being incorporated into commercial bone cements. This material exhibits none of the drawbacks typical of commercial bone cements, such as a high exotherm, monomer toxicity, and shrinkage, yet maintains comparable mechanical strength. Furthermore, the silorane biomaterial has been shown to have improved biocompatibility in comparison to commercial PMMA bone cements.^{7,9} Due to the lower curing temperature (~26 °C) and different polymerization mechanism, our silorane bone cement may be an effective delivery device for a broad range of antimicrobials. The capacity of this material to effectively deliver chemically- and heat-sensitive antimicrobials was assessed. The antimicrobial activity, elution profiles, and mechanical properties of

antimicrobial-laden silorane and PMMA cements were compared to each other and ISO 5833 (Implants for surgery — Acrylic resin cements).⁴⁷ While a commercial ALBC was available for one of the antibiotics tested, the decision was made not to use it due to the improved elution properties associated.¹⁴⁵ Samples were prepared and provided to Grahmm Funk and Damon Mar at the University of Kansas Medical Center for elution and mechanical testing.

Proof of Concept Studies

As vancomycin has broad spectrum applicability and is one of the few antibiotics available in commercial ALBCs, it was selected as for the first of the preliminary antimicrobial studies. The structure of vancomycin is given in Figure 3.3.



103

Figure 3.3. Vancomycin (**103**) structure.

Vancomycin was incorporated into the silorane bone cement at a low (2.40 wt.%) and high (11.11 wt.%) dose. The compressive strengths and moduli of the vancomycin-laden silorane cement are depicted in Figures 3.4 and 3.5 and listed in Table 3.2 (n=5/group). As the vancomycin content was increased, a general reduction both in the compressive strength and modulus was observed. However, there were no significant differences between the control and 2.4% samples, whereas the 11.11% vanc samples differed significantly from the control ($p<0.05$).

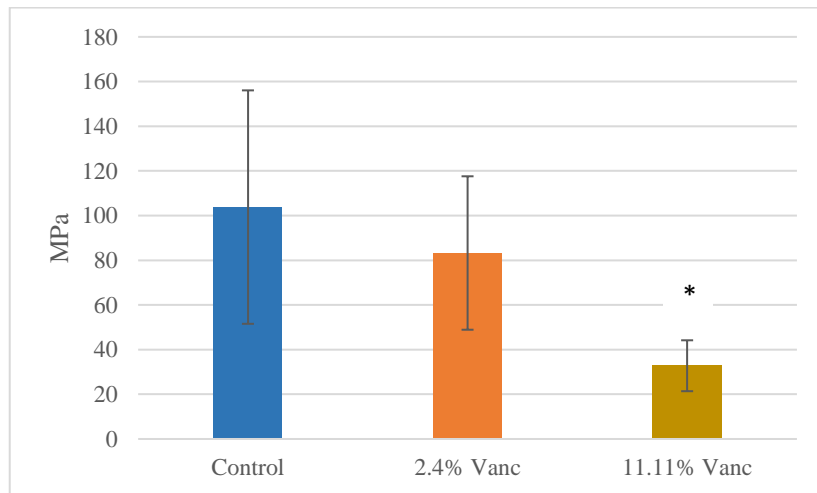


Figure 3.4. Compressive strength of vancomycin-laden silorane cement (* $p<0.05$).

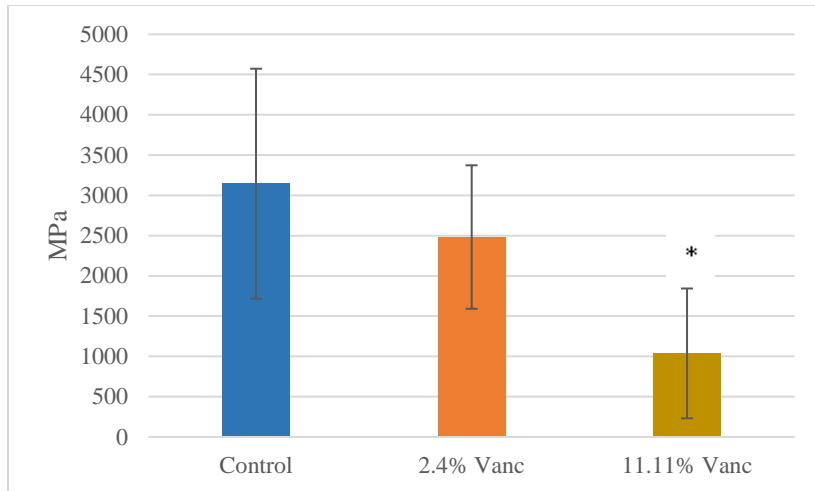


Figure 3.5. Compressive modulus of vancomycin-laden silorane cement (*p<0.05).

Table 3.2. Compressive strength and modulus of vancomycin-laden silorane biomaterial.

	Avg. Compressive Strength (MPa)	Avg. Modulus (MPa)
Control	103 ± 52	3145 ± 1428
2.4% Vanc	83 ± 34	2483 ± 891
11.11% Vanc	33 ± 11	1038 ± 806

Based on the preliminary mechanical testing, a low dose (2.4% by weight) of vancomycin was added to both the silorane (n=10) and SmartSet™ (n=10) cements. The amount of vancomycin eluted was determined using flow injection spectrophotometric analysis. Before soaking in PBS solution, the mass of each pellet was taken and the density of each cement was calculated. It was found that the silorane-based biomaterial was denser ($1.83 \times 10^{-3} \text{ g/mm}^3$) than the commercial PMMA bone cement ($1.25 \times 10^{-3} \text{ g/mm}^3$). The preliminary

results showed that silorane eluted vancomycin at comparable concentrations to PMMA over the 10-day period while remaining above the literature reported MIC (Figure 3.6).¹⁴⁶

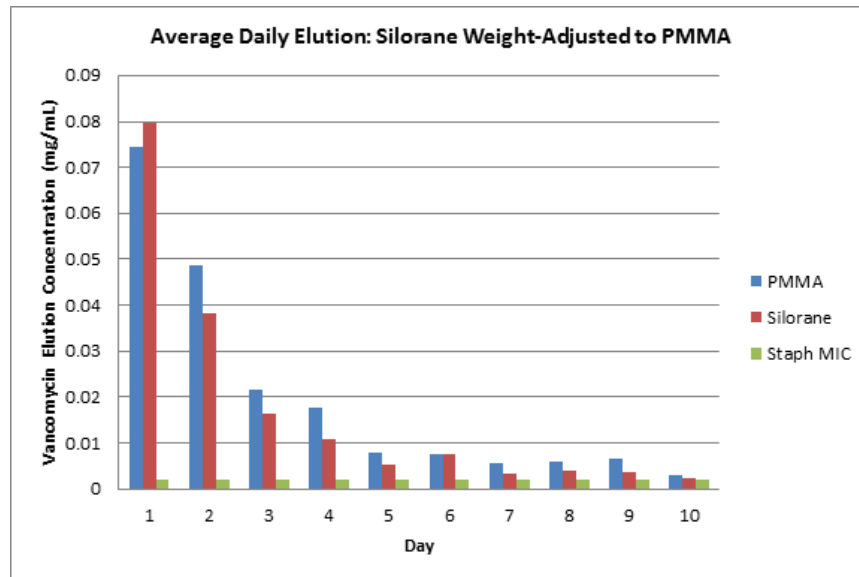


Figure 3.6. Weight-adjusted daily elution for vancomycin-incorporated PMMA and silorane bone cements.

Due to the rarity of fungal PJIs, less is known about the effects of antifungals on bone cements. Amphotericin B is an ideal candidate for antifungal-laden bone cements due to its broad spectrum applicability, thermal stability, and effectiveness against *Candida* species, the most common fungal PJI pathogen (Figure 3.7).^{87,128,147}

Table 3.3. Amphotericin B-laden silorane biomaterial formulations.

Sample	%LCSM	%LMC	%Filler	%Amp B	Polymerization time (min)
Control	34.60	0.40	65.00	0.00	30 min
Low dose	33.77	0.40	63.43	2.40	30
High dose	30.76	0.40	57.74	11.11	7 h

Due to the effects of the high dose of amphotericin B on the polymerization time of the silorane cement, the elution and mechanical properties were characterized for the low dose only for both silorane and PMMA samples. Amphotericin B was successfully eluted from silorane samples over seven days while concentrations fell below the limit of detection for PMMA samples after day 3 (Figure 3.8).

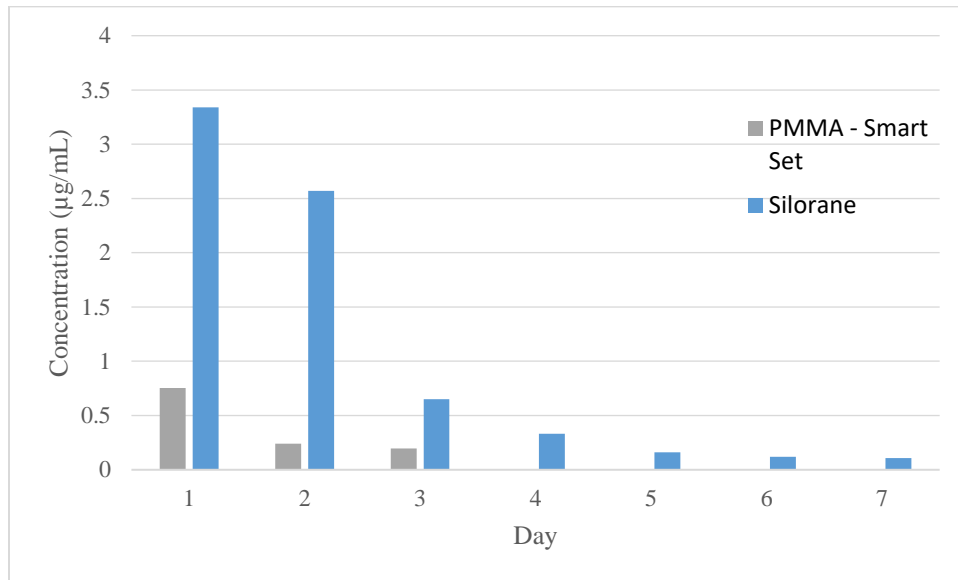


Figure 3.8. Weight-adjusted average amphotericin B daily elution. Silorane (n=3) PMMA (n=5).

The effects of amphotericin B on the mechanical properties of the silorane biomaterial are depicted in Figures 3.9 and 3.10 and given in Table 3.4. No significant differences were observed in either the compressive strength or modulus between the amphotericin B-laden and silorane control samples ($p>0.05$). At first glance, the compressive strength of SM Amp B appears to be enhanced after the antifungal incorporation. This discrepancy is most likely due to the variability in sample preparation and not a result of an interaction between amphotericin B and the silorane biomaterial. Evidence of this was demonstrated in the compressive strength values of the control as one sample was in agreement with the SM Amp B samples, one was much lower (~ 70 MPa), and the third failed before a value could be recorded. Uniform pellet formation with the silorane cement was previously noticed during the vancomycin testing and is apparent in the large standard deviations. Regardless, the compressive strength remained above the 70 MPa threshold set by ISO 5833 for both samples.⁴⁷

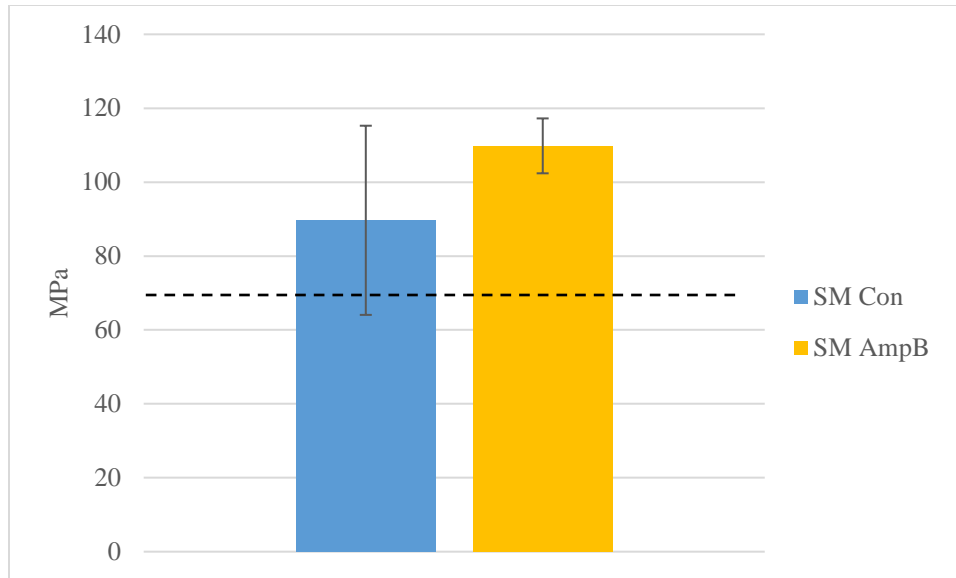


Figure 3.9. Compressive strength of amphotericin B-laden silorane biomaterial on Day 7 (n=3). The dotted line represents the ISO 5833 minimum threshold (70 MPa).

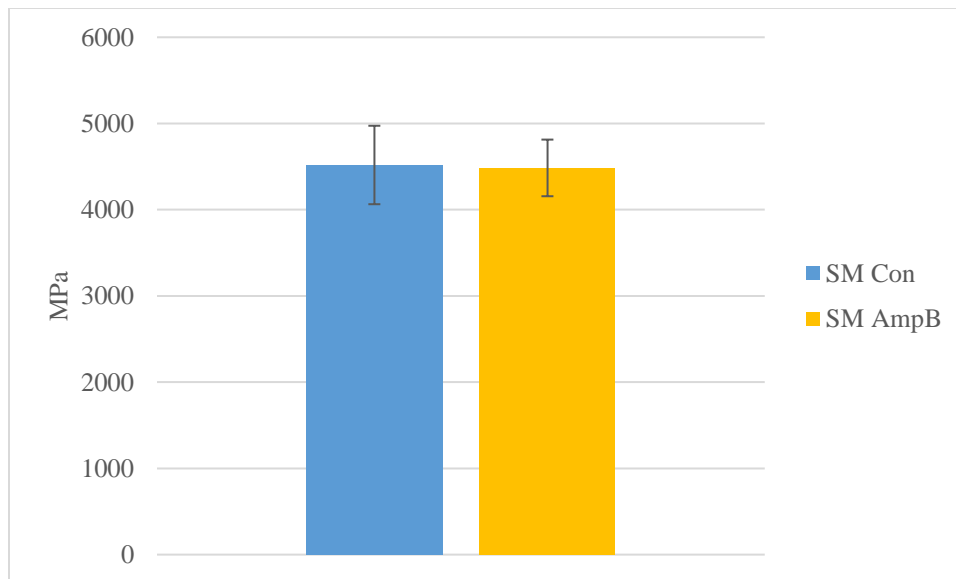


Figure 3.10. Compressive modulus of amphotericin B-laden silorane biomaterial on Day 7 (n=3).

Table 3.4. Compressive strength and modulus of amphotericin-laden silorane biomaterial.

	Avg. Compressive Strength (MPa)	Avg. Modulus (MPa)
Control	90 ± 26	4519 ± 455
2.4% Amp B	110 ± 7	4485 ± 328

In summary, the preliminary studies demonstrated the ability of this silorane-based biomaterial to serve as an antimicrobial delivery device. The silorane-based cement eluted vancomycin at comparable concentrations to the commercial PMMA bone cement, SmartSet™. Furthermore, silorane was able to release amphotericin B in higher concentrations and over a longer duration compared to PMMA. While no diminished mechanical properties were observed for the low dose antimicrobial-laden silorane cements, the same could not be said of their high dose counterparts. It appears the silorane biomaterial suffers from the same problem associated with high load rates of antimicrobials in commercial PMMA cements. Based on our previous experience optimizing the silorane cement formulation, a maximum threshold for the filler exists at approximately 75% filler content in which once reached the material becomes begins to fall apart and crumbles easily without much pressure. We think the antimicrobials may function as an additional filler in our material. This may account for the deleterious mechanical effects observed in the high dose samples. If this is the case, it may be possible to address this pitfall by adjusting the filler content prior to antimicrobial incorporation. Due to the promising results and limited sample size, it was determined a full-scale investigation into the ability of the silorane biomaterial to effectively incorporate and deliver antimicrobials was needed.

Antimicrobial-Incorporated Silorane Bone Cement

Vancomycin Incorporation

Based on the preliminary studies, a low dose of vancomycin was incorporated into silorane and commercial SmartSet™ PMMA bone cements and the elution and mechanical properties were investigated. Due to the aforementioned differences in densities, the load rates were adjusted to achieve equivalent concentrations of antibiotic per volume of cement. The composition of each group is given in Table 3.5.

Table 3.5. Formulations of samples for the vancomycin investigation.

Sample	%LCSM	%LMC	%Filler	%Vanc
SM Con	34.60	0.40	65.00	0.00
SM Vanc	33.94	0.40	63.77	1.89
SmartSet™ Con	n/a	n/a	n/a	0.00
SmartSet™ Vanc	n/a	n/a	n/a	2.4

Both the silorane and PMMA cement samples were able to elute clinically relevant concentrations of vancomycin over the 14 days (Figure 3.11). While the elution profiles were comparable, the SM Vanc samples released 1.5-times more vancomycin than SmartSet™ Vanc samples.

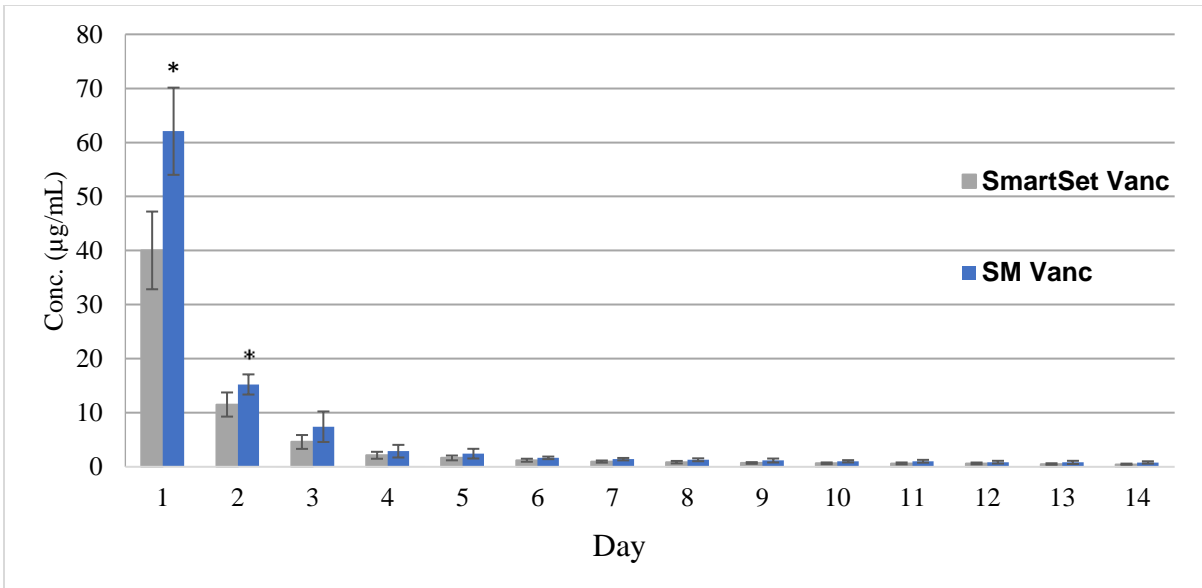


Figure 3.11. Elution profiles for vancomycin-incorporated SmartSet™ and silorane (SM) bone cements (* $p < 0.05$).

The compressive strength and modulus are illustrated in Figures 3.12 and 3.13, respectively. No differences in compressive strength were observed for any of the vancomycin samples ($p > 0.05$). Surprisingly, the SM Vanc samples exhibited reduced compressive modulus compared to SM controls.

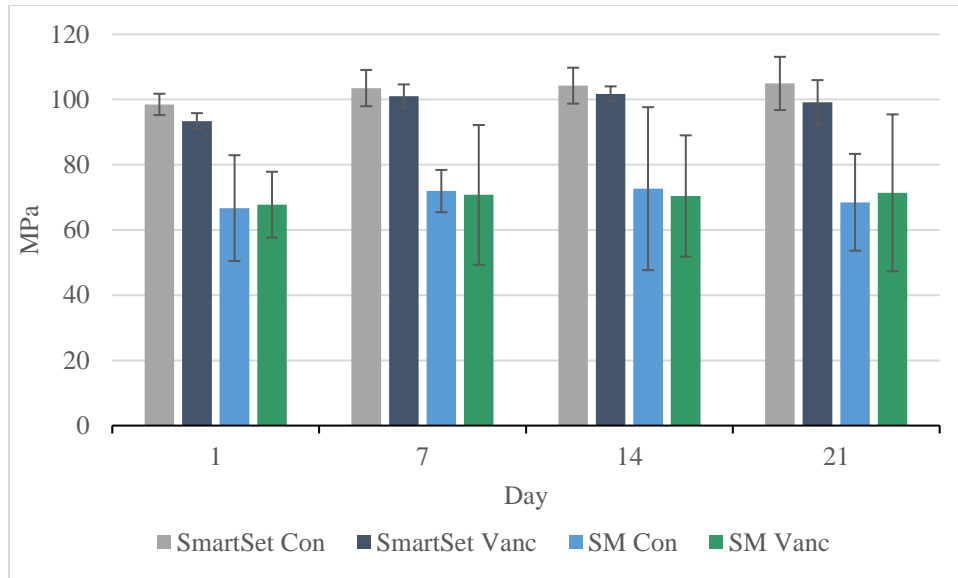


Figure 3.12. Effect of vancomycin-incorporation on the compressive strength of SmartSet™ and silorane (SM) bone cements over time.

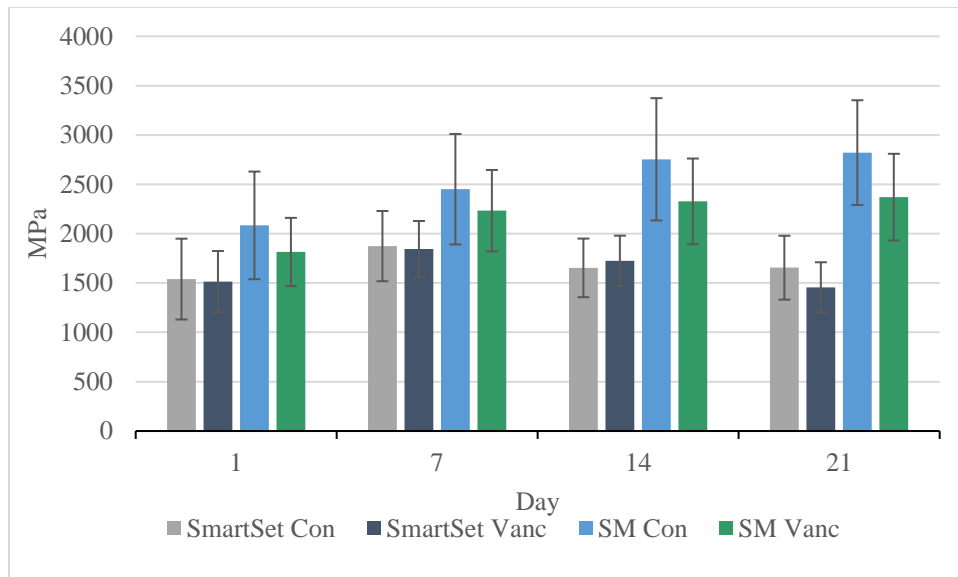
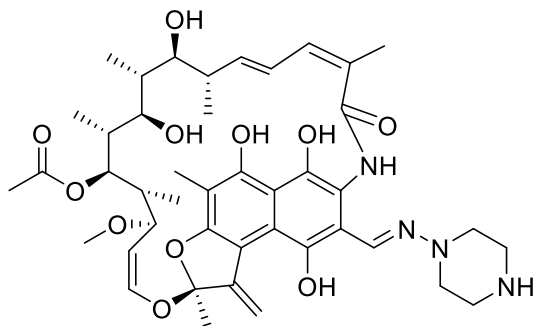


Figure 3.13. Effect of vancomycin-incorporation on the compressive modulus of SmartSet™ and silorane (SM) bone cements over time.

Rifampin Incorporation

PMMA Incompatibility

After the successful incorporation of vancomycin, we set out to investigate the ability of silorane to incorporate a PMMA-incompatible antibiotic, specifically rifampin (Figure 3.14). Rifampin (**105**) is an antibiotic effective against biofilms and is often indicated in methicillin-resistant *S. aureus* infections.



105

Figure 3.14. Chemical structure of rifampin (**105**).

However, following rifampin addition to PMMA-based bone cements, delayed polymerization and reduced mechanical strength have been observed.^{123,125,126} Previously, McPherson *et. al.* proposed that rifampin may act as a free radical scavenger and as such inhibit PMMA polymerization.¹²⁵ We set out to further understand the nature of the incompatibility between PMMA and rifampin. This information could potentially be utilized to screen and identify other potential PMMA-incompatible antimicrobials prior to incorporation. Since rifampin was

proposed to behave as a free radical scavenger, the effect of rifampin on a stable free radical, α, α -diphenyl- β -picrylhydrazyl (DPPH), was investigated. This assay was chosen because it is well-established, robust, quick, and did not require the generation of a radical species.¹⁴⁸⁻¹⁵⁰ The DPPH radical species displays a vibrant purple color in solution with an absorption around 517 nm in methanol. Once reduced, the solution becomes a pale yellow and a loss of absorbance is observed. An example of the resulting UV-vis spectra and the general reaction scheme for the DPPH[•] interaction with a hydrogen donor is provided in Figures 3.15 and 3.16, respectively.

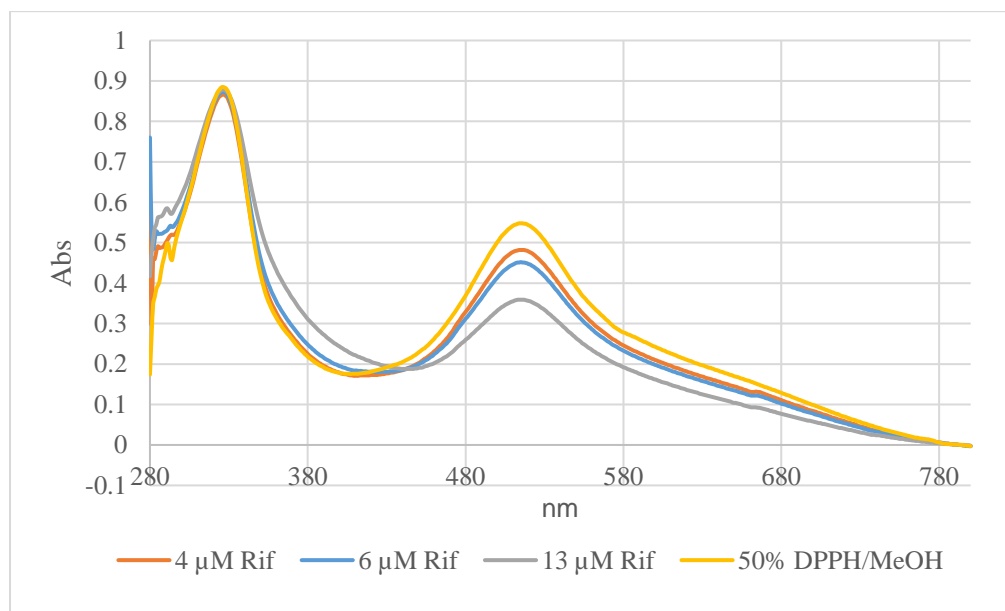


Figure 3.15. Typical UV-Vis spectra of DPPH assay.

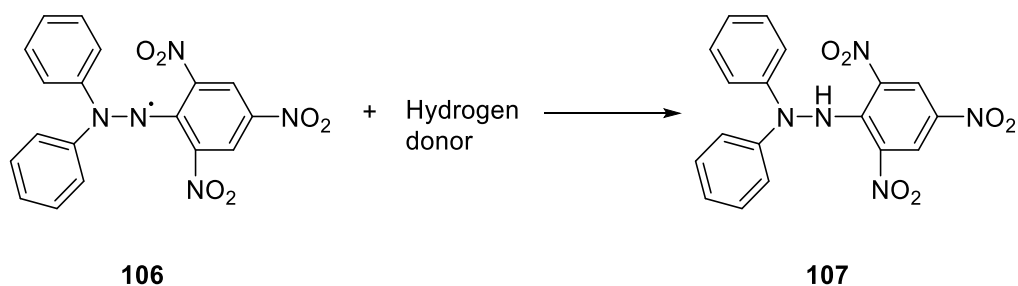


Figure 3.16. Schematic of the reduction reaction of DPPH \cdot .

Six analytes were chosen in addition to rifampin based on one of three categories: known ability to act as a radical scavenger (ascorbic acid (AA)), relationship to the rifampin structure (hydroquinone (HQ) and 1-methylpiperazine (Pip)), and antibiotics that can be successfully incorporated into commercially available bone cements (gentamicin (Gent) and vancomycin (Vanc)) (Figure 3.17).

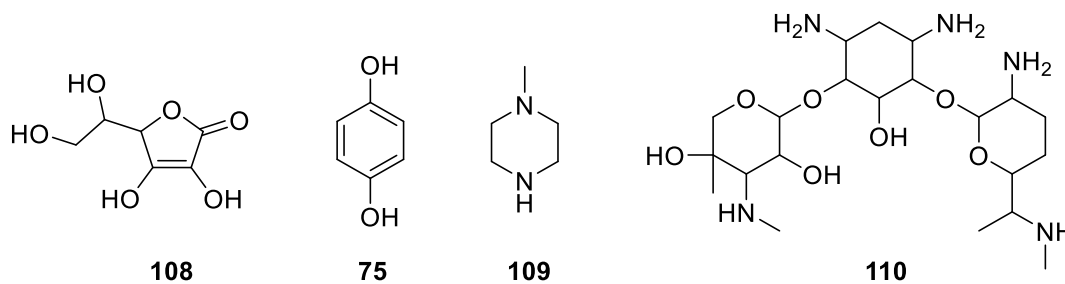


Figure 3.17. Structures of ascorbic acid (**108**), hydroquinone (**75**), 1-methylpiperazine (**109**), and gentamicin (**110**).

The free radical scavenging activity of the six analytes was evaluated using the EC₅₀ value or the concentration required to reduce the control absorbance by 50% as proposed by Bondet *et.*

al. and are depicted in Figure 3.18.¹⁵⁰ This value is inversely related to the potency of the free radical scavenger. While not as quick or potent as ascorbic acid or hydroquinone, both known radical scavengers, rifampin did exhibit free radical scavenging activity.¹¹³ Gentamicin and vancomycin, antibiotics available in commercially available ALBCs, did not behave as radical scavengers using the DPPH assay.¹¹³ In addition to the hydroquinone moiety, the piperazine moiety contained within rifampin has the potential to react with free radicals. However, no interaction was observed over the concentrations and time period tested.¹¹³ While EPR studies are necessary to definitively confirm the mechanism in which rifampin retards PMMA polymerization, the EC50 values are a good indication that rifampin can behave as a free radical scavenger. This ability is the likely cause of the PMMA incompatibility.

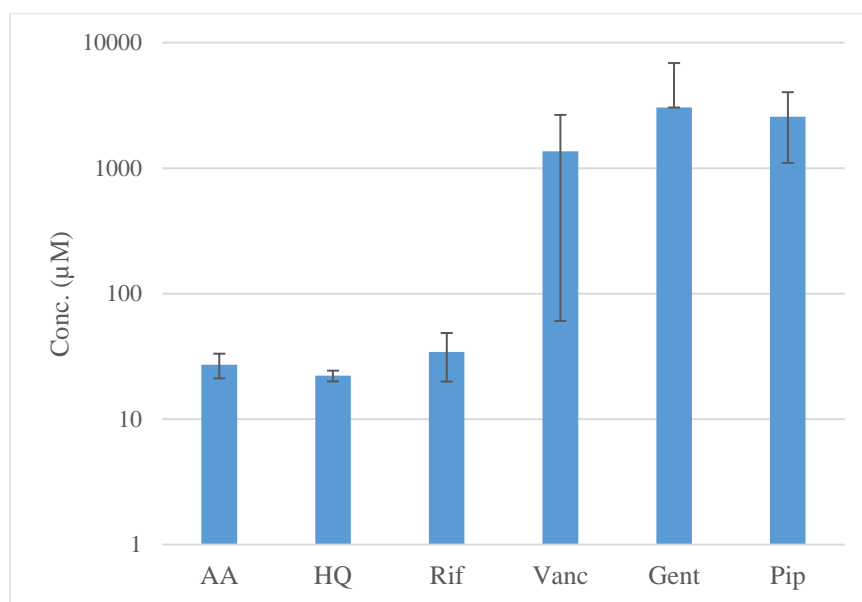


Figure 3.18. Log scale EC50 values. The EC50 value is inversely related to the potency of the free radical scavenger.

Based on the DPPH assay, only the three analytes that exhibited free radical scavenging ability (ascorbic acid (AA), hydroquinone (HQ), and rifampin(RIF)) were incorporated into commercially available SmartSet™, a PMMA-based bone cement (CON), in order to evaluate their effects on the setting time and compressive strength.

In agreement with previous reports, the incorporation of rifampin significantly retarded PMMA polymerization. Rifampin-incorporated PMMA took approximately 5 times longer to set than the control (33 min vs. 7.2 min, Table 3.6).¹¹³ Similar results were observed for hydroquinone. The diminished peak exothermic temperature is further confirmation of the interference in the free radical polymerization of PMMA. The maximum exothermic temperatures were 92.5 °C, 42.5 °C, and 27.6 °C, for control, rifampin, and hydroquinone samples, respectively.¹¹³ Surprisingly, ascorbic acid did not behave as expected in that only a slight reduction in the exothermic temperature and setting time was observed. Upon further inspection, it was noted that ascorbic acid is insoluble in the MMA monomer, unlike rifampin and hydroquinone. As such, the availability of ascorbic acid is limited explaining the slight attenuation in setting time and peak exothermic temperature compared to the control.

Table 3.6. Setting time and maximum curing temperature for rifampin-, hydroquinone-, and ascorbic acid-laden SmartSet™ bone cement.¹¹³

Group	Setting Time (Min:Sec)	Peak Exothermic Temp (°C)
Control	7:20	92.5
Rifampin	33:05	42.5
Hydroquinone	34:45	27.6
Ascorbic Acid	7:30	90.1

After studying the effects of the free radical scavengers on the setting time and maximum curing temperatures, the effects on the compressive strength were examined. The results are displayed in Figure 3.19.¹¹³ All groups showed significantly reduced compressive strength compared to the control ($p < 0.05$). For rifampin- and hydroquinone-laden samples the compressive strength fell below the minimum ISO 5833 threshold of 70 MPa. Therefore, rifampin-incorporated PMMA bone cement is contraindicated for use in weight-bearing applications.

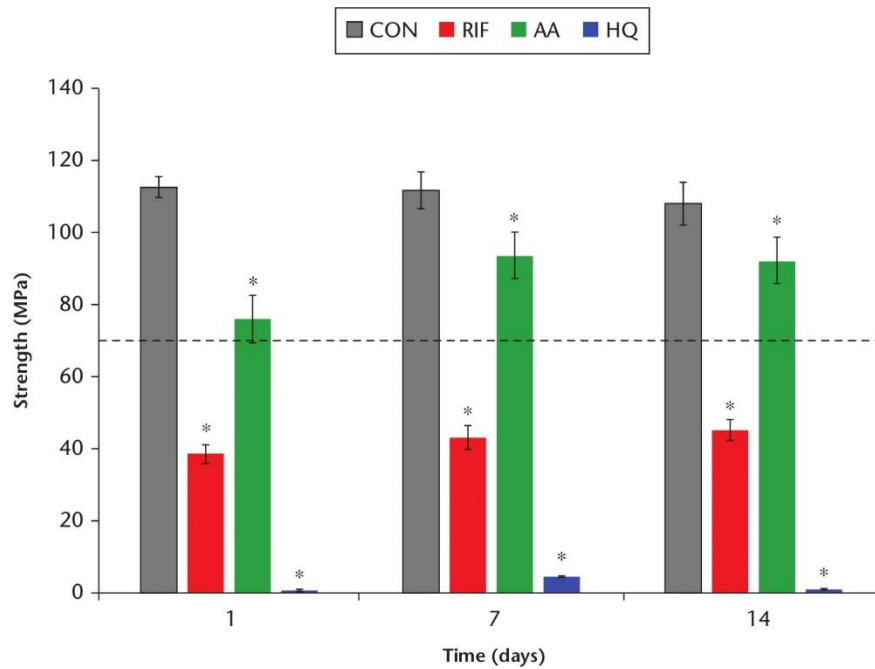


Figure 3.19. Effects of rifampin (RIF), ascorbic acid (AA), and hydroquinone (HQ) on the compressive strength of SmartSet™ over time. The dashed line represents the ISO 5833 threshold ($*p < 0.05$).¹¹³

While ill-suited for weight-bearing applications, several researchers have suggested it could be suitable for non-weight-bearing applications (e.g., beads).^{123,124,126,151} However, after the incorporation of rifampin into PMMA, a noticeable MMA odor was present. Funk *et. al.* reported a steady release of MMA monomer for 24 h with a 500% increase in release of MMA monomer compared to the control.¹¹³ Therefore, rifampin-laden PMMA bone cement is ill-suited for both weight-bearing applications and non-weight-bearing.

Rifampin-Incorporated Silorane-Based Bone Cement

Due to the difference in polymerization chemistry (cationic vs. free radical) of our silorane-based biomaterial, it was expected that rifampin could be incorporated and delivered without the deleterious effects observed in PMMA. Prior to performing elution and mechanical testing, the effects of rifampin on silorane polymerization time were evaluated. Rifampin was incorporated into the silorane-based bone cement in concentrations ranging from 0-15% and the polymerization time was assessed using the GNT. The formulations and polymerization times are given in Table 3.7. As expected, no change in polymerization was observed as the load rate of rifampin increased.

Table 3.7. Formulations and polymerization times of silorane-based bone cement with increasing concentrations of rifampin.

Sample	%LCSM	%LMC	%Filler	%Rifampin	Polymerization time (min)
1	34.60	0.40	65.00	0.00	30
2	33.77	0.40	63.43	2.40	30
3	32.86	0.40	61.74	5.00	30
4	30.75	0.40	57.74	11.11	45
5	29.39	0.40	55.21	15.00	45

Since no effect on polymerization time was observed, the elution and mechanical properties of rifampin-laden silorane bone cement were investigated. For the elution and mechanical testing, a low dose was utilized. However, on account of the density differences between the two cements, the load rate was adjusted to ensure equivalent dosage based on cement volume. The composition of each group is given in Table 3.8.

Table 3.8. Sample formulation for rifampin-incorporated elution and mechanical testing.

Sample	%LCSM	%LMC	%Filler	%Vanc
SM Con	34.60	0.40	65.00	0.00
SM Rif	33.94	0.40	63.77	1.89
SmartSet™ Con	n/a	n/a	n/a	0.00
SmartSet™ Rif	n/a	n/a	n/a	2.4

The silorane cement was able to successfully incorporate and elute rifampin over the 14-d period at clinically relevant concentrations while retaining its bioactivity (Figure 3.20). By comparison, the SmartSet™ Rif samples fell below detection limits after Day 2. On average, SM Rif samples released 125% more rifampin than SmartSet™ Rif.

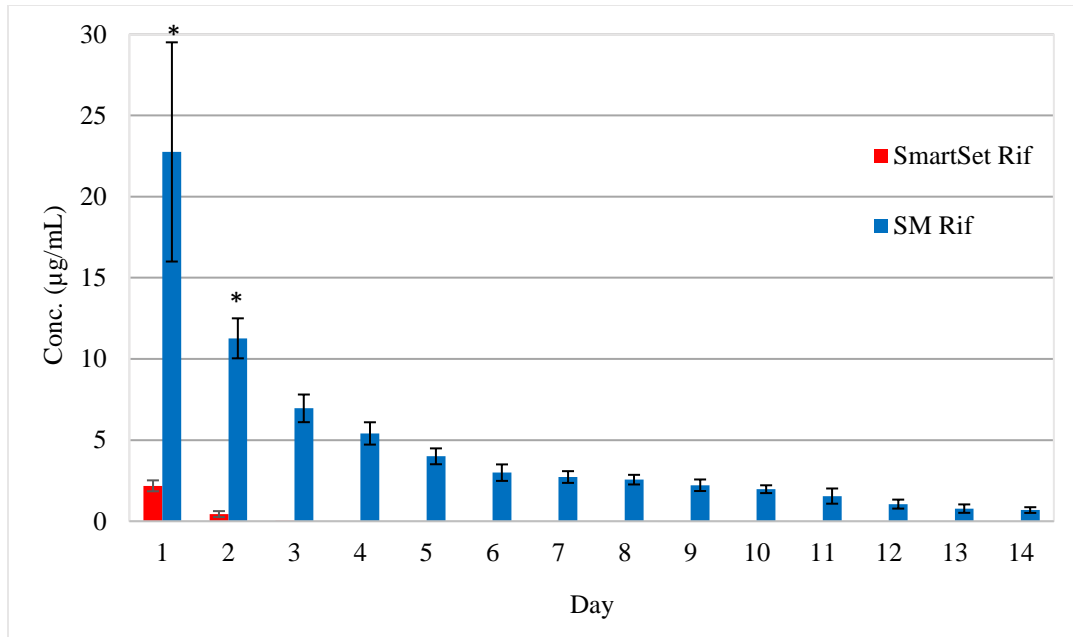


Figure 3.20. Elution profiles for vancomycin-incorporated SmartSet™ and silorane bone cements (*p<0.001).

While elution is a key component of antibiotic-loaded bone cements, preservation of the mechanical properties is also critical especially if intended for weight-bearing applications. The incorporation of rifampin did not affect the compressive strength or modulus in silorane samples ($p>0.05$) (Figure 3.21 and 3.22). However, the compressive strength and modulus were both significantly reduced in the PMMA samples ($p<0.001$).

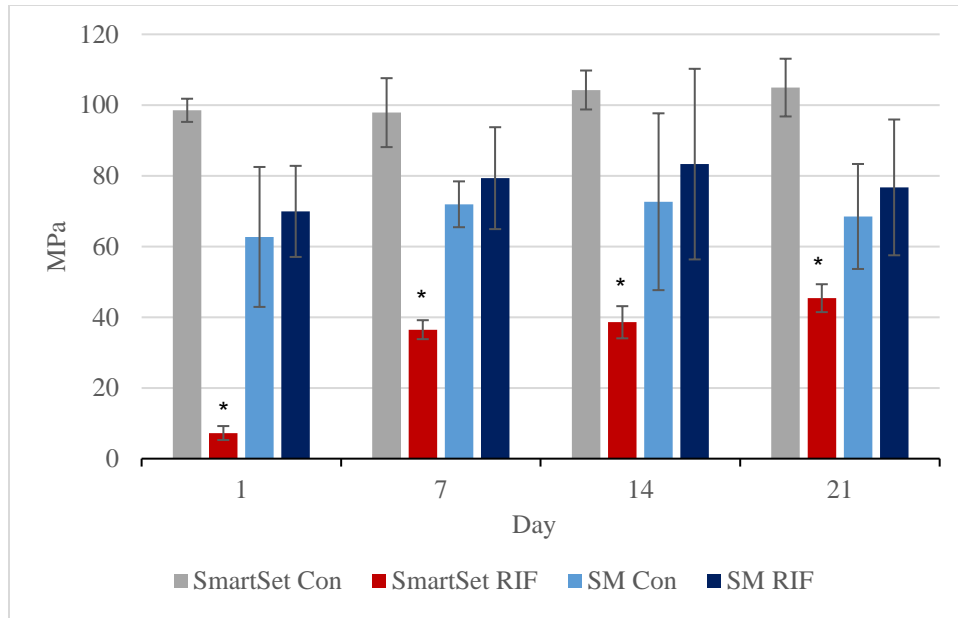


Figure 3.21. Effects of rifampin incorporation on the compressive strength of SmartSet™ and silorane (SM) bone cements (*p<0.001).

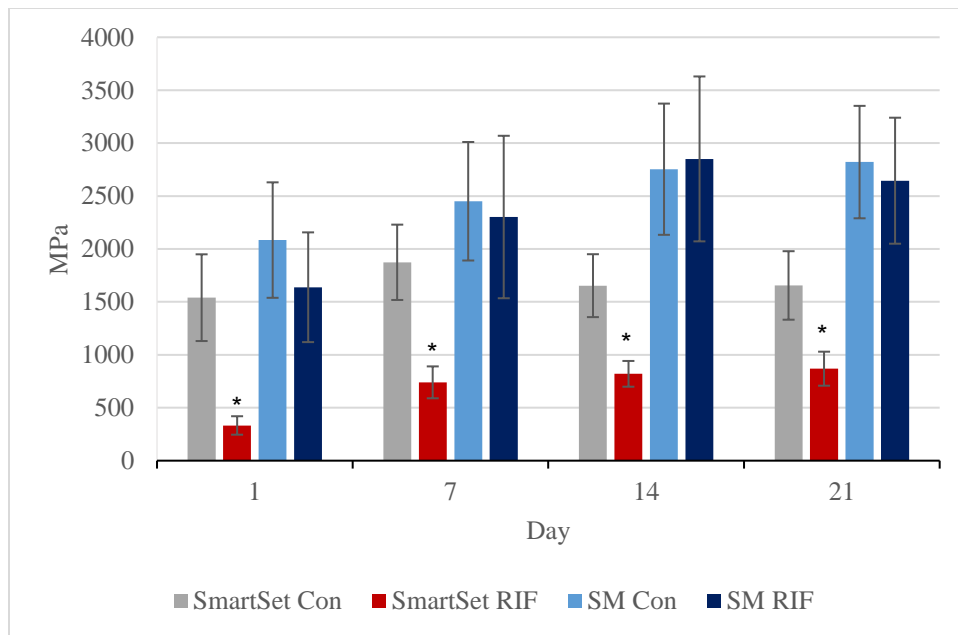


Figure 3.22. Effects of rifampin incorporation on the compressive modulus of SmartSet™ and silorane (SM) bone cements (*p<0.001).

Summary

The ability of rifampin to serve as a free radical scavenger has been implicated in the inhibition of PMMA bone cement polymerization. Utilizing the DPPH assay, it was determined that rifampin can act as a free radical scavenger explaining the increased setting time and decreased mechanical properties observed upon incorporation into PMMA. In addition to the incomplete polymerization, a steady release of the toxic MMA monomer occurred over 24 h. As a result, rifampin-laden PMMA bone cement is contraindicated for both weight-bearing and non-weight-bearing orthopaedic applications. Additionally, the antimicrobial structure must be evaluated for any potential interactions with the PMMA free radical polymerization mechanism prior to incorporation to avoid any adverse effects.

Due to the chemical composition and nature of polymerization, PMMA-based cements are limited in terms of local antimicrobial delivery. As a result, there is an imminent need for an alternative delivery device that can release a broad spectrum of active antimicrobials due to the growing number of PJI cases and the increase in resistant microbials. Moreover, current non-PMMA-based alternatives are ill-suited for weight-bearing applications. The silorane-based biomaterial has the potential to fulfill these needs as an alternative delivery vehicle for a breadth of antimicrobials. This material displays none of the characteristic drawbacks of commercial bone cements while exhibiting a lower exotherm (~ 26 °C), less shrinkage, and improved biocompatibility. Furthermore, the silorane-based biomaterial has comparable mechanical properties *in vitro* and *in vivo* to commercial bone cement. The lower exotherm should allow for a larger arsenal of antimicrobials to be incorporated. Additionally, the difference in the polymerization mechanism should further limit the number of incompatible

antimicrobials. We have shown that our silorane-based bone cement is capable of eluting the PMMA-compatible antibiotic, vancomycin, at comparable concentrations. Furthermore, this material can effectively incorporate and elute a low dose (2.4%) of PMMA-incompatible antimicrobials, rifampin and amphotericin B, without comprising the mechanical strength. Thus, making it suitable for both weight-bearing and non-weight-bearing applications.

Future Work

The silorane-based biomaterial has demonstrated superior elution of PMMA-incompatible antibiotics at low concentrations. However, for the treatment of PJIs, surgeons prefer a higher concentration of antimicrobials to ensure complete eradication of the infection. This was problematic in the current study as it appears the silorane material suffers from the same detrimental effects observed in PMMA after increased antibiotic incorporation. In spite of this, our material has the potential to be tailored for specific antimicrobial load rates by modifying the amount of filler and catalyst included. The effects of decreasing the filler content while increasing the antimicrobial concentration on the mechanical properties should be studied in attempts to identify an optimal formulation for a high dose antimicrobial therapy. In addition to modifying the formulation, further studies on antimicrobial-laden silorane-based biomaterial are necessary to understand its capabilities beyond antibiotics. This includes running a full investigation of amphotericin B-laden cement as well as incorporating new antimicrobial therapies, such as other antimicrobial peptides.

During the course of this study, it was noted that the silorane biomaterial demonstrated reduced biofilm formation compared to the SmartSet™ samples. As biofilm formation

contributes to the difficulty in treatment and recurrence rate of PJIs, a material that impedes the microbial adhesion and biofilm formation is of immense interest. The silorane cement is visually smoother than the PMMA cement, as judged by SEM. Yet, it is unknown at this time if the reduction in biofilm formation is due to the surface smoothness or if it is an inherent property of the silorane biomaterial. Characterization of biofilm growth on silorane and SmartSet™ cements were underway during the preparation of this dissertation.

Materials and Methods

Silorane Biomaterial (Antibiotic/Antifungal Incorporation Control). The silorane biomaterial was prepared as described for the pig study specimens above. Prior to Lamoreaux's catalyst addition, the sample was divided into smaller (~5 g) samples. The material was transferred to a 5 mL syringe and injected into a polytetrafluoroethylene (PTFE) mold to form 6 x 12 mm pellets. This process was repeated for the remaining samples utilizing the same mold for all samples. Samples were cured at 37 °C for 1 h. After being removed from the molds, the pellets were weighed and inspected for visual defects. The final composition of the silorane biomaterial was: 34.60% LCSM, 0.40% LMC, and 65.00% DY5-1TOSU filler.

Antimicrobial-laden Silorane Biomaterial. Filled SilMix was prepared as previously described. Antibiotics were mixed in by hand until uniformly distributed. Lamoreaux's catalyst was added with a syringe (by weight) and hand mixed for approximately 45 s. The material was transferred to 5 mL syringe and injected into polytetrafluoroethylene mold to form 6 x 12 mm pellets. This process was repeated for the remaining material utilizing the same mold for all samples. Samples were cured at 37 °C for 1 h. The final composition of antibiotic incorporated silorane biomaterial was: 33.94% LCSM, 0.40% LMC, 63.77% DY5-1TOSU filler and 1.89% antibiotic (rifampin or vancomycin).

Antimicrobial-laden SmartSet™ Cement. Antimicrobials were combined with the powdered component and mixed by hand until the sample appeared homogenous. Once mixed, the liquid monomer was added and the polymerizing cement was placed in a PTFE mold to form cylindrical pellets (6 x 12 mm). The samples were cured at 37 °C for 1 h.

Antimicrobial Elution. The pellets were transferred to 15 mL centrifuge tubes containing 2.5 mL of phosphate buffered saline (PBS) solution and incubated at 37 °C for 14 days. PBS solution was collected and replaced daily with fresh PBS. The elution profile was determined using HPLC with measurements taken at 1, 6, and 24 h followed by days 2-14.

Compression Testing. Compressive strength was determined according to ISO 5833 (Implants for surgery -- Acrylic resin cements) and tested on a MTS 858 Mini Bionix II. Forty cylindrical specimens (6 x 12 mm) were prepared for each cement group and tested prior to elution (day 0) and following elution at days 7, 14, and 21 (n=10/day). The thirty samples that were tested after elution were submerged in PBS as described in the elution studies

DPPH Radical Scavenging Assay. The DPPH radical scavenging activity was determined using an adapted method from Blois.¹⁴⁸ A DPPH stock solution of 593 μ M (2.34 mg in 10 mL MeOH) was prepared and care was taken to limit light and air exposure. The dark purple solution was further diluted to 81 μ M in order to achieve an absorbance close to one. Stock solutions of the antioxidants were prepared in MeOH and serially diluted to between 3 – 101 μ M. A full spectrum scan was taken for MeOH, DPPH, and each antioxidant (AOX). Each of the AOX solutions were combined with the DPPH working solution in a 1:1 ratio in a plastic cuvette and mixed with a pipet. The samples were incubated in the dark for 30 min at which time a full spectrum scan was taken and the absorbance at 515 nm recorded. An EC50 value or the efficient concentration required to reduce the DPPH absorbance by 50% as described by Bondet¹⁵⁰ was determined for each analyte. This assay was performed in triplicate.

References

1. Day, J. S.; Lau, E.; Ong, K. L.; Williams, G. R.; Ramsey, M. L.; Kurtz, S. M. *J. Shoulder Elbow Surg.* **2010**, *19*, 1115–1120.
2. Padegimas, E. M.; Maltenfort, M.; Lazarus, M. D.; Ramsey, M. L.; Williams, G. R.; Namdari, S. *Clin. Orthop. Relat. Res.* **2015**, *473*, 1860–1867.
3. W-Dahl, A.; Robertsson, O.; Lidgren, L. *Acta Orthop.* **2010**, *81*, 161–164.
4. Kurtz, S. M.; Lau, E.; Ong, K.; Zhao, K.; Kelly, M.; Bozic, K. J. *Clin. Orthop. Relat. Res.* **2009**, *467*, 2606–2612.
5. Charnley, J. J. *Bone Joint Surg. Br.* **1960**, *42-B*, 28–30.
6. Charnley, J. J. *Bone Joint Surg. Br.* **1964**, *46-B*, 518–529.
7. Hendriks, J. G. E.; van Horn, J. R.; van der Mei, H. C.; Busscher, H. J. *Biomaterials* **2004**, *25*, 545–556.
8. Lewis, G. J. *Biomed. Mater. Res. B Appl. Biomater.* **2008**, *84B*, 301–319.
9. Smith, D. C. *Orthop. Clin. North Am.* **2005**, *36*, 1–10.
10. Kühn, K.-D. What is Bone Cement. In *The Well-Cemented Total Hip Arthroplasty: Theory and Practice*; Breusch, S.; Malchau, H., Eds.; Springer Berlin Heidelberg: Berlin, Heidelberg, 2005; p 52–59.
11. Demian, H. W.; McDermott, K. *Biomaterials* **1998**, *19*, 1607–1618.
12. Endogan, T.; Serbetci, K.; Hasirci, N. *J. Appl. Polym. Sci.* **2009**, *113*, 4077–4084.
13. Kuehn, K.-D.; Ege, W.; Gopp, U. *Orthop. Clin. North Am.* **2005**, *36*, 17–28.
14. Gosavi, S. S.; Gosavi, S. Y.; Alla, R. K. *Dent. Res. J.* **2010**, *7*, 82–87.
15. Leggat, P. A.; Kedjarune, U. *Int. Dent. J.* **2003**, *53*, 126–131.
16. Soares, D.; Leite, P.; Barreira, P.; Aido, R.; Sousa, R. *Acta Orthop. Belg.* **2015**, *81*, 184–190.

17. Gilbert, J. L.; Hasenwinkel, J. M.; Wixson, R. L.; Lautenschlager, E. P. *J. Biomed. Mater. Res.* **2000**, *52*, 210–218.
18. Haas, S. S.; Brauer, G. M.; Dickson, G. *J. Bone Joint Surg. Am.* **1975**, *57*, 380–391.
19. Orr, J. F.; Dunne, N. J.; Quinn, J. C. *Biomaterials* **2003**, *24*, 2933–2940.
20. Vallo, C. I.; Schroeder, W. F. *J. Biomed. Mater. Res. B Appl. Biomater.* **2005**, *74B*, 676–685.
21. Bohner, M. *Injury* **2000**, *31*, D37–D47.
22. 3M ESPE US Filtek™ Silorane Low Shrink Posterior Restorative 2007.
23. Weinmann, W.; Thalacker, C.; Guggenberger, R. *Dent. Mater.* **2005**, *21*, 68–74.
24. Schweikl, H.; Schmalz, G.; Weinmann, W. *J. Dent. Res.* **2004**, *83*, 17–21.
25. Lien, W.; Vandewalle, K. S. *Dent. Mater.* **2010**, *26*, 337–344.
26. Braga, R. R.; Ferracane, J. L. *Crit. Rev. Oral Biol. Med.* **2004**, *15*, 176–184.
27. Belfield, K. D.; Zhang, G. *Polym. Bull.* **1997**, *38*, 165–168.
28. Eick, J. D.; Barragan-Adjemian, C.; Rosser, J.; Melander, J. R.; Dusevich, V.; Weiler, R. A.; Miller, B. D.; Kilway, K. V.; Dallas, M. R.; Bi, L.; Nalvarte, E. L.; Bonewald, L. F. *J. Biomed. Mater. Res. B Appl. Biomater.* **2012**, *100B*, 850–861.
29. Schweikl, H.; Schmalz, G.; Weinmann, W. *Mutat. Res. Toxicol. Environ. Mutagen.* **2002**, *521*, 19–27.
30. Eick, J. D.; Kotha, S. P.; Chappelow, C. C.; Kilway, K. V.; Giese, G. J.; Glaros, A. G.; Pinzino, C. S. *Dent. Mater.* **2007**, *23*, 1011–1017.
31. Aoki, S. U.S. Patent 6,255,428, July 3, 2001.
32. Crivello, J. V.; Bi, D. *J. Polym. Sci. Part Polym. Chem.* **1994**, *32*, 683–697.
33. Miller, B. D. Synthesis and Analysis of Siloranes for Use as a Biomaterial and Extended Twisted Molecular Ribbons. Ph.D. Dissertation, University of Missouri – Kansas City, Kansas City, MO, 2013.

34. Stansbury, J. W. *J. Dent. Res.* **1992**, *71*, 1408–1412.
35. Bailey, W. J. *J. Elastoplast.* **1973**, *5*, 142–152.
36. Bailey, W. J. *J. Macromol. Sci. Part A - Chem.* **1975**, *9*, 849–865.
37. Weiler, R. A. The Study of Initiation Systems and Formulations for the Development of a Novel Silorane Biomaterial. Ph.D. Dissertation, University of Missouri – Kansas City, Kansas City, MO, 2015.
38. 3M ESPE US Filtek™ Silorane Low Shrink Posterior Restorative Study Booklet 2007.
39. Crivello, J. V. *J. Polym. Sci. Polym. Chem.* **1999**, *37*, 4241–4254.
40. Crivello, J. V.; Lam, J. H. W. *Macromolecules* **1977**, *10*, 1307–1315.
41. Crivello, J. V.; Ahn, J. *J. Polym. Sci. A Polym. Chem.* **2003**, *41*, 2570–2587.
42. Ortyl, J.; Popielarz, R. *Polimery* **2012**, *57*, 510–517.
43. Strassler, H. E. *Compend. Contin. Educ. Dent.* **2011**, *32*.
44. Stansbury, J. W. *J. Esthet. Restor. Dent.* **2000**, *12*, 300–308.
45. Kwon, T.-Y.; Bagheri, R.; Kim, Y. K.; Kim, K.-H.; Burrow, M. F. *J. Investig. Clin. Dent.* **2012**, *3*, 3–16.
46. Crivello, J. V.; Lam, J. H. W. *J. Polym. Sci. Polym. Chem. Ed.* **1978**, *16*, 2441–2451.
47. International Organization for Standardization, ISO 5833: Implants for surgery – Acrylic resin cements.
48. Ranaweera, R. A. A. U.; Schuman, T. P.; Wang, R.; Miller, B. D.; Kilway, K. V. *J. Appl. Polym. Sci.* **2015**, *132*, 41831.
49. Hartwig, A.; Schneider, B.; Lühring, A. *Polymer* **2002**, *43*, 4243–4250.
50. Crivello, J. V.; Lee, J. L. *J. Polym. Sci. A Polym. Chem.* **1990**, *28*, 479–503.
51. Crivello, J. V. *Appl. Organomet. Chem.* **2010**, *24*, 169–178.

52. Mudgalkar, N.; Ramesh, K. *Anesth. Essays Res.* **2011**, *5*, 240–242.
53. Donaldson, A. J.; Thomson, H. E.; Harper, N. J.; Kenny, N. W. *Br. J. Anaesth.* **2009**, *102*, 12–22.
54. Khanna, G.; Cernovsky, J. *Contin. Educ. Anaesth. Crit. Care Pain* **2012**, *12*, 213–216.
55. Lamoreaux, H. F. U.S. Patent 3,220,972, November 30, 1965.
56. Kurtz, S.; Ong, K.; Lau, E.; Mowat, F.; Halpern, M. *J. Bone Jt. Surg.* **2007**, *89*, 780–785.
57. Meehan, J. P.; Danielsen, B.; Kim, S. H.; Jamali, A. A.; White, R. H. *J. Bone Jt. Surg. Am.* **2014**, *96*, 529–535.
58. Prokopetz, J. J.; Losina, E.; Bliss, R. L.; Wright, J.; Baron, J. A.; Katz, J. N. *BMC Musculoskelet. Disord.* **2012**, *13*, 251.
59. Kurtz, S. M.; Lau, E.; Watson, H.; Schmier, J. K.; Parvizi, J. *J. Arthroplasty* **2012**, *27*, 61–65.
60. Padegimas, E. M.; Maltenfort, M.; Ramsey, M. L.; Williams, G. R.; Parvizi, J.; Namdari, S. *J. Shoulder Elbow Surg.* **2015**, *24*, 741–746.
61. Althoff, A.; Cancienne, J. M.; Cooper, M. T.; Werner, B. C. *J. Foot Ankle Surg.* **2018**, *57*, 269–272.
62. Eka, A.; Chen, A. F. *Ann. Transl. Med.* **2015**, *3*, 233.
63. Everhart, J. S.; Altneu, E.; Calhoun, J. H. *Clin. Orthop. Relat. Res.* **2013**, *471*, 3112–3119.
64. Tande, A. J.; Patel, R. *Clin. Microbiol. Rev.* **2014**, *27*, 302–345.
65. Vasarhelyi, E. M.; MacDonald, S. J. *J. Bone Joint Surg. Br.* **2012**, *94-B*, 100–102.
66. Voloshin, I.; Schippert, D. W.; Kakar, S.; Kaye, E. K.; Morrey, B. F. *J. Shoulder Elbow Surg.* **2011**, *20*, 158–168.
67. Somerson, J. S.; Boylan, M. R.; Hug, K. T.; Naziri, Q.; Paulino, C. B.; Huang, J. I. *Shoulder & Elbow* **2019**, *11*, 116–120.

68. Fink, B.; Sevelde, F. *BioMed Res. Int.* **2017**, *2017*, 4582756.
69. Peersman, G.; Laskin, R.; Davis, J.; Peterson, M. *Clin. Orthop.* **2001**, *392*, 15–23.
70. Kurtz, S. M.; Lau, E.; Schmier, J.; Ong, K. L.; Zhao, K.; Parvizi, J. *J. Arthroplasty* **2008**, *23*, 984–991.
71. Natsuhara, K. M.; Shelton, T. J.; Meehan, J. P.; Lum, Z. C. *J. Arthroplasty* **2019**, *34*, S337–S342.
72. Lum, Z. C.; Natsuhara, K. M.; Shelton, T. J.; Giordani, M.; Pereira, G. C.; Meehan, J. P. *J. Arthroplasty* **2018**, *33*, 3783–3788.
73. Kurtz, S. M.; Lau, E. C.; Son, M.-S.; Chang, E. T.; Zimmerli, W.; Parvizi, J. *J. Arthroplasty* **2018**, *33*, 3238–3245.
74. Kamath, A. F.; Ong, K. L.; Lau, E.; Chan, V.; Vail, T. P.; Rubash, H. E.; Berry, D. J.; Bozic, K. J. *J. Arthroplasty* **2015**, *30*, 1492–1497.
75. Delanois, R. E.; Mistry, J. B.; Gwam, C. U.; Mohamed, N. S.; Choksi, U. S.; Mont, M. A. *J. Arthroplasty* **2017**, *32*, 2663–2668.
76. Kubista, B.; Hartzler, R. U.; Wood, C. M.; Osmon, D. R.; Hanssen, A. D.; Lewallen, D. *G. Int. Orthop.* **2012**, *36*, 65–71.
77. Kunutsor, S. K.; Wylde, V.; Beswick, A. D.; Whitehouse, M. R.; Blom, A. W. *Sci. Rep.* **2019**, *9*, 232.
78. Parvizi, J.; Pawasarat, I. M.; Azzam, K. A.; Joshi, A.; Hansen, E. N.; Bozic, K. J. *J. Arthroplasty* **2010**, *25*, 103–107.
79. Elkins, J. M.; Kates, S.; Lange, J.; Lange, J.; Lichstein, P.; Otero, J.; Soriano, A.; Wagner, C.; Wouthuyzen-Bakker, M. *J. Arthroplasty* **2019**, *34*, S181–S185.
80. Gbejuade, H. O.; Lovering, A. M.; Webb, J. C. *Acta Orthop.* **2015**, *86*, 147–158.
81. Gahukamble, A. D.; McDowell, A.; Post, V.; Salavarieta Varela, J.; Rochford, E. T. J.; Richards, R. G.; Patrick, S.; Moriarty, T. F. *J. Clin. Microbiol.* **2014**, *52*, 1595–1606.
82. Sabaté Brescó, M.; Harris, L. G.; Thompson, K.; Stanic, B.; Morgenstern, M.; O'Mahony, L.; Richards, R. G.; Moriarty, T. F. *Front. Microbiol.* **2017**, *8*, 1401.

83. Zimmerli, W.; Sendi, P. *APMIS* **2017**, *125*, 353–364.
84. Piper, K. E.; Jacobson, M. J.; Cofield, R. H.; Sperling, J. W.; Sanchez-Sotelo, J.; Osmon, D. R.; McDowell, A.; Patrick, S.; Steckelberg, J. M.; Mandrekar, J. N.; Fernandez Sampedro, M.; Patel, R. *J. Clin. Microbiol.* **2009**, *47*, 1878–1884.
85. Pottinger, P.; Butler-Wu, S.; Neradilek, M. B.; Merritt, A.; Bertelsen, A.; Jette, J. L.; Warne, W. J.; Matsen, F. A. *J. Bone Jt. Surg. Am.* **2012**, *94*, 2075–2083.
86. Darouiche, R. O.; Hamill, R. J.; Musher, D. M.; Young, E. J.; Harris, R. L. *Clin. Infect. Dis.* **1989**, *11*, 89–96.
87. Azzam, K.; Parvizi, J.; Jungkind, D.; Hanssen, A.; Fehring, T.; Springer, B.; Bozic, K.; Della Valle, C.; Pulido, L.; Barrack, R. *J. Bone Jt. Surg. Am.* **2009**, *91*, 142–149.
88. Stewart, P. S. *Microbiol. Spectr.* **2015**, *3*.
89. Ciofu, O.; Tolker-Nielsen, T. *Front. Microbiol.* **2019**, *10*, 913.
90. Vuong, C.; Voyich, J. M.; Fischer, E. R.; Braughton, K. R.; Whitney, A. R.; DeLeo, F. R.; Otto, M. *Cell. Microbiol.* **2004**, *6*, 269–275.
91. Jesaitis, A. J.; Franklin, M. J.; Berglund, D.; Sasaki, M.; Lord, C. I.; Bleazard, J. B.; Duffy, J. E.; Beyenal, H.; Lewandowski, Z. *J. Immunol.* **2003**, *171*, 4329–4339.
92. Hollmann, B.; Perkins, M.; Walsh, D. Hollmann, B. Biofilms and their role in pathogenesis. <https://www.immunology.org/public-information/bitesized-immunology/pathogens-and-disease/biofilms-and-their-role-in> (accessed Sep 15, 2019).
93. Lewis K. Multidrug Tolerance of Biofilms and Persister Cells. In *Bacterial Biofilms. Current Topics in Microbiology and Immunology*; Romeo T., Ed; Springer: Berlin, Heidelberg, 2008, Vol 322; p 107-131.
94. Wood, T. K.; Knabel, S. J.; Kwan, B. W. *Appl. Environ. Microbiol.* **2013**, *79*, 7116–7121.
95. Ma, D.; Shanks, R. M. Q.; Davis, C. M.; Craft, D. W.; Wood, T. K.; Hamlin, B. R.; Urish, K. L. *J. Orthop. Res.* **2018**, *36*, 452-458.
96. Zimmerli, W.; Trampuz, A.; Ochsner, P. E. *N. Engl. J. Med.* **2004**, *351*, 1645–1654.

97. Qasim, S. N.; Swann, A.; Ashford, R. *SICOT J* **2017**, 3, 2.
98. Azzam, K.; McHale, K.; Austin, M.; Purtill, J. J.; Parvizi, J. *Clin. Orthop. Relat. Res.* **2009**, 467, 1706–1714.
99. Haleem, A. A.; Berry, D. J.; Hanssen, A. D. *Clin. Orthop.* **2004**, 428, 35–39.
100. Hanssen, A. D.; Trousdale, R. T.; Osmon, D. R. *Clin. Orthop.* **1995**, 321, 55–67.
101. Bejon, P.; Berendt, A.; Atkins, B. L.; Green, N.; Parry, H.; Masters, S.; Mclardy-Smith, P.; Gundle, R.; Byren, I. *J. Antimicrob. Chemother.* **2010**, 65, 569–575.
102. van de Belt, H.; Neut, D.; Schenk, W.; van Horn, J. R.; van der Mei, H. C.; Busscher, H. *J. Acta Orthop. Scand.* **2001**, 72, 557–571.
103. Mazzucchelli, L.; Rosso, F.; Marmotti, A.; Bonasia, D. E.; Bruzzone, M.; Rossi, R. *Curr. Rev. Musculoskelet. Med.* **2015**, 8, 373–382.
104. Buchholz, H. W.; Elson, R. A.; Heinert, K. *Clin. Orthop.* **1984**, 190, 96–108.
105. Anagnostakos, K.; Wilmes, P.; Schmitt, E.; Kelm, J. *Acta Orthop.* **2009**, 80, 193–197.
106. Anagnostakos, K.; Fürst, O.; Kelm, J. *Acta Orthop.* **2006**, 77, 628–637.
107. Ger, E.; Dall, D.; Miles, T.; Forder, A. *South Afr. Med. J.* **1977**, 51, 276–279.
108. Lautenschlager, E. P.; Marshall, G. W.; Marks, K. E.; Schwartz, J.; Nelson, C. L. *J. Biomed. Mater. Res.* **1976**, 10, 837–845.
109. Seldes, R. M.; Winiarsky, R.; Jordan, L. C.; Baldini, T.; Brause, B.; Zodda, F.; Sculco, T. P. *J. Bone Jt. Surg.* **2005**, 87, 268–272.
110. Downes, S.; Maughan, P. A. *Clin. Mater.* **1989**, 4, 109–122.
111. Lewis, G. *J. Biomed. Mater. Res. B Appl. Biomater.* **2009**, 89B, 558–574.
112. Pelletier, M. H.; Malisano, L.; Smitham, P. J.; Okamoto, K.; Walsh, W. R. *J. Arthroplasty* **2009**, 24, 454–460.
113. Funk, G. A.; Menuey, E. M.; Cole, K. A.; Schuman, T. P.; Kilway, K. V.; McIff, T. E. *Bone Jt. Res.* **2019**, 8, 81–89.

114. Centers for Disease Control and Prevention. Antibiotic/Antimicrobial Resistance. https://www.cdc.gov/drugresistance/biggest_threats. (accessed Oct 1, 2017).
115. Centers for Disease Control and Prevention. Healthcare-associated infections. https://www.cdc.gov/hai/organisms/visa_vrsa/visa_vrsa.html (accessed Oct 1, 2017).
116. Hanssen, A. D.; Spangehl, M. J. *Clin. Orthop.* **2004**, *427*, 79–85.
117. Joseph, T. N.; Chen, A. L.; Di Cesare, P. E. *J. Am. Acad. Orthop. Surg.* **2003**, *11*, 38–47.
118. Picknell, B.; Mizen, L.; Sutherland, R. *J. Bone Joint Surg. Br.* **1977**, *59-B*, 302–307.
119. Frommelt, L.; Kühn, K.-D. In *The Well-Cemented Total Hip Arthroplasty: Theory and Practice*; Breusch, S.; Malchau, H., Eds.; Springer Berlin Heidelberg: Berlin, Heidelberg, 2005; p 86–92.
120. Weiss, B. D.; Weiss, E. C.; Haggard, W. O.; Evans, R. P.; McLaren, S. G.; Smeltzer, M. S. *Antimicrob. Agents Chemother.* **2009**, *53*, 264–266.
121. Marks, K. E.; Nelson, C. L.; Lautenschlager, E. P. *J. Bone Joint Surg. Am.* **1976**, *58*, 358–364.
122. Anagnostakos, K.; Kelm, J.; Regitz, T.; Schmitt, E.; Jung, W. *J. Biomed. Mater. Res. B Appl. Biomater.* **2005**, *72B*, 373–378.
123. Anguita-Alonso, P.; Rouse, M. S.; Piper, K. E.; Jacofsky, D. J.; Osmon, D. R.; Patel, R. *Clin. Orthop.* **2006**, *445*, 239–244.
124. Gálvez-López, R.; Peña-Monje, A.; Antelo-Lorenzo, R.; Guardia-Olmedo, J.; Moliz, J.; Hernández-Quero, J.; Parra-Ruiz, J. *Diagn. Microbiol. Infect. Dis.* **2014**, *78*, 70–74.
125. McPherson, E.; Portugal, D. *Reconstr. Rev.* **2011**, *1*, 34–36.
126. Shiels, S. M.; Tennent, D. J.; Akers, K. S.; Wenke, J. C. *Injury* **2017**, *48*, 2095–2100.
127. Sanz-Ruiz, P.; Carbó-Laso, E.; Del Real-Romero, J. C.; Arán-Ais, F.; Ballesteros-Iglesias, Y.; Paz-Jiménez, E.; Sánchez-Navarro, M.; Pérez-Limiñana, M. Á.; Vaquero-Martín, J. *J. Orthop. Res.* **2018**, *36*, 459–466.

128. Goss, B.; Lutton, C.; Weinrauch, P.; Jabur, M.; Gillett, G.; Crawford, R. *J. Arthroplasty* **2007**, *22*, 902–908.
129. Kweon, C.; McLaren, A. C.; Leon, C.; McLemore, R. *Clin. Orthop. Relat. Res.* **2011**, *469*, 3002–3007.
130. Sealy, P. I.; Nguyen, C.; Tucci, M.; Benghuzzi, H.; Cleary, J. D. *Ann. Pharmacother.* **2009**, *43*, 1606–1615.
131. Cunningham, B.; McLaren, A. C.; Pauken, C.; McLemore, R. *Clin. Orthop. Relat. Res.* **2012**, *470*, 2671–2676.
132. Houdek, M. T.; Greenwood-Quaintance, K. E.; Morrey, M. E.; Patel, R.; Hanssen, A. D. *J. Arthroplasty* **2015**, *30*, 2308–2310.
133. Marra, F.; Robbins, G. M.; Masri, B. A.; Duncan, C.; Wasan, K. M.; Kwong, E. H.; Jewesson, P. J. *Can. J. Surg.* **2001**, *44*, 383–386.
134. Wendling, A.; Mar, D.; Wischmeier, N.; Anderson, D.; McIff, T. *Bone Jt. Res.* **2016**, *5*, 26–32.
135. Nugent, M.; McLaren, A.; Vernon, B.; McLemore, R. *Clin. Orthop. Relat. Res.* **2010**, *468*, 2101–2106.
136. Inzana, J. A.; Schwarz, E. M.; Kates, S. L.; Awad, H. A. *Biomaterials* **2016**, *81*, 58–71.
137. Nandi, S. K.; Mukherjee, P.; Roy, S.; Kundu, B.; De, D. K.; Basu, D. *Mater. Sci. Eng. C* **2009**, *29*, 2478–2485.
138. Kanellakopoulou, K.; Giamarellos-Bourboulis, E. J. *Drugs* **2000**, *59*, 1223–1232.
139. Makadia, H. K.; Siegel, S. J. *Polymers* **2011**, *3*, 1377–1397.
140. McLaren, A. C. *Clin. Orthop.* **2004**, *427*, 101–106.
141. Wachol-Drewek, Z.; Pfeiffer, M.; Scholl, E. *Biomaterials* **1996**, *17*, 1733–1738.
142. Gitelis, S.; Brebach, G. T. *J. Orthop. Surg.* **2002**, *10*, 53–60.
143. Mousset, B.; Benoit, M. A.; Delloye, C.; Bouillet, R.; Gillard, J. *Int. Orthop.* **1995**, *19*, 157–161.

144. Hanssen, A. D. *Clin. Orthop.* **2005**, *437*, 91–96.
145. Nelson, C. L.; Griffin, F. M.; Harrison, B. H.; Cooper, R. E. *Clin. Orthop.* **1992**, *284*, 303–309.
146. CLSI. Performance Standards for Antimicrobial Susceptibility Testing. 29th ed. CLSI supplement M100. Wayne PA: Clinical and Laboratory Standards Institute; 2019.
147. Gallis, H. A.; Drew, R. H.; Pickard, W. W. *Clin. Infect. Dis.* **1990**, *12*, 308–329.
148. Blois, M. S. *Nature* **1958**, *181*, 1199–1200.
149. Kedare, S. B.; Singh, R. P. *J. Food Sci. Technol.* **2011**, *48*, 412–422.
150. Bondet, V.; Brand-Williams, W.; Berset, C. *LWT - Food Sci. Technol.* **1997**, *30*, 609–615.

VITA

Elizabeth Michol Menuey was born on July 12, 1988, in Iowa City, Iowa. She received a Bachelor of Science degree in biochemistry from Rockhurst University in 2010. In the fall of 2013, she joined the research group of Dr. Kathleen V. Kilway where her research focused on the development of a silorane-based biomaterial as an antimicrobial delivery device and the theoretical investigation into the twisted nature of longitudinally twisted acenes.

During her tenure at UMKC, Elizabeth was the recipient of a number of honors including two UMKC School of Graduate Studies Research Grants (2016 and 2018) and the Mr. & Mrs. Fong Wu Cheng Scholarship for Demonstration of Exceptional Achievement or Potential in Chemical Research (2015 and 2018). She was selected for the 21st Century Leadership Academy (2014) and the Graduate Student Leadership Program (2016). Elizabeth has presented her research at several meetings including the American Chemical Society Midwest Regional Meeting, the Physical Organic Chemistry Gordon Research Conference, and the International Symposium on Novel Aromatics. In addition to her scholastic endeavors, she was actively involved the Graduate Student Council serving in numerous capacities including president, conference co-chair, board member, and student government association senator. She also served as the secretary, vice president, and president for the Chemistry Graduate Student Association during her time at UMKC.

Publications:

Funk, G. A.; **Menuey, E. M.**; Cole, K. A.; Schuman, T. P.; Kilway, K. V.; McIff, T. E. "Radical Scavenging of Poly(methy methacrylate) Bone Cement by Rifampin and Clinically Relevant Properties of the Rifampin-Loaded Cement." *Bone Joint Res.* **2019**, *8*, 81-89. DOI: 10.1302/2046-3758.82.BJR-2018-0170.R2.

Clevenger, R. G.; Kumar, B.; **Menuey, E. M.**; Kilway, K. V. "Synthesis and Structure of a Longitudinally Twisted Hexacene." *Chem. Eur. J.* **2018**, *24*, 3113-3116. DOI: 10.1002/chem.201705676.

Clevenger, R.G.; Kumar, B.; **Menuey, E. M.**; Lee, G.-H.; Patterson, D.; Kilway, K.V., "A Superior Synthesis of Longitudinally Twisted Acenes," *Chem. Eur. J.* **2018**, *24*, 243–250, DOI: 10.1002/chem.201704501.

Presentations (* designates presenter if not first author):

Menuey, E.; Clevenger, R. G.; Kilway, K. V. "Towards Configurationally Stable LTAs." Presented at the 2019 International Symposium on Novel Aromatics Conference, Sapporo, Japan, July 21-26, 2019.

Kilway, K. V.; **Menuey, E.**; Clevenger, R. G. "Aggregate-Induced Emission of LTAs." Presented at the 2019 International Symposium on Novel Aromatics Conference, Sapporo, Japan, July 21-26, 2019.

Menuey, E.; Clevenger, R. G.; Kilway, K. V. "Investigation of configurationally stable LTAs." Presented at the 2019 Physical Organic Chemistry Gordon Research Conference, Holderness, NH, June 24-28, 2019.

Menuey, E. Funk, G.; Cole, K.; Schuman, T. P.; Kilway, K. V.; McIff, T. "Investigation of PMMA-Incompatible Rifampin." Presented at the 2018 Midwest Regional American Chemical Society Meeting, Ames, IA, October 22, 2018.

Abnos, M.; **Menuey, E. M.**; Kilway, K.V. "The Study of Amphotericin B Incorporated Silorane Bone Cement." Presented at the 2018 SUROP Poster Celebration, Kansas City, MO, August 30, 2018.

Connor, M.; **Menuey, E. M.**; Clevenger, R. G.; Kilway, K.V. "Determination of the Barrier to Interconversion through Variable Temperature NMR Spectroscopy." Presented at the 2018 SUROP Poster Celebration, Kansas City, MO, August 30, 2018.

Noori, S.; **Menuey, E. M.**; Kilway, K.V. "Effect of Amphotericin B on Physical Properties of Bone Cement." Presented at the 2018 SUROP Poster Celebration, Kansas City, MO, August 30, 2018.

Connor, M.; **Menuey, E. M.**; Funk, G.; McIff, T.; Kilway, K.V. "Attack of bone infections: An alternative to commercial bone cement." Presented at UMKC's 18th Annual Symposium of Undergraduate Research, Scholarship, and Creative Work, Kansas City, MO, April 12, 2018.

Funk, G.; **Horn, E.**; Cole, K.; Kilway, K.; McIff, T. “Polymerization Inhibition of Poly(Methyl Methacrylate) by Rifampin Through a Radical Scavenging Mechanism.” Presented at the Society for Biomaterials 2018 Annual Meeting and Exposition, Atlanta, GA, April 13, 2018.

Connor, M.; **Menuey, E. M.**; Funk, G.; McIff, T.; Kilway, K.V. “Attack of bone infections: An alternative to commercial bone cement.” Presented at Undergraduate Research Day @ the Capitol, Jefferson City, MO, April 5, 2018.

Funk, G.; Cole, K.; **Horn, E.**; Kilway, K.; McIff, T. “Characterization and Failure of Rifampin-loaded Poly(Methyl Methacrylate) Bone Cement.” Presented at the ORS 2018 Annual Meeting, New Orleans, LA, March 10-13, 2018.

Menuey, E.; Clevenger, R. G.; Kilway, K. V. “A Computational Study of Stability and Twist Bias for LTAs.” Presented at the 2017 International Symposium on Novel Aromatics Conference, Stony Brook, NY, July 23-28, 2017.

Clevenger, R. G.; **Menuey, E.**; Staudinger, M.; Kilway, K. V.* “Study and Analysis of Twisted Acenes and Their Precursors.” Presented at the 2017 International Symposium on Novel Aromatics Conference, Stony Brook, NY, July 23-28, 2017.

Menuey, E.; Clevenger, R. G.; Kilway, K. V. “A Computational Study of Stability and Twist Bias for LTAs.” Presented at the 2017 Physical Organic Chemistry Gordon Research Conference, Holderness, NH, June 24-30, 2017.

Clevenger, R. G.; **Menuey, E.**; Staudinger, M.; Kilway, K. V.* “Study and Analysis of Twisted Acenes and Their Precursors.” Presented at the 2017 Physical Organic Chemistry Gordon Research Conference, Holderness, NH, June 24-30, 2017.

Patel, M.; **Menuey, E. M.**; Funk, G.; McIff, T.; Kilway, K.V. “Scale Up and Production Optimization of our Silorane –Based Bone Cement.” Presented at UMKC's 17th Annual Symposium of Undergraduate Research, Scholarship, and Creative Work, Kansas City, MO, April 20, 2017.

Patel, M.; **Menuey, E. M.**; Funk, G.; McIff, T.; Kilway, K.V. “Scale Up and Production Optimization of our Silorane –Based Bone Cement.” Presented at Undergraduate Research Day @ the Capitol, Jefferson City, MO, April 4, 2017.

Menuey, E.; Clevenger, R. G.; Kilway, K. V. “Twist Bias of Twisted Acene Derivatives.” Presented at the 2016 Midwest Regional American Chemical Society Meeting, Manhattan, KS, October 28, 2016.

Patel, M.; **Menuey, E. M.**; Funk, G.; McIff, T.; Kilway, K.V. “The Application of a Novel Silorane-Based Bone Cement as an Effective Antibiotic Delivery Device.” Presented at the 2016 Summer Undergraduate Research Opportunity (SUROP) Poster Celebration, Kansas City, MO, September 1, 2016.

Menuey, E.; Clevenger, R.; Li, Y.; Scheel, K.; Peng, Z.; Kilway, K. V. “A Structure-Property Relationship Study of Acene and Thiophene Derivatives.” Presented at the 2016 UMKC Community of Scholars Symposium, Kansas City, MO, April 28, 2016.

Kilway, K.V.; Peng, Z.; Li, Y.; Clevenger, R.G.; Lu, J.; **Menuey, E. M.**; Bryan, J.; Scheel, K., “A Structure – Function Study of Substitution in Thiophenes and Aces on Optical Properties,” 16th International Symposium on Novel Aromatic Compounds (ISNA2015), Madrid, Spain, July 5-10, 2015.

Menuey, E.; Clevenger, R. G.; Li, Y.; Scheel, K.; Peng, Z.; Kilway, K. V. “A Structure-Property Relationship Study of Acene and Thiophene Derivatives.” Presented at the 2015 Physical Organic Chemistry Gordon Research Conference, Holderness, NH, June 21-26, 2015.

Horn, E. “Computer Modeling of Carbon Nanotubes” Presented at the Rockhurst Outstanding Research Seminar, Kansas City, MO, April 2010.

Horn, E.; Morokuma, K.; Bobadova-Parvanova, P. N. “Computer Modeling of Large Materials: How to Select the Correct Model” Presented at the 24th National Conference of Undergraduate Research, Missoula, MT, April 2010.

Horn, E.; Morokuma, K.; Bobadova-Parvanova, P. N. “Selecting the Correct ONIOM Model for Computational Studies of Carbon Nanotubes” Presented at the American Chemical Society 44th Midwest Regional Meeting, Iowa City, IA, October 2009.